Title
Lattice dynamics of substitutional alloys through a combined vibrational and compositional expansion

Author
Kuo, Yu-Sheng

Publication Date
2019

Peer reviewed|Thesis/dissertation

UNIVERSITY OF CALIFORNIA

Los Angeles

Lattice dynamics of substitutional alloys through a combined vibrational and compositional expansion

A dissertation submitted in partial satisfaction
of the requirements for the degree
Doctor of Philosophy in Materials Science and Engineering

by

Yu-Sheng Kuo

2018

ABSTRACT OF THE DISSERTATION

Lattice dynamics of substitutional alloys through a combined vibrational and compositional expansion

by

Yu-Sheng Kuo
Doctor of Philosophy in Materials Science and Engineering
University of California, Los Angeles, 2018
Professor Dwight Streit, Co-Chair
Professor Vidvuds Ozolins, Co-Chair

A general method incorporating both vibrational and configurational degrees of freedom is proposed by expanding energy into vibrational clusters. Our approach captures vibrational properties in substitutional alloys with arbitrary atomic configurations which can serve as an accurate surrogate model for first-principles calculations. Compressive sensing is applied to robustly and accurately select the important configuration dependent force constants and determine their value by learning from first principles calculations in one shot. Unlike virtual crystal approximation which tends to overestimate lattice thermal conductivity at high concentration range. Great agreements with experimental results across all composition for PbTe-Se demonstrates our VCE method is an accurate approach to generate high fidelity potential energy surface across a wide range of alloy materials.

The dissertation of Yu-Sheng Kuo is approved.

Jamian Marian

Mosleh Ali

Dwight Streit, Committee Co-Chair

Vidvuds Ozolins, Committee Co-Chair

University of California, Los Angeles

2018

To my wife and my daughter . . .

who—among so many other things—

have shown how strong I could be

TABLE OF CONTENTS

LIST OF FIGURES

LIST OF TABLES

ACKNOWLEDGMENTS

To my life-saviour, my dear wife ChiehChun Chou: because I owe it all to you. Many Thanks!

First and foremost, I have to thank my advisor, Professor Vidvuds Ozolins. Without his guidance and patience this work would not have been possible. He has always shown great support while I needed him. His special magic in elaborating complex concepts into approachable words has greatly helped me conquer the high mountains in this field. He is the best mentor, advisor and friends and the years spent with him to me is truly a bless. A very special gratitude goes to my mentor Fei Zhou, who has shown enormous patience, to guide me whenever I felt lost. Fei, your intelligence is out of this world and has amazed me times after times. But what makes you so powerful is how humble and so warm you are whenever someone is in need.

Special thanks to our lab's alumni Chi-ping Liu, Weston Nielson, and Yi Xia for leading a smooth transition for me while I first joined the group. You have been so welcoming and generous to teach all the precious experiences and knowledge you have learn for years in the lab.

I am grateful to my lab-mate Junsoo Park, Jiatong Chen, Brad Magnetta, and Daniel Eth. Your company makes my PhD career so colorful and enjoyable. It will down to one of the best journey I could have because of you all. Not to mentioned how welcoming and supportive you are whenever I am in need.

A very special gratitude goes out to all of my friends here in Los Angeles and Taiwan. Your supports have been my fountains to refresh me again and again.

And of course, all the thanks to my family who has been the biggest power which carries me forward. Thanks all of you!

Thanks for all your encouragement!

CHAPTER 1

Introduction

It is fair to say human advancement is pretty much defined by the innovation of materials. Ever since the usage of stone, the innovation of bronze, brass and steel and the modern Silicon era, whenever there is a new material being well exploited, the human civilization takes a great step forward. Traditionally, the discovery of materials often occurs in accidence or led by laboring experimentalists with countless time and expenses. According to recent National Research Council's report, a "new consumer product from invention to widespread adoption typically takes 2 to 5 years, but doing the same for a new material may take 15 to 20 years"[1]. This is the number has not taken numerous days and nights for experimentalists working in academic or industrial labs. The strong need of new and unique functional materials ranging from batteries with faster charge time, longer sustainability and safer usage in wide range of operating conditions, to better energy harvesting devices without intermittent issue, and higher conversion rate can hardly be kept up by the innovation of new materials.
The fundamental reason of the slow materials innovation is one can hardly relies on its limited understanding and intuition to systematically discover the important features of materials out of astronomically large materials space. The strong pressure between unbalance demand and supply in materials innovations has urged the development of "virtual lab". Unlike conventional lab investing money and time for one jack-pot material, virtual lab leverage the advancement of understanding of physics, advanced numerical methodologies and high performance computing to accelerate the materials discovery process which used to be guided by intuitions and experiences.

Though the idea of creating new materials using computer sounds like distant scenario in sci-fi movies, the advancement of first-principles methods, especially the development of

density functinoal theory(DFT)[2, 3, 4] has helped us making great breakthrough to get closer to this goal. By realizing external potential is a unique functional of electron density, DFT has successfully transform the original Schrödinger equation which directly deal with wave-functions for N electrons to a question of 1 electron alike question. This breakthrough riding on the wave of unprecedented progress of computing power has successfully built the foundation for modern first-principles calculations[5, 6]. Unlike most empirical models requires wide range of experimental inputs to infer the parameters to build the models, DFT has attracted significant attention because it requires no experimental data in advance. It liberate all the possibilities to design and analyze the materials from bottom up. The use of DFT has successfully guided the engineering design like desired band-gap[7] for electronic devices[8], high-voltage and high charging rate li-ion batteries[9, 10], high energy conversion thermoelectrics[11], nano scale optical devices[12], porous frameworks[13], and high entropy alloys[14] with unprecedented strength. We have now arrived at the point where the properties of hundreds and even thousands of materials can be screened in an automated fashion with minimized human intervention[15, 16].

Indeed, the initiative of Materials Project[17] and Open Quantum Materials Database[18] have largely summarized the significant progress of first-principles calculations.

1.0.1 Issues of first-principles calculations

Through high-performance computing and state-of-art screening algorithms, thousands of materials have been calculated and recommended to scientists with specific domain-expertise everyday. Though being demonstrated as powerful tool, with the computation complexity approximately scale with the number of electrons to the cubic, DFT is still well limited to calculate the ground state, at most, for few thousand atoms in a molecule or a periodic supercell even with the most advanced computation platform nowadays.

Therefore, though with impressive improvements, out of the computational necessity, most of DFT-based calculations have been conducted for perfect materials, which has no long-range disorder, at zero temperature. In reality, materials are fabricated and operated

at finite temperature with intrinsic defects and solubility of other elements. The fact is the material properties at real environment can rarely be represented by the calculation at perfect and zero temperature conditions. Non-perfect materials usually means the introduction of atomic configurational disorder. One of the common configurational disorder is defects, which can be vacancy or doping atoms. Obviously, most of the time, defect stands for detrimental effect in materials performance[19]. Accurately predict the effect of defect plays important role to properly estimate the performance of proposed materials. Furthermore, in terms of compositional disorder, calculating only perfect materials cast out a large class of compositional alloy materials

Alloys, also known as solid solution, is arguably one of the most popular material system. From the innovation of bronze and brass all the way to the modern micro-electronics, alloys plays important role in the success of engineering advancement. Due to the similarity in both physical and chemical properties, the alloy bonding allows the guest elements to interchange positions with host elements without significant increase of free energy. This special property allows stochastic distribution of elements with no definite relative positions. Unlike compound system with highly ordered atomic configurations, one of the most special property in alloys is its tunability. By alloying, graduate change of material properties between end-member can easily fill the gap which can not be easily obtained by existing compounds. For instance, it is well known by doping Indium into AlGaN, a continuous change of direct bandgap[20] can achieve wide range of lighting colors which can hardly be matched by other light emitting semiconductor compounds. Beside the graduate change, the alloying system can also create some unique properties only exhibited when intrinsic disorder is allowed. For instance, titanate-perovskite materials based on the substition of Ti for Mn, Nb, Zn, and Zr, exhibit a remarkable dielectric response at non-stoichiometric compositions near the morphotropic phase boundary[21], which is as well inaccessible in the end-member compounds themselves. High entropy alloys(HEA)[22] is another impressive example when disorder becomes essential. By equiatomically mixing more than 5 elements, HEA performs superb radiation resistance which makes it an ideal material for space mission and nuclear

power plant.

Other than configurational disorder, thermal disorder is another disorder which often can not be approximated by 0K temperature calculations. Indeed, without thermal disorder consideration, various predicted promising materials would simply fall flat because the violated thermodynamic stability. The finite temperature effect plays important role not only in predicting promising materials, but also essential for fabrication and synthesis. Even with materials which are stable at finite temperature, the synthesis of these materials often involve a series of meta-states which highly depend on finite temperature effects. The ability to accurate capture these meta materials is key to successfully fulfill the idea of virtual lab beyond the materials properties predictions.

Thermal and configurational disorder present serious challenge to researchers who only have access to standard electronic structure packages which are designed to handle perfectly ordered structures at zero temperature. This kind of calculations contain very limited thermodynamic information. Even now, it is common some fascinating materials are screened and recommended but never fulfill its promise because its property depends sensitively on the temperature and defect level. Series of phase transformations and segregation also are sensitive to the doping of carriers while optimizing the best performance[23]. For example, it is well known ferroelectric and piezoelectric exhibit its unique dielectric and piezoelectric properties only within certain critical temperature and doping concentration range. Above examples can not further emphasize the importance to expand the current DFT capability to incorporate thermal and configurational disorder.

1.1 Multi-scale Modeling

A typical approach to address computational complexity issue is applying multi-scale modeling coupling with first-principless calculations[24, 25, 26]. Instead of directly use first-principles calculations to explicitly incorporate thermal and configurational disorder across large time and length scale. The key idea of multi-scale modeling is if there is a higher

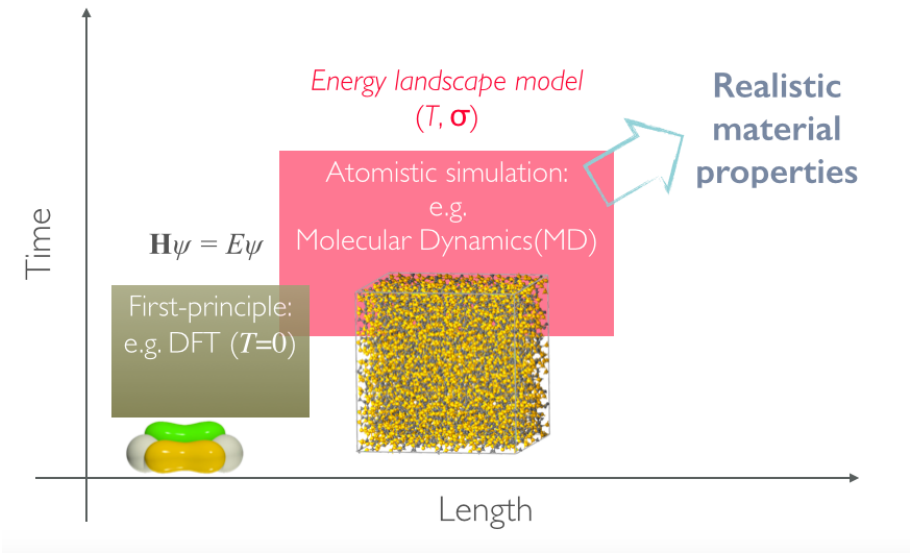

Figure 1.1: Schematic illustration of multi-scale modeling

level model, or say representation, which faithfully inherit all the targetting information from first-principles calculations but with only a fraction of computational cost, we can then use this higher level model as the surrogate model for further calculations to bypass the expensive calculations.

An question one would ask is if it is possible to find this kind of model given the complex level of underlying quantum mechanics? One of the fundamental approximation to enable multi-scale modeling is the application of Born-Oppenheimer approximation(BOA)[27], also known as adiabatic approximation. Due to the significant masses differences between electron and nuclear, BOA allows the separation of ion and electron wave function. By assuming that the electrons are close to their ground state, we can express ground state energy landscape which determines most materials properties as a simple function of the nuclear coordinates $\{\mathbf{R}_i\}$ and ion type $\{Z_i\}$ at lattice site i:

$$E \approx E_{\mathrm{BO}}^{\mathrm{GS}}(\{\mathbf{R}_i\}, \{Z_i\}) \tag{1.1}$$

We often refer this ground state energy as the potential energy surface(PES). This PES determines the ground state order, dynamics, statistical mechanics, and thermodynamics of targeting system. And all of this can be available to us by building this entire PES landscape

in a closed, parameterized functional form if our PES is smooth enough. Fortunately, this is the case for most of the time. By rapidly sampling the approximated PES obtained from the surrogate model instead of the exact yet time-consuming DFT calculations, we could efficiently extract the entire statistical mechanics, dynamics etc. This enables much larger scale simulation in both time and length.

To intuitively explain how first-principles mutli-scale modeling work as a whole, we know that at some scale, and for some problems, often time we do not need to know how atoms interact with each other, nor do we need to know how atoms are arranged exactly. For instance, an engineer does not need to know where the atoms in a bridge are to know how much the bridge will bend under the weight of a truck. Knowledge of the elastic properties of the supporting beams, together with the material they are made of, is sufficient as long as the response of the material to elastic deformations is known. For microscopic parameter like elastic deformation, we can then obtain from knowing the landscape of PES. And PES can be built from first-principles calculations. In this fashion, if we had a set of workable physical models at all length and time scales of our interest, we could compute the microscopic parameters of the larger scale model from the next scale down, and thus be done with a first-principless model of the world as a whole. As schematic represented in Figure 1.1, the key to bring first-principles into larger scale is an accurate description of PES. However, building this PES model is a challenging work, and the process gets even tougher when compositional disorder comes into the picture. Most of the PES models tend to oversimplify the PES with very few degree of freedom using well crafted empirical functional like famous Lenard-Jones potential. The results are usually these empirical models are not accurate and can hardly be improved. For those exact methods derived models like lattice dynamics ,though enjoy high accuracy, often have the atomic type Z_i or fixed R_i implicitly implied when the model is built. It makes the study of dynamic in compositional disorder materials extremely cumbersome and time-consuming, and practically impossible to compute.

To address these issues, we propose to develop a vibrational cluster expansion(VCE) method that can construct physically-accurate and mathematically rigorous model with sig-

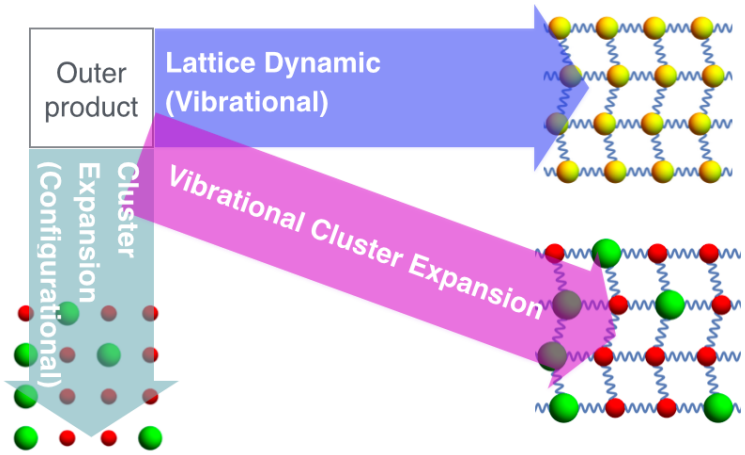

Figure 1.2: A schematic representation of VCE. The core of VCE is a combination of lattice dynamics and cluster expansion through the tensor product. Lattice dynamics handles vibrational degrees of freedom while cluster expansion handles configurational degree of freedom as highlighted by spring and different color, respectively. The product of VCE is thus the model which can directly handle both of degrees of freedom

nificant advantage to simulate materials under realistic condition with complexities such as random site disorder, local and low-dimensional orderings, static and anharmonic thermal displacements, and temperature-composition instability.

VCE method incorporates both configurational and vibrational degrees of freedom by merging the ideas of lattice dynamics (LD) and cluster expansion (CE) to accurately construct PES for alloys as depicted in Figure 1.2. It requires no prior knowledge or empirical potential form in potential design. Unlike empirical potential form, because both LD and CE are derived from exact models, accurate vibratinoal properties can be recovered with controlled approximations. Because of the capability to explicitly incorporate both vibrational and configuration degree of freedom, the VCE model will be suitable for the modeling of a host of functional materials whose performance-critical properties are sensitive to disorder and finite-temperature effects, such as battery components, ferroelectrics, piezoelectrics, thermoelectrics, thermal coatings, superconductors, thin-film solar cells, and transparent conductors.

Though with numerous applications, to limit our scope, in this study we try to demonstrate how our VCE method can help us tackle one of the multi-scale modeling applications which requires accurate PES representation that can incorporate configurational disorder: Lattice thermal conductivity of alloys.

1.2 Lattice thermal conductivity of alloys

Thermal conductivity describes the heat transportation process in materials. Thermal conductivity in semiconductors alloys plays important role in modern technology. Tuning thermal conductivity in semiconductor alloys through adjusting compositions allows one to obtain thermal properties that cannot be obtained from pure compounds. Moreover, in the real world, there can hardly find any perfect crystals. In other words, if we want to have trustworthy description of heat transport in solids, we can not ignore the impurities. Likes of microelectronics and thermoelectrics applications all rely on highly accurate thermal conductivity control to achieve high performances and durabilities. In microelectronics, the need of high performance devices and the pursuit of Moore's law, a well known heuristic rule predict density of transistors doubles every two years, causing heat budget a serious issue when size kept shrunk down. In the mean time, semiconductor alloys are ubiquitous in microelectronics nowadays. Thermal conductivity of alloys thus need to be well understood for better reliability in the ever-complex integrated circuits. For thermoelectrics, a device which can directly convert wasted heat into power is an emerging alternative of green energy sources. State-of-art power plants can only convert 60% of energy while the rest 40% caused 15 terawatts of energy lost per year[28]. The dissipated heat also caused the detrimental effect to our environments. These facts make numerous research and development efforts contribute to the discovery of high performance thermoelectrics. The performance of thermoelectrics is commonly characterized by the dimensionless figure of merit $ZT = \frac{S^2\sigma T}{\kappa}$. Where S, σ, T, κ correspond to Seeback coefficient, electrical conductivity, temperature and thermal conductivity, respectively. One of the major approach to improve ZT from existing materials is reducing thermal conductivity while keeping electron transportation minimally affected

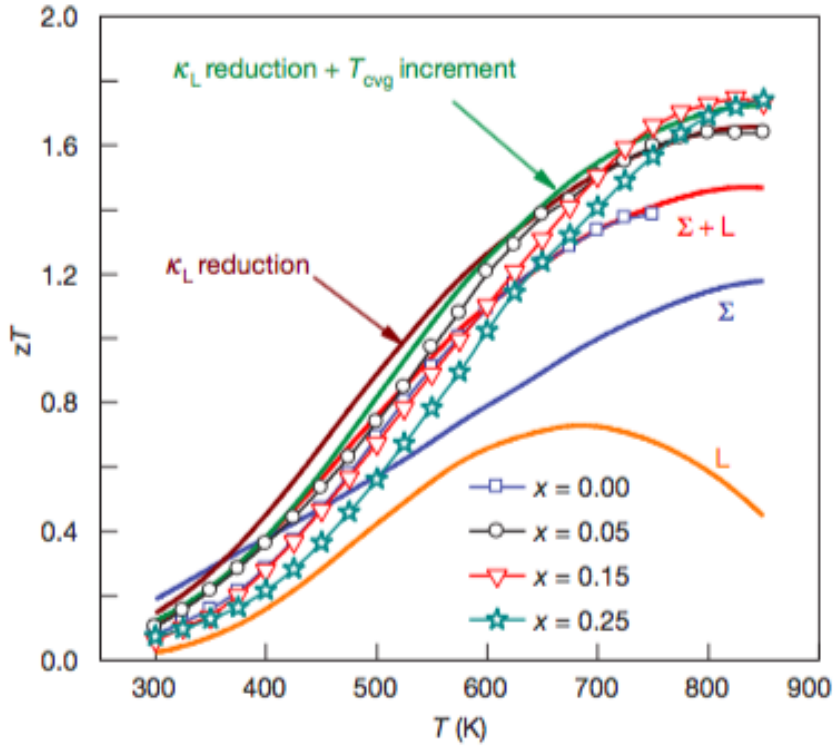

Figure 1.3: Temperature dependence of the thermoelectric figure of merit, zT, for $PbTe_xSe_{1-x}$. A significant improvement of ZT can be seen when Se atom is introduced to PbTe compared with pure PbTe compound. Image Courtesy of Pei et al.[30]

to achieve phonon gas electron crystals(PGEC)[29]. Various approaches has been proposed, yet alloying is still considered as the most promising and practical avenue to achieve high performance thermoelectrics due to its stability across wide temperature range and low cost fabrications. As depicted in Figure 1.3 from the work of Pei et al.[30], through alloying, numerous studies demonstrated more than double of optimum ZT can be achieved. To fully exploit and optimize this tunablity for materials design and development, an accurate calculation of thermal conductivity for alloys at different concentrations is crucial.

For solids there are two main types of thermal conductivity. The first type of thermal conductivity is often referred as electron thermal conductivity(κ_e) and the second type is lattice thermal conductivity(κ_L). The κ_e is mainly contributed from the electron as the carrier to transport the energy while κ_L is mainly caused by the ion vibrations. In non-metallic

systems, the dominant thermal conductivity is κ_L, which originates from ionic vibrations due to its low free electron density.

1.2.1 Limitation of Existing Methods

To describe lattice thermal conductivity, one of the most important atomic feature is ion vibration. To be able to describe ion vibrations, all computational methods have to start from some representations of PES along with corresponding multi-scale modeling approaches. Given the significant importance of lattice thermal conductivity, numerous multi-scale models have been proposed to handle thermal conductivities in semiconductor alloys. Two of the most popular methods are phonon methods and molecular dynamics. These two models originated from two distinctive perspectives. First is from the phonon, a quasi-particle describing the quantized ion vibration. In phonon, all of the vibrations are transformed into the reciprocal space. Another starts from the real space perspective is the well-known molecular dynamics(MD) to directly simulate the ion dynamics over the time.

1.2.2 Phonon Based Methods

The discovery of phonons[31], a quantized vibrations, can be tracked back to 1907 when Einstein first proposed this elegant yet powerful quasi-particle picture to describe lattice vibrations in diamond. The behavior of phonons is commonly characterized in reciprocal space and discussed within the framework of Born von Karmans[32] lattice dynamics models, where periodic boundary condition is applied for its simplicity and great applicability in crystalline structures. For decades, phonons in crystalline structures have been extensively developed into various tractable models to accurately describe thermodynamic properties in solids. By assuming ion is moving in harmonic PES, phonon properties, including density of state, dispersion relation, and group velocity can be analytically calculated.

However, if with harmonic PES only, phonons would not interact with each other and hence there are no finite thermal conductivity in perfect bulk materials. This obviously disagrees with the experimental observations. This result has first been addressed by Peril

in 1929[33], that due to the solution form of phonons in harmonic PES, any perturbation persist forever. To enable thermal conductivity calculations in phonon framework, high order phonon interactions thus need to be included as perturbations by considering anharmonicity part of PES for the calculations of finite phonon life time. With the help of Boltzmann transport equation[34], which is discussed in Section 4.1, thermal conductivity can then be numerically calculated once the phonon properties and phonon life time is derived. One of the great advantage of phonon method is it's seamless incorporation of first-principles calculations. The recent advancement of first-principles calculation based on density functional theory greatly enhance the predictability of thermal conductivity with phonon theory. For harmonic phonon, Pioneer work from Giannozzi et al.[35] successfully apply the density-functional perturbation theory to compute the phonon properties for Si and Ge. The excellent agreement between computed and experimentally measured phonon frequencies corroborate the validity of DFT calculations. For anharmonic part, linear response or finite differences calculations can derive the finite phonon line-width caused by anharmonicity. Broido et al.[36] obtained the anharmonic effects with linear response and solved the phonon Boltzmann equation exactly using an iterative process. These first-principles approaches, which are free from any adjustable parameters, is found to yield an excellent agreement between the calculated and experimentally measured thermal conductivities for Si and Ge. Li et.al. also applied finite difference method to construct more efficient extraction scheme for anharmonicity from DFT forces calculations to compile excellent thermal conductivity agreement between computation and experimental measurement for InAs[37]. Though phonon theory has been successful in most compound systems, one can still find phonon calculations hard to be directly used for alloy systems. There are two major reason to inhibit the thermal conductivity calculation of alloys using phonon theory. First, and the most fundamental reason of it is due to the definition of phonon modes is based on periodicity of primitive cell. However, in alloy system, no periodicity is expected and if one decide to use a large supercell to simulate disorder, one would quickly found vanished thermal conductivity is the only expected result due to the vanished phonon group velocity. This issue is first pointed out by Allen and Feldman[38]. They suggested that when the number of atom

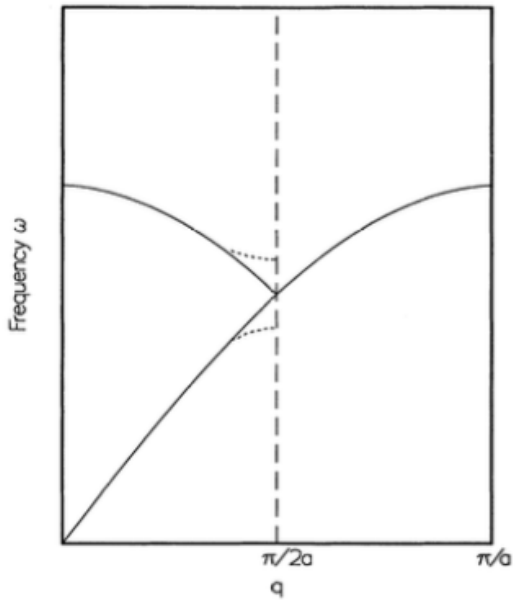

Figure 1.4: A schematic plot of zone folding for one dimensional phonon due to reduced symmetry when enlarge the modeling cell for alloys. The induced flat band, which has zero group velocity, at zone edge reduce the propagation of energy.(Image from [38])

N of concerning primitive cell increases when longer range disorder is explicitly taken into account, then $3N$ phonon bands would repel each other like described in Figure 1.4. In the limit of N approaches infinity the repelled band would cause the flat phonon band and thus vanished group velocity. In Garg's simulation study[39], it also suggests similar trend for Si-Ge alloys. They found κ_L drops with N in a $1/N^{0.24}$ rate. Thus in the limit of an infinitely large supercell, directly using phonon theory in large disorder supercell would yield zero thermal conductivity. These results show phonon is inadequate to explicitly describe disorder system. Virtual crystal approximation(VCA), a work around method, is proposed by giving up the explicitly description of local environment but treat the disorder system as an order system with an virtual PES calculated from weight-averaged PES. The disorder effect is then treated as perturbation from mass disorder on top of anharmonicity from virtual PES. The facile calculation processes in VCA makes it the most popular method when it comes to alloy thermal conductivity calculations. But the fact VCA only consider the average PES makes it inaccurate to handle materials which is strongly affected by local environments

e.g. highly anharmonic materials. One of significant case is from Garg et.al.[40]. They successfully match their computation works of Si-Ge with experiments, however with the same technique, it fails to predict PbTe-Se[41], a highly anharmonic materials. The second issue of phonon comes with the effect of anharmonicity. Since phonon relaxation time is mainly due to the anharmonic phonon interaction, accurate relaxation time theoretically requires arbitrary high order of phonon interaction until converging values. This is widely regarded as impractical approach due to the great complexity to calculate phonon interaction, even only consider up to 4th order. This is well evidenced by most state-of-art BTE solvers only capable of 3rd order phonon calculations[37]. Moreover, from our study, it is not uncommon that these high order phonon interaction would be sensitive to the local environments. Indeed, most promising thermoelectrics come with the strong anharmoncity and thus often time current phonon calculations can hardly accurately predict their thermal conductivities. In short, lack of ability to explicitly treat local environment and high anharmonicity makes phonon hardly be the ideal approach to accurately calculate the lattice thermal conductivity of alloys.

1.2.2.1 Molecular Dynamics with Emperical Potentials

Unlike phonon operated in reciprocal space, one another major approach is directly considering the ion movements in real space. The most popular method for this approach is molecular dynamics(MD). By knowing ion trajectory with respect to time, we can calculate thermal conductivity either through Green-Kubo formalism[42] or Fourier transport equation[42] depending on the choice of ensemble. Due to its real space property, it is straightforward to use large disorder supercell to simulate long-range disorder system. Moreover, the real space property also allows interaction of phonon up to full order without the need to handle complicated formalism, but incorporat implicitly by monitoring ion trajectories. The most important ingredient for MD to faithfully represent thermal conductivity is an accurate description of PES. However, obtaining quality PES from first-principles calculations is a fairly challenging work. To that end, various empirical potential like Tersoff[43] and Stillinger-

Weber[44] are proposed and widely used instead. Unsurprisingly, though commonly used in MD community, they are far from satisfying PES. Poor phonon dispersion and force prediction shows inaccurate representation of PES using empirical potentials. Skye et al.[45] tries to use equilibrium MD to simulate Si-Ge but failed with overestimated thermal conductivity. Broido et al. [46] benchmarked force constants derived from several different empirical potentials, including, Stillinger-Weber, Tersoff and environment dependent potentials comparing to linear response force constants from ab initio calculations. The results show none of these empirical potentials gives satisfying agreement compared to experimentally measured values of thermal conductivity in fi calculations. Though the advancement of machine learning techniques allow better first-principles calculations incorporation for empirical potentials, the fixed potential form inhibits accurate vibrational property of ions, which is very sensitive the shape of PES landscape. It can be evidenced by commonly poor phonon dispersion extraction from this kind of approaches. Its fixed functional form also means its an uncontrolled approximation, in other word, no systematically improvable approach can be applied to these empirical potentials. What makes the matter worse is, these potential forms are highly tailored for specific materials. The lack of transferability of empirical potentials between materials not only renders potential design a challenging task but also undermines the predictive power for unknown materials. To the best of our knowledge, no general method is available to obtain quality empirical potential for all materials exists.

Indeed, the advancement of ab initio MD(AIMD) which directly samples from first-principles calculations alleviate the inaccuracy issue in emperical potentials. Some very recent works[47] show, with proper extrapolation scheme, great match between highly anharmonic compounds can be achieved even at high temperature. Though excellent results has been shown for highly anharmonic materials, the computation cost limits the advanced AIMD scheme can only work for small unit cell materials.

To conclude, disorder makes phonon based methodology hardly an ideal candidate given its incapability to handle explicit environments and undermine its accuracy at high temperature and highly anharmonic materials. MD, on the other hand, is a compelling method

with its ability to directly incorporate phonon scattering to full order with ability to explicit simulate disorder in supercell. The main issue for MD is from poor PES description from empirical potentials which can not accurately simulate ion vibrations and thus caused the unreliable thermal conductivity calculations. Though AIMD can sample along exact PES, the great computational requirements makes it prohibitive for alloys calculations. The question now is: how can we be able to address these issues so we can sample accurate PES without the need of intensive self-consistent calculations for each time stamp in MD? Here, our proposed VCE method is an exact method with controlled approximation which can represent near DFT accuracy but with only a fraction of cost. Moreover, this method explicitly incorporate arbitrary disorder into account thus we can sample over various supercell configuration within the same model rapidly. This makes it an ideal PES generator for alloy systems which has strong anharmonicity.

1.3 Goal and motivations

The core of this work is demonstrating a model building process which can accurately construct the PES landscape for alloy systems. Given the importance of thermal conductivity calculations, we try to address the issues in current approaches to calculate thermal conductivity with our accurate PES model. By combining with first-principles calculations, the accurate thermal conductivity prediction can thus be used to compliment the sparse experimental results, in which only around 1% of 100,000 known inorganic materials has published measurement results. To achieve this, we develop a general formalism can be used as the representation of arbitrary disorder alloys with the proposed VCE method.

The acquired VCE model then can be used in MD calculations to accomplish the lattice thermal conductivity calculations.

In Ch.2, we would give an in-depth backgrounds review to cover the materials which are required for the development of VCE model. This includes two important building blocks, LD and CE, two powerful techniques to model the energy surface with respect to

ion trajectory and atomic configuration, respectively. Kanzaki theory, the preliminary works aiming to solve the configuration disorder in lattice dynamics also are discussed and are given as the theoretical framework of our VCE model. To robustly infer the parameters, we also introduce an emerging mathematical technique called compressive sensing, a signal recovery protocol. As an advanced signal processing technique CS can handle highly under-determined problem by exploiting the sparsity in the system. Lastly, a brief introduction of molecular dynamics is included to make this report as self-explainable as possible.

In Ch.3 we introduce how we construct VCE model mathematically and discuss the significance of its physical meanings. With group theory, we can apply the symmetry to identify the independent parameters to dramatically reduce the necessary dimension of parameters. By using compressive sensing, we can further robustly and accurately construct the VCE model efficiently. Prototypical studies on Si-Ge and PbTe-Se are shown to demonstrate the exceptional ability to construct accurate PES for alloys with arbitrary configurations.

In Ch.4 Thermal conductivity calculations process is discussed in detail. Both phonon calculations and MD calculations are performed for Si-Ge and PbTe-Se to further demonstrate the accuracy of our VCE model. For PbTe-Se, we show the constructed PES from our VCE method can replicate the force fields with near-DFT accuracy. VCE generated PES is then used in MD simulations to accurately predict thermal conductivity with respect to the change of concentrations. An in-depth discussion of why VCA can work well with Si-Ge but not PbTe-Se also demonstrate VCE as a more general and future-proof tool to calculate thermal conductivity. This also demonstrates VCE as an ideal tool to analyze and understand the non-trivial interaction between anharmonicity and configurations. Finally, we propose the future works in Ch.5 to discuss the potential of VCE and the prospective applications beyond thermal conductivity calculations before the conclusion words in Ch. 6.

CHAPTER 2

Backgrounds

Before going through the construction of VCE, it is helpful to first understand existing methods which serve as the theory foundation of our VCE model. To harness the predictive power of first-principle calculations, the first and most important topic need to be discussed is density functional theory(DFT). Arguably the most popular first-principles method for solid-state physics and the main driving force of modern computational materials, a brief theory review of DFT is presented at first.

2.1 Density functional theory

Directly calculating material properties from quantum mechanics has long been considered an intractable approach due to the complexity of solving a many-body Schrödinger equation. In 1964, the seminal work by Hohenberg and Kohn[3] successfully demonstrated that for all non-degenerate ground state properties of materials can be determined by its electron density $n(r)$. This striking results successfully cast the original N electrons problem with 3N degrees of freedom into a single-electron alike problem with only 3 degrees of freedom. This lays down the foundation of density functional theory which serve as the main tool to practically studying the electronic properties of many-electrons systems. The theoretical basis of density functional theory is based on two following theorem:

1. For a system of interacting particles in an external potential V_{ext}, the potential is uniquely defined (up to a constant) by the ground state particle density $n_0(r)$.

2. For any V_{ext}, a universal energy functional $E[n]$ can be defined in terms of the den-

sity. For any specific V_{ext}, the ground state energy can be found by minimizing this functional.

The Hohenberg-Kohn expression of energy functional $E(n(\mathbf{r}))$ of electron density is then expressed as:

$$E[n(r)] = T[n(r)] + \frac{1}{2}\int \frac{n(\mathbf{r})n(\mathbf{r})}{|\mathbf{r}-\mathbf{r}'|}d\mathbf{r}\mathbf{r}' + \int v_{ext}(\mathbf{r})n(\mathbf{r})d\mathbf{r} + E_{xc}[n] \tag{2.1}$$

These terms in appearance order correspond to 1) kinetic energy 2) classic Coulomb interaction, 3) external potential contribution and 4) the self-interaction correction. Though Hohenberg-Kohn successfully reformulated the problem from many-body to electron density, it does not offer practical solution to solve it since no explicit functional form of kinetic Hamiltonian $T[n]$ and self-interaction correction $E_{\mathrm{xc}}[n]$ can be obtained. Famous Kohn-Sham equation[4] address this issue by assuming an interacting system is equal to a non-interacting system with all the complicated exchange and correlation terms lumped into the unknown exchange-correlation functional E_{xc}^{KH}:

$$E[n(r)] = T_0[n(r)] + \frac{1}{2}\int \frac{n(\mathbf{r})n(\mathbf{r})}{|\mathbf{r}-\mathbf{r}'|}d\mathbf{r}\mathbf{r}' + \int V_{ext}^{\mathrm{KH}}(\mathbf{r})n(\mathbf{r})d\mathbf{r} + E_{xc}^{\mathrm{KH}} \tag{2.2}$$

With T_0 represents non-interacting particle kinetic interaction and the local effective potential V_{eff}^{KH}, the only unknown functional form is E_{xc}^{KH}. To handle E_{xc}^{KH}, various approximation has been made. Depending on the expansion process, common exchange correlation functional are local density approximation(LDA)[4] and generalized gradient approximation(GGA)[48]. Since each of them suffer different source of errors, the choice of E_{xc}^{KH} nowadays still needs to be vindicated by one which best match the interested experiment results.

2.2 Lattice Dynamics

One of a key building block of our VCE leverages the power of lattice dynamics(LD), which is commonly used for phonon calculations. The subject of lattice dynamics is the study of atom vibration in crystals. Understand how atom vibrates plays important role to understand various critical physical phenomenon in crystalline solids. For example, by understanding how wave propagate through ion vibration we are able to understand the acoustic sound wave and light-matter interactions. Most importantly, understand vibration is the foundation of almost all of the thermodynamics and mechanical properties in solids. It can thus answer questions ranging from heat capacity, phase transformation to elasticity and thermal expansion. Though plays such an important role, we used to have very small understanding on how to quantitatively describe it until the pioneering work from Einstein[31]. Often time crystalline solids are pictured by countless atom staying statically at lattice sites bonded by neighboring atoms, while the fact is at finite temperature, even the solid is staying quietly, the atoms inside are unceasingly vibrating. After the discovery of atom from Brownian's motion[49], Einstein propose the quantized vibration which is responsible for strong temperature dependent heat capacity in 1902. The theory is further extended and completed by Born and von Karman by starting with the assumption that the crystal is infinite and has a perfect periodicity. Debye, in the meantime also successfully adopted the idea of lattice dynamics to accurate predict the heat capacity in solids at low temperature by introducing more realistic phonon distribution. Born and Huang's work[50] further elaborate how harmonic vibrations relate to the elastic properties. Before a more rigorous discussion, we need to be aware that the main framework of LD is discussed within the Born-Openherimer approximation(BOA). The core motivation of this assumption is the fact that the mass of an atomic nucleus in a molecule is much larger than the mass of an electron (more than 1000 times). Because of this difference, the nuclei move much more slowly than the electrons. Within this approximation, no ion-electron interaction is considered, and hence we can decouple the overall wave function into ion wave function and electron wave function as:

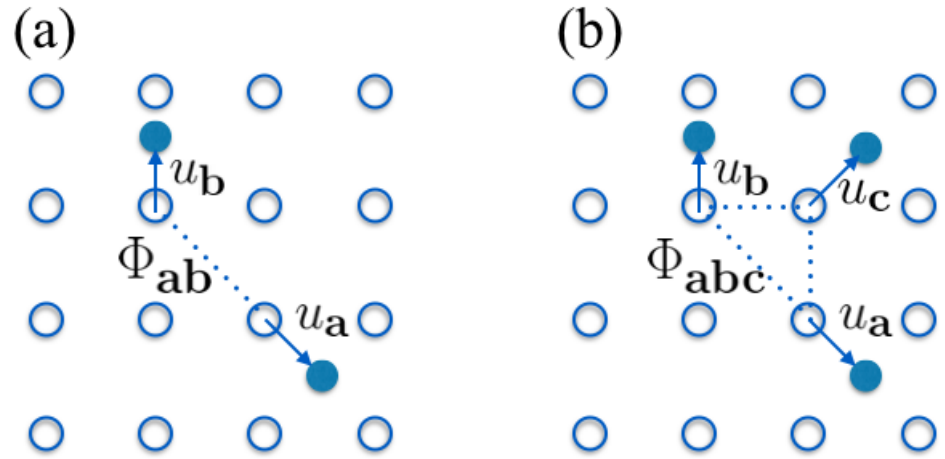

Figure 2.1: Illustration of a) Second and b) third order force constant tensor(FCT). Second order FCT represent the strength of coupling between atom a and b. Along with the displacement deviated away from the reference points $\mathbf{u}_{\mathrm{a}}$ and $\mathbf{u}_{\mathrm{b}}$ determines the energy differences. Same principle applied to third and higher order FCTs

$$\Psi_{tot} = \psi_{electronic} \times \psi_{nuclear} \tag{2.3}$$

Consider the electron system to be in its ground state then electron and ion Hamiltonian are:

$$H_e = -\frac{1}{2}\sum_i \nabla_i^2 - \sum_{i,I} \frac{Z_I}{r_{Ii}} + \sum_{i>j} \frac{1}{r_{ij}} \tag{2.4}$$

$$H_I = -\frac{1}{2M_I}\sum_I \nabla_I^2 + \sum_{i>j} \frac{Z_I Z_J}{R_{ij}} + U_e(R) \tag{2.5}$$

where r, R, U, Z represents the distance between electron pair, distance between ion pair, potential from electron, and charge of ion, respectively. Clearly, we can use equation 2.5 to describe the dynamics of crystal lattice if potential $U_e(R)$ were available. Given the fact

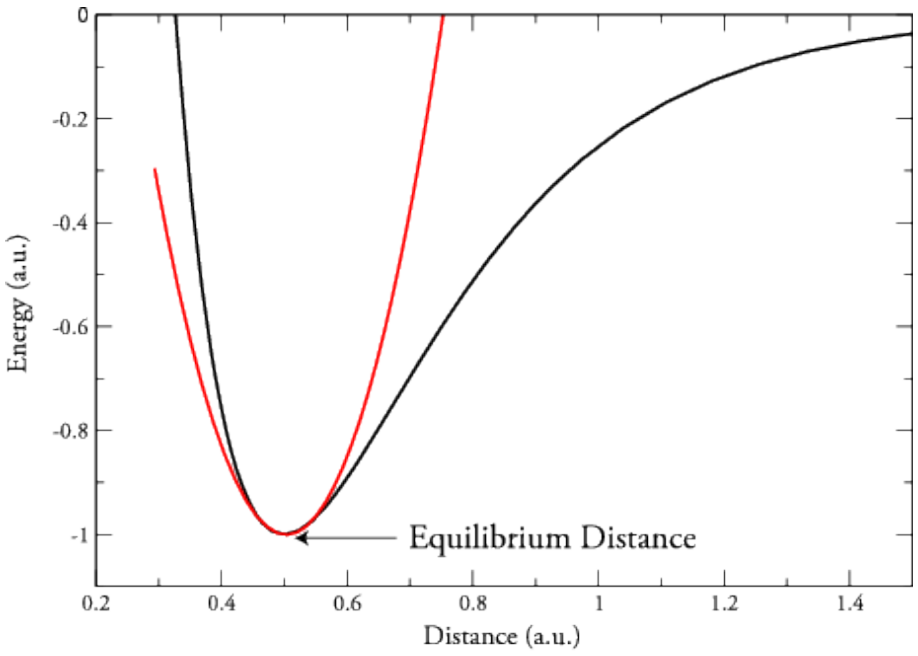

Figure 2.2: A typical potential energy surface(PES) of solids cause by the repulsive short-range force and attractive binding force. The bottom part of PES can often be well approximated by the harmonic potential well(red curve)

that potential $U_e(R)$ is position-dependent and no energy exchange exist between ion and electron due to BOA, we can expand $U_e(R)$ with respect to displacement $\mathbf{u} = R - u_{\text{eq}}$ of ions if only small distortion from equilibrium position u_{eq} is considered.

Instead of applying some empirical potential form like Lenard-Jones to get the full PES, lattice dynamics is a mathematical framework which provides exact description of interatomic potentials. From Born and Huang's approach we can expand $U(\mathbf{u})$ using Taylor expansion. We then have an explicit form of U as a function of $\mathbf{u}$

$$U(\mathbf{u}) = U_0 + \sum_a \Phi_a \mathbf{u_a} + \sum_{ab} \frac{1}{2!} \Phi_{ab} \mathbf{u_a u_b} + \sum_{abc} \frac{1}{3!} \Phi_{abc} \mathbf{u_a u_b u_c} + \cdots \tag{2.6}$$

In the traditional three dimensional Euclidean space, the coefficient $\Phi^{(n)}$, commonly

termed as force constant tensor(FCT) of any order n can form an n-dimensional tensor from the derivative of PES $U(u)$. For example, the 2nd and 3rd order FCT can be determined from:

$$\Phi_{\mathrm{ab}} \equiv \Phi_{ij}(ab) = \partial^2 U / \partial u_{\mathrm{a}} \partial u_{\mathrm{b}} \tag{2.7}$$

$$\Phi_{\mathrm{abc}} \equiv \Phi_{ijk}(abc) = \partial^3 U / \partial u_{\mathrm{a}} \partial u_{\mathrm{b}} \partial u_{\mathrm{c}} \tag{2.8}$$

Where ijk represents the Cartesian coordinate x,y,z. The physical meaning of FCT is straightforward. As depicted in figure 2.1 first order FCT Φ_a represent the static force exerted on atom a. Similarly, second order FCT Φ_{ab} represent force exerted on atom a if atom b is displaced along $\mathbf{u}$. Higher order terms can then be deduced based on the similar pattern.

In conventional LD, the expansion is derived from equilibrium position, and thus the first order coefficient is always equal to zero.

Theoretically, to fully express potential with respect to displacement, one should collect high order terms to meet the required convergence. However, the number of parameters grows exponentially along the order of force constant tensor. Fortunately in solids, where there is an equilibrium lattice positions, the PES would be more or less alike a parabolic potential well as depicted in Figure 2.2. Therefore, it is common to approximate PES according to the harmonic approximation.

2.2.1 Dynamical matrix and phonon dispersion

Though theoretically one can use lattice dynamics to expand to arbitrary anharmonic order just like one can expand any interesting continuous function with Taylor expansion, out of the computational necessity and the practical applications, harmonic approximation are commonly used for phonon calculations. From the experimental data, we do know the anharmonicity plays important role in finite thermal conductivity, thermal expansion, and

countless high temperature effects. However, for most of the solids, while at relatively low temperature, the atom would spend most of their time vibrating within the parabolic like well. This fact makes harmonic approximation works surprisingly well in most of the cases. Most importantly, harmonic approximation offers elegant solution to equation of motion and hence the notion of phonon can be constructed. Indeed, the whole phonon theory is based on the harmonic approximation. Starting from the equation of motion. When the atoms in a crystal vibrate, the Hamiltonian can be written into the sum of kinetic and potential energy. By applying harmonic approximation for the potential energy,

$$\begin{aligned} \mathrm{H} &= K.E. + P.E. \\ &= \sum_a \frac{\mathbf{p}_a^2}{/} 2m + U_0 + \frac{1}{2}\sum_{ab} \Phi_{ab}\mathbf{u}_a\mathbf{u}_b \end{aligned} \tag{2.9}$$

And taking Cartesian coordinate as the general coordinate q_i, the canonical Hamiltonian equation can be written as:

$$\dot{\mathbf{u}_a} = \frac{\partial H}{\partial \mathbf{p}_a} = \frac{\mathbf{p_a}}{m_a} \tag{2.10}$$

$$\dot{\mathbf{p}_\mathbf{a}} = -\frac{\partial H}{\partial \mathbf{u_a}} = -\sum_{ab} \Phi_{ab}\mathbf{u}_b \tag{2.11}$$

By deriving equation 2.10 and equation 2.11, the equation of motion can thus be obtained:

$$m_a\ddot{\mathbf{u}_a} = -\sum_b \Phi_{a,b}\mathbf{u}_b \tag{2.12}$$

To solve this partial differential equation, it is common to transform the basis to Fourier space to convert the question into linear equations. Knowing boundary condition with supercell size $\mathbf{R}$ is $\mathbf{u}(\mathbf{r}) = \mathbf{u}(\mathbf{r} - \mathbf{R})$ and displacement $\mathbf{u}$ can be transformed into reciprocal

space as $\mathbf{u}(\mathbf{r}) = \sum_q \epsilon_{q,m} e^{i(\mathbf{qr})-\omega_m t}$ Now the displacement of atom become a summation over all possible plane waves which is characterized by the wave vector q and frequency mode ω_m. Since these Fourier basis are orthonormal, these plane waves also are known as normal modes. Moreover, this collective motion is quantized by the boundary condition, and these modes are actually the well known phonons. By alternating summation order, and exploiting the orthogonality between phonon modes, we can rewrite the equation of motion as:

$$\omega^2(\mathbf{q})\epsilon_{m,q} = D_{ab}(\mathbf{q})\epsilon_{m,q} \tag{2.13}$$

Where D is the dynamical matrix defined as:

$$D_{ab}(\mathbf{q}) = \frac{1}{\sqrt{m_a m_b}} \sum_{a,b} \Phi e^{i\mathbf{q}(\mathbf{u}_a - \mathbf{u}_b)} \tag{2.14}$$

Once the dynamic matrix $D_{ab}(\mathbf{q})$ is established, phonon frequency and dispersion relation can easily be obtained from equation 2.14. One can also easily obtain phonon density of state $D(\omega)$ by counting the number of phonon modes in each frequency width $DOS\omega = \omega(\mathbf{q} - \mathbf{q}')$:

$$D(\omega) = \frac{1}{2\pi} \int dq \delta(\omega - \omega(q)) \tag{2.15}$$

By comparing phonon properties with experimental results at low temperature can therefore serve as an important metric for the quality of PES representation.

2.2.2 Anharmonicity

Though harmonic approximation generates great results for specific heat, free energy and phonon dispersions across various materials, there are situations where harmonic approximation fails completely. As introduced in the Introduction, without anharmonicity, phonon

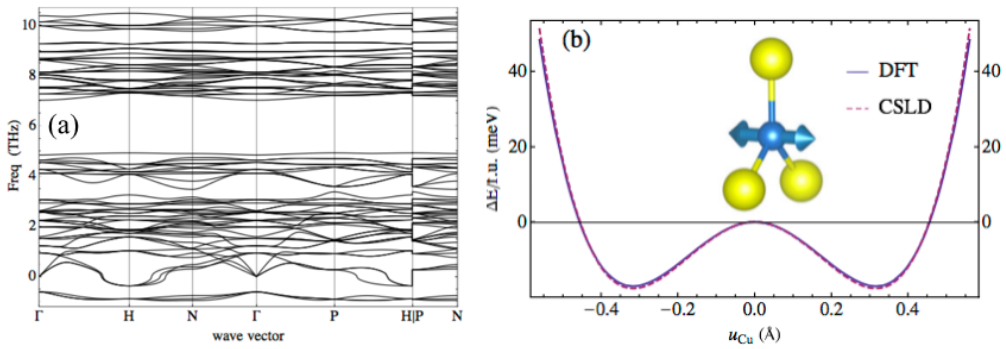

Figure 2.3: (a) Phonon dispersion of tetrahedrite($Cu_12Sb_4S_13$) calculated from finite displacement[52]. The flat imaginary mode, represented by negative part of dispersion, is shown along the high symmetry k path. (b)The potential well with double well is the cause of the imaginary mode. The potential calculated directly by DFT and LD are shown as comparison to demonstrate the accuracy of extracted force constant for phonon dispersion

is not interacting with each other. No thermal resistance is expected in harmonic approximations thus. In addition, due to the symmetry in harmonic potential well, no thermal expansion is expected to deviate away from its fixed equilibrium positions. Even for specific heat, when the temperature start to get higher, the interaction between phonons can not be ignored. In Ti-AlN at T $>$ 1500K[51], free energy is found to be overestimated by harmonic approximation. In body-center cubic(BCC) metals, existence of imaginary mode is another important demonstration showing including harmonic approximation is not sufficient. As depicted in figure 2.3, The double well like potential turns the sign of force constant and generate the imaginary modes, which is phonon with imaginary frequency. In phonon dispersion, imaginary modes are commonly drawn in the area where $\omega < 0$. Due to the ill-defined phonon mode in imaginary phonons, all the phonon related applications can not be applied anymore.

Above mentioned scenario states the importance of accurate anharmonicity is not only important for the sake of theoretical satisfaction, but plays important role to explain and extend the application which can not be solved by harmonic approximations.

With inclusion of anharmonicity, instead of a fixed parametric fitting, LD can be seen as an infinite set of functions derived from Taylor expansions. It empowers LD to model any PES with controlled approximations. However, in LD, the number of parameters need to be inferred in model building process grows with $(N_a)^n$ where N_a and n is the number of atom and order of inter-atomic interactions, respectively. It is prohibitive expensive to build one alloy even for a 512 atom supercell up to 3rd order. What makes it worse is even it is possible to simulate one cell, it is common an ensemble averaging over multiple different configurations need to be considered. This makes LD can hardly be applied to model PES of alloys practically. Therefore, an efficient scheme which can explicitly incorporate alloys configuration is desired.

2.3 Cluster Expansion

Model configuration is a very challenging work. How to find a compact representation to efficiently sample the vast configuration space is the objective of cluster expansion(CE). CE is an invaluable technique building from the expansion of material properties with respect to the atomic configuration distribution. Because of its ability to incorporate configuration distribution, it serves great help for the development of alloys theory including total energy[53], thermodynamics[54] and band gaps[55].

The fact that accurate alloy property has to sample over large configurational space, direct first principle calculations simply is not a practical approach. Have been proposed for alloys system, the motivation of CE is to construct a multi-scale model which explicitly take configuration into account to rapidly visit important configurational space.

The strong benefit of cluster expansion is from its efficient computation process along with high accuracy for configurational problem. By using lattice configurations, which is the occupations of the lattice sites by different atoms, as an approximate indicator for different systems and possible energy states, forward mapping from configuration to energy is made possible. Using this simplified picture, the cluster expansion maps the true alloy Hamilto-

nian onto a very simple Ising-like form. In short, the cluster expansion (CE) is a method for representing a property that depends on discrete and topologically ordered degrees of freedom in a system. In alloys theory, the cluster expansion is essentially a parameterization of the energy in terms of discrete variables that give the occupancy of each lattice point in the crystal. Obviously, energy can not be solely represented by discrete and topologically ordered parameters only, the constraints and the underlying assumption of cluster expansion is based on the coarse graining. In general, energy of solids can be treated as a function of configuration, atomic vibration, electronic states. Through coarse graining, a dimension reduction process, the states which has more rapid variation either in time or space can be averaged out. Here, configuration can be treated as the larger scale property compared to vibration and electronic state and thus a simpler indicator based on configuration can be obtained from the sampling and integration. Unfortunately, the sampling and integration can be practically infeasible. A simplification often adopted in alloy theory is replacing the summation process to finding the minimum energy.

$$E(\{\sigma\}) = \min E(\sigma, v, e) \tag{2.16}$$

.

Where σ, v, e represent configuration, vibration, and electronic degree of freedom, respectively. With minimum energy, the lattice points is no longer a variable but implicitly staying on the relaxed positions which usually are close to the ideal undistorted lattice positions.

Mathematically speaking, CE is an expansion of the interested property in a set of linearly independent basis function that span the whole(or relevant) configuration space. In most forms, the basis set of the cluster expansion is desired to be mathematically complete by design. Thus with the full expansion, a perfect representation can be obtained. The key to construct useful CE is finding this basis set which is physically relevant and computationally efficient. Through proper basis set, one can reduce the dimension with systematically truncation while retain the most information. The goal in developing an effective CE is to identify a expansion set along with the systematical model building process for accurate

mapping between configuration and interested material properties.

2.3.1 Formalism

Cluster expansion is mainly built on the foundation of Ising model[56]. Ising model was first proposed by physicist Ernst Ising to explain ferromagnetism in statistical mechanism. In the simplest 1-D case, Ising model uses discrete state σ_i such that $\sigma_i \in \{+1/-1\}$ to describe either spin-up or spin-down state at lattice site i. The whole Ising model Hamiltonian then can be expanded in the configuration space:

$$H(\sigma) = \sum_i J^i \sigma i + \sum_{i,j} J^{ij} \sigma_i \sigma_j \tag{2.17}$$

Where the energy is assumed to be dependent on self energy and the pair interaction as represented by the first and second term in the left hand side of equation 2.17, respectively. Cluster expansion inherits the same idea of Ising model but generalizing it to configurational space with respect to the atoms occupancy instead of spin. Spin variable $\sigma \in \{+1, -1\}$ is borrowed to represent atom type A or B. In the simplest case, any configuration of a system can simply be represented by an N component $\boldsymbol{\sigma} = \{\sigma_1, ..., \sigma_N\}$. And any configurational function should be able to be represented by this vector as $f(\sigma)$, such as energy $E(\sigma)$. To calculate $f(\sigma)$, we can start with the definition of inner product in configurational space first. The inner product for any two function of configuration $f(\sigma)$ $g(\sigma)$ is defined as:

$$\langle f(\sigma), g(\sigma) \rangle = \rho_0 \sum_\sigma f(\sigma) g(\sigma) \tag{2.18}$$

The sum in equation is over all possible configurations in the space, and it is normalized to unity by ρ_0. Once we have the definition of inner product, it is intuitive to define the basis in configurational space which is complete and orthogonal for future convenience. For each binary site, degree of freedom is 2. Therefore, we can first construct the constant function

$w(\sigma_i) = 1$ and the point function $w(\sigma_i) = \sigma_i$ to represent possible configuration degree of freedom on each site. We can then have an orthogonal point function set by applying Gram-Shimidt procedure. Given we have an orthogonal point function set $\{\theta_0, \theta_1\}$, we can choose them by letting $\theta_0 = w_0 = 1$ and $\theta_1(\sigma_i) = \beta(\sigma_i - 1)$, where β is the normalization factor. After constructing the orthogonal basis for each site, we need to assure there is orthogonality between each point functions belonging to different sites. To achieve this we utilize the fact that the alloy occupation on one site does not depend on other atom on the other site. Mathematically it can be expressed as:

$$\langle \theta_i(\sigma_i), \theta_j(\sigma_{i'}) \rangle = \delta_{i,j}\delta_{i,i'} \tag{2.19}$$

where $\delta_{i,j}$,$\delta_{ii'}$ is the Kronecker's delta. The completeness can also be shown using the same basis:

$$\theta_0^2 + \theta_1(\sigma_i)\theta_1(\sigma_{i'}) = \delta(\sigma_i, \sigma_{i'}) \tag{2.20}$$

The constructed proper orthogonal point function basis can simply be assigned to each site and form the tensor product assuming each site's occupancy does not depends on others:

$$\begin{bmatrix} 1 \\ \theta_1(\sigma_1) \end{bmatrix} \times \begin{bmatrix} 1 \\ \theta_1(\sigma_1) \end{bmatrix} \times ... \times \begin{bmatrix} 1 \\ \theta_1(\sigma_N) \end{bmatrix} = \{\Pi_\alpha(\sigma)\} \tag{2.21}$$

Because each site has an orthogonal and complete basis, the tensor product would spontaneously show the orthogonality and completeness without further worries. The product series can be characterized by cluster α, where α is simply the possible combination of sites $\alpha = (i, i', ..)$. And these correlation functional Π_α can be our basis in the configurational space. The orthogonality and completeness along with the finite dimension property allow

us to expand any configuration function $f(\sigma)$ as:

$$f(\boldsymbol{\sigma}) = f_0 + \sum_{\alpha} f_\alpha \Pi_\alpha(\boldsymbol{\sigma}) \tag{2.22}$$

And for the coefficient of cluster α , we can simply apply inner product to both side:

$$f_\alpha = \langle \Pi_\alpha(\boldsymbol{\sigma}), f(\boldsymbol{\sigma}) \rangle \tag{2.23}$$

Since here our inner product is defined over all possible configurations without any constraints on concentration, this CE also are described as grand canonical CE[57]. In grand canonical CE, we can easily choose the point function $\theta_1(p)$ as σ since $\langle 1, \sigma_p \rangle = 0$ and $\Phi_\alpha(\sigma) = \prod_{p\in\alpha} \sigma_p$. However, in alloys calculations we are interested in energy with different configurations but fixed concentration. In other words, we are interested in the canonical case. The first hurdle need to be addressed in canonical CE is the violated independent relation between site functions θ Once the concentration is fixed, one can easily understand this dependency by imaging 2 lattice site with fixed concentration c. If first one is σ_p, then the other one has to be $2c - \sigma_p$ which violates our assumption that each site is independent. To resolve this issue, we need to take the thermodynamic limit that $N \to \infty$ to effectively remove the dependency. In canonical CE, point function $\theta_1(\sigma)$ now becomes $(\sigma_p - \bar{\sigma})/(1-\bar{\sigma}^2)^{\frac{1}{2}}$. Where $\hat{\sigma} = 2c - 1$ as the average spin in the system. By giving up the normalization factor, one can get the orthogonal cluster function

$$\Pi_\alpha(\sigma) = \prod_{\alpha} \sigma_i - \bar{\sigma} \tag{2.24}$$

which is almost identical to grand canonical cluster functions except it captures the deviation from the mean field. With canonical CE, we can easily express any configuration dependent

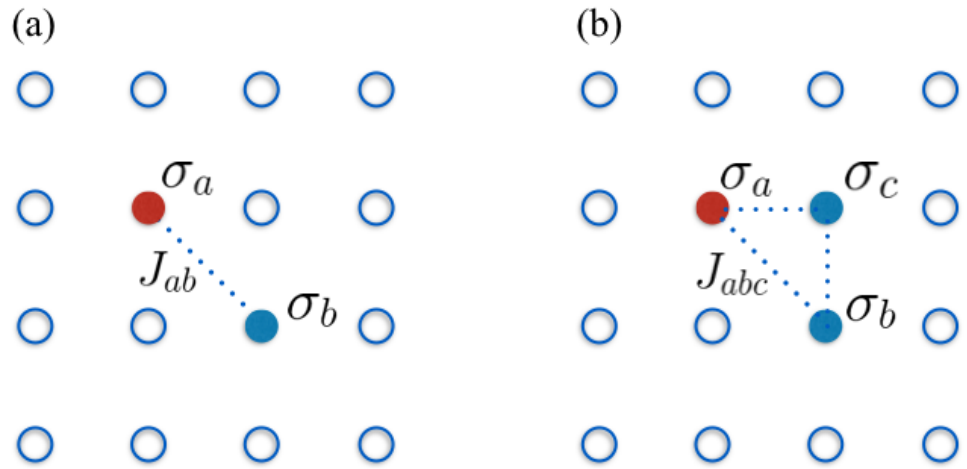

Figure 2.4: Illustration of effective cluster interaction(ECI) J for (a) pair and b) triplet configurational cluster. Pair ECIs represents the strength of coupling between the atomic configuration of atom a and atom b with respect to uniform mean field. Triplet and higher order ECIs can be understood by the similar principle

function with fixed atomic position into:

$$E(\sigma) = J_0 + \sum_{\alpha} J_\alpha \Pi_\alpha(\sigma) \tag{2.25}$$

The coefficient J for each cluster is called effective cluster interaction(ECI) as described in Figure 2.4. Given the configuration sets $(\{\sigma_1\}, \cdots, \{\sigma_L\})$, the above equation can be constructed as the linear matrix multiplication:

$$f = M \cdot J \tag{2.26}$$

where M is the correlation matrix constructed through CE:

$$M = \begin{bmatrix} 1 & \phi(\sigma_1^1) & \cdots & \phi(\sigma_1^1)\phi(\sigma_1^2) & \cdots \\ & & \cdots & \cdots & \\ 1 & \phi(\sigma_L^1) & \cdots & \phi(\sigma_L^1)\phi(\sigma_L^2) & \cdots \end{bmatrix} \tag{2.27}$$

Same as LD, by parameterizing energy into configuration space with known ECI, one can rapidly enumerate energy for different configurations. Physically, CE is trying to illustrate if we change the occupancy of one site i, how the energy would change accordingly. From this perspective, we only need to take those clusters with significant contribution to energy differences into account. And it is straightforward to believe if the pair clusters include the site j that far apart from i, it is expected to have diminished effect since j can hardly feel the change of i in most cases. Though theoretically there are infinite clusters, CE show it is reasonable to truncate most of them and only focus on few nearest neighbor and thus greatly alleviate the computational complexity. This great feature makes CE a very popular method to search for ground state configuration and thermodynamic stability of alloys over other configuration expansion scheme.

The success of the cluster expansion formalism has been proven in studies of metals, semiconductors, and ceramics. And its ability to reproduce experimental thermodynamic data has been confirmed repeatedly in binary systems[58], and multi-component systems[59]. However, One major issue of CE is it can hardly handle the vibration property, which is essential for heat transport and thermodynamics , since it is expanded on either fixed or ensemble averaged atomic positions. It makes CE a convenient method only for fixed temperature simulations. The work around method is to directly incorporate T as the variable by rewriting energy $E(\sigma)$ into temperature dependent physical property like free energy $F(\sigma, T)$ or lattice thermal conductivity $\kappa_L(\sigma, T)$. However, the problem of calculating $F(\sigma, T)$ over large set of σ is a much more computational demanding task than $E(\sigma)$ due to the integration process to incorporate temperature effect. Same issue occurs to $\kappa_L(\sigma, T)$ that each data points typically requires long MD simulations [60]. Lack of efficient way to incorporate vibrational property is the fundamental problem of CE to be successful for temperature dependent physical properties.

But as the reader has figured, the similarity of clusters between LD and CE and the complimentary features between LD makes them perfect match for the construction of con-

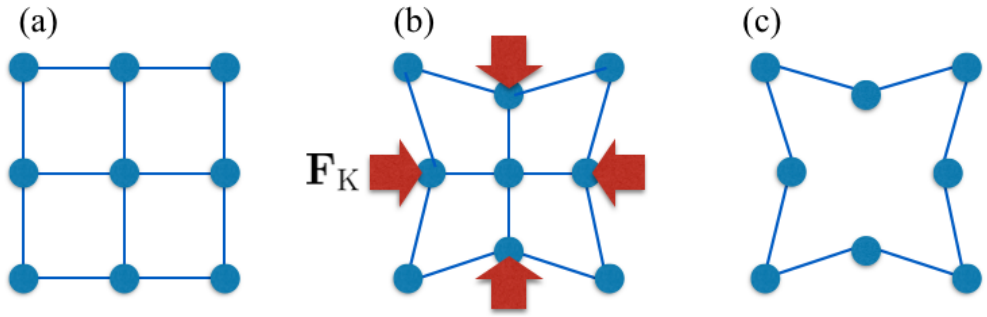

Figure 2.5: Schematic illustration of Kanzaki force calculation. (a) Represent the ideal crystal without vacancy, (b) is the ideal crystal with external Kanzaki force F_{k} to force atom at the same position as (c) fully relaxed position due to the presence of vacancy.

figuration sensitive PES for alloys. What if we can parameterize not only on vibration or configuration, but both of them simultaneously? But what would the physics scheme be like in this case? The pioneer work from Kanzaki tries to address this issue by answering how configuration would affect the elastic properties of solids. He successfully incorporate both of the configuration and vibration effect by formulating the Kanzaki force.

Later on, we will show by combining both of them, Kanzaki demonstrates a preliminary yet pioneering work to study how strain are explicitly affected by atomic configurations.

2.3.2 Kanzaki Force

Before getting into VCE, some works focusing on parameterizing configurational dependent PES would be introduced. One of the pioneering approach is done by Kanzaki in 1957[61]. Kanzaki force is a classical combination of CE and LD designed to solve the substitutional point defect problem in perfect lattice. The insight of Kanzaki force is it explicitly stated the problem of a defect in crystal at equilibrium position is equivalent to a perfect lattice site without defect with an external force F_{k} as described in figure 2.5. The Hamiltonian of this problem is:

$$H_{\{\sigma\},\{u\}} = H_{chem}(\{\sigma\}) + H_{rel}(\{\sigma\},\{u\}) \tag{2.28}$$

The chemical part H_{chem} is the energy from all atoms fixed at ideal positions of the parent lattice, and another Hamiltonian H_{rel} is from the relaxation strain, showing the energy required to drift lattice away form their ideal positions to reach equilibrium positions.

The chemical part can be easily handled by CE as mentioned earlier. However, for most of the applications, we are not really interested in the chemical part here but the relaxation energy which is controlled by both local configuration $\{\sigma\}$ and displacement $\{\mathbf{u}\}$.

In Kanzaki's model, we can see how configuration interact with relaxation explicitly in H_{rel}. Under the harmonics approximation we can separate H_{rel} into two parts. One is from Kanzaki force, which is caused by configuration and one is from the configuration-independent pair interaction by assuming configuration has minimal effect on strain, and thus is the same as LD:

$$H_{rel}(\{\sigma\},\{u\}) = -\sum_{a} F(\sigma)_a^K \mathbf{u_a} + \sum_{ab} \frac{1}{2}\Phi_{ab}\mathbf{u_a}\mathbf{u_b} \tag{2.29}$$

For each configuration $\{\sigma\}$, if the energy difference between ideal and normal structures H_{rel} and distortion displacement $\{u\}$ are given, one can quickly linearly solve the corresponding Kanzaki force F^K by solving the linear equation 2.29. Equivalently, if F^K is given, then one can easily know the relaxation displacement for any configuration by letting $H_{rel} = 0$.

It is easy to notice the force here originates from the configuration disorder, in other words, a function of configuation. To be more specific, this is the force occur when you change the site from original atom to a vacancy. Shchyglo et al. successfully show one can brings in the cluster expansion into Kanzaki force[62]. Realizing at equilibrium position, the chemical part can be expressed using CE:

$$H_{\text{chem}}(\{\sigma\}) = \sum_{\alpha} J_\alpha \sigma_\alpha \tag{2.30}$$

and the Kanzaki part can then be explicitly expressed as:

$$F_a^K = \sum_{b \neq a} K_\alpha \sigma^\alpha \tag{2.31}$$

The main advantage of adopting this framework is the explicit incorporation of configurations into LD. The only change from LD is that the expansion is no longer done from the equilibrium position but from the "ideal position", and the residue force can be expanded in the configurational space.

Some exciting results[63] have shown Kanzaki force can be a powerful tool to make accurate force/relaxation energy prediction in alloy system simply by correcting the first order configurational effect with controlled cutoff. In general, more accurate results could be expected if higher order effects can also be corrected by configurational effect. However, to the best of our knowledge, although the idea of higher order expansion of configurational force constants was proposed, only first order force with high order cluster expansion parameterization jobs[63] have been done. Given the fact that the high order FCT which is important for thermal conductivity, the short cutoff order of FCT greatly limits the power of the Kanzaki force to fully capture the interplay between configuration and vibration. So how can we construct a generalize Kanzaki force scheme to arbitrary order of FCT as well as the ability to accurately infer the model is the focal point of Chapter 3.

2.4 Compressive Sensing

The signal $f(t)$ can be linearly recorded by sensing waveform $\phi_k(t)$:

$$y_k = \langle f, \psi_k \rangle \,, \;\; k = 1, ..., m \tag{2.32}$$

The above equation is simply showing we can correlate the interested function with sensing basis ψ. Physically speaking, this sensing basis ψ is the tool to make $f(t)$ observable to

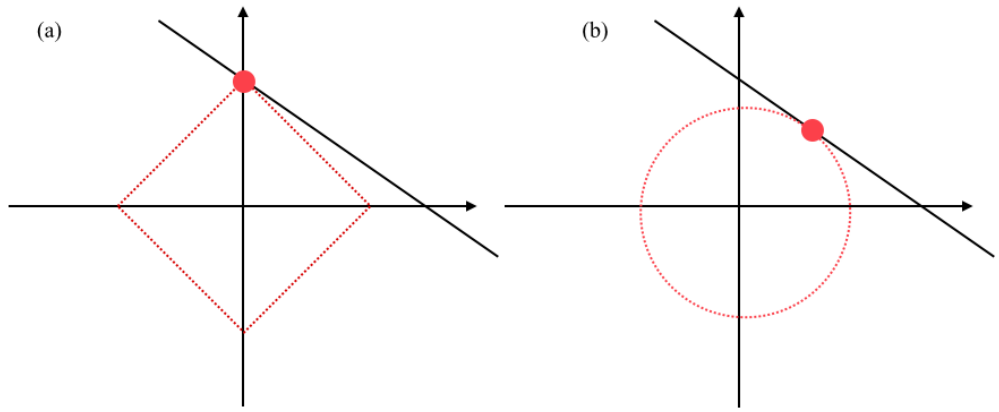

Figure 2.6: Schematic illustration of regularization effect for optimal solution. As can be seen in (a), the L1 regularized optimal solution(red spot) has more sparse solution than (b) using L2

us. In other words, it is the equipment for us to measure. Meanwhile, one can also find an intrinsic representation basis ϕ of $f(t) \in \mathbb{R}^n$ which can be used to model the signals:

$$f(t) = \sum_{i=1}^{n} x_i \phi_i(t). \tag{2.33}$$

From a set of measurements $\{y_i\}$, how can we find the coefficient x_i for representative basis is the core of signal recovery. For a long time, common wisdom in signal recovery believes to exactly recover the signals from measurements, the sampling frequency should be at least higher than twice the signal bandwidth. This frequency is the well known Nyquist sampling rate. The very fundamental idea of Nyquist sampling rate is inspired from the fact that a unique linear equation can not be solved in undetermined setup. To accurately recover signal from Nyquist sampling requires the good prior of what is the highest frequency. In general, this is not necessary known in advanced, and another issue is the number of measurements m is usually much smaller than the dimension of representation basis espeicially for those expensive measurements. The question CS is trying to answer is whether it is possible to

accurately reconstruct signal even when measurement m « N?? The answer is yes if your signal in your representative space is sparse. Instead of directly finding the unique solutions from high-dimensional space, compressive sensing is finding the minimal number of non-zero components which can reproduce the original signal. When the basis set is orthogonal and the signal is sparse, which is only few non-zero components, a unique solution can be obtained with far fewer samples than required by Nyquist sampling rate. The process of finding the least number of non-zero components to reconstruct the original signal can be formulated as an l_0 optimization problem:

$$\begin{aligned} &\min \|\mathbf{X}\|_0 \\ &s.t. \mathbb{A}\mathbf{X} = \mathbf{y} \end{aligned} \tag{2.34}$$

Where $\mathbb{A}$ is the correlation matrix. However, this is known to be a NP-hard problem, which means one can only thoroughly try out all the combinatorial combinations. To efficiently solve this problem, Candes and Tao proves if the sensing matrix $\mathbb{A}$ follows restricted isometry property(RIP)[64], which implies that the sparse signal cannot be in the null space of $\mathbb{A}$, one can replicate l_0 results by using l_1 norm:

$$\begin{aligned} &\min \|\mathbf{X}\|_1 \\ &s.t. \mathbb{A}\mathbf{X} = \mathbf{y} \end{aligned} \tag{2.35}$$

. The convexity property of l_1 norm grants great advantages over l_0 norm in terms of computational complexity, while still preserves sparsity. Figure 2.6 shows an intuitive geometrical argument on why l_1 norm can produce sparse solutions. Unlike l_2 norm, l_1 norm have strong tendency to select sparse solutions. The real power of compressive sensing comes from the high probability that one can use $M \approx \sqrt{2 \log N}$ measurements[64], where N is the number of total representation components, to accurately recover the sparse signal. The key to achieve this significant reduction of required data sampling is selecting an N random structures for

minimal correlations. In practice, these are commonly done by orthonormalizing n vectors sampled from uniform random ball.

In real world applications, very few signal is uncorrupted and thus hardly any real sparse signal existed. One another strong advantages comes along the l_1 solutions is its ability to deal with noise. By setting up the equation with noise bound:

$$\begin{aligned} &\min \|\mathbf{X}\|_1 \\ &s.t. \|\mathbb{A}\mathbf{X} - y\| < \epsilon \end{aligned} \tag{2.36}$$

Indeed, one might found the whole equation setup pretty much the same as the famous least absolute shrinkage and selection operator(LASSO) regression which use l_1 as the regularization terms to produce sparse features. However, the key differences between CS and LASSO is the fact LASSO is no more than an embedded feature selection process for any given regression problem but CS is a full suite signal sampling protocol starting from the sampling to recovery process. By applying CS, a highly efficient and accurate model building process can then be achieved for sparse systems.

Ever since the practical proposal made by Candes and Tao et.al.[65], CS has been successfully applied to wide spectrum of problems ranging from signal processing[66], machine learning[67] to physical modeling[68]. CS, as a new paradigm for data sampling/sensing techniques to deliver highly accurate signal reconstruction with much fewer required sampling points than conventional data acquisition processes.

2.5 Molecular Dynamics

Molecular dynamics(MD) is a simulation technique trying to capture the atomic movement with respect to time. As a sampling scheme trying to resemble the real dynamics of atoms, MD is a deterministic process based on classical Newton's equation of motion. Unlike most sampling scheme utilize the stochastic process, the unique dynamic property preserved in

MD makes it an ideal tool to asses time dependent physical quantities like transport coefficients[69], time-dependent responses to perturbations[70], rheological properties[71] and thermodynamic properties[72]. To explain atomic dynamics, a good analogy is our video camera. What camera do is taking snapshot every few micro-seconds consecutively. By putting them into order, a smooth motion can thus be shown to audiences. Same principle applies to MD. By recording the atomic position at each time-stamp, a full dynamic process can be estimated. Similar to the video, the shorter the time interval are taken, the more realistic these snapshots resembles the real dynamic properties. Though the choice of interval depends on the interested properties and atomic vibration frequency, it is common to choose time interval around femtosecond(10^{-15} second). To generate snapshots, the MD simulation is composed by 4 main iterative steps:

1. Initialize: initialize the atomic position and velocity
2. Evaluate: calculate the forces on all of the atoms
3. Integrate: integrate the equations of motion to advance the time step and determine new atomic positions
4. Sample: sample the system to calculate properties

Similar to other stochastic sampling scheme, initializing MD involves setting up the corresponding atomic positions and velocity. A proper initialization can make the MD simulation converges much faster. One common approach is to select the initial configuration that all atom stays at their ideal or equilibrium positions, while randomly assign velocity according to the targeting temperature. For high temperature condition where the classical dynamics is dominant, one can sample velocity from the Maxwell-Boltzmann distribution with temperature T:

$$f(v) = \sqrt{(\frac{m}{2\pi k_b T})^3} 4\pi v^2 \exp^{-\frac{mv^2}{2k_b T}} \tag{2.37}$$

.

After the initial step, the subsequent step is to evaluate the corresponding force and potential energy at that particular configuration from the PES. This step is the most computational intensive step in MD, and thus lots of optimization and parallelization has been developed for this step. The major differences between MD and other stochastic sampling scheme is the integration step. Once initial position, velocity and force are computed, Newtonian equation of motion is applied to infer the position and velocity for next time step with designed integration scheme. One common integration scheme is Verlet algorithm[73]. Verlet algorithm is constructed from Taylor expansion of particle's position at time t-δt and time t+δt:

$$\mathbf{r}(t+\delta t) = \mathbf{r}(t) + \mathbf{v}(t)\delta t + \frac{1}{2}\mathbf{a}(t)\delta t^2 + O(\delta t^3) \tag{2.38}$$

$$\mathbf{r}(t-\delta t) = \mathbf{r}(t) - \mathbf{v}(t)\delta t + \frac{1}{2}\mathbf{a}(t)\delta t^2 + O(\delta t^3) \tag{2.39}$$

The new position of $t+\delta t$ can thus be calculated

$$\mathbf{r}(t+\delta t) = 2\mathbf{r}(t) - \mathbf{r}(t-\delta t) + \mathbf{a}(t) \tag{2.40}$$

Where $\mathbf{a}(t) = \frac{1}{m}\mathbf{F}(t)$

One major issue of Verlet algorithm[74] is there is no explicit velocity term in Verlet algorithm. Indeed, velocity can be inferred from :

$$\mathbf{v}(t) = \frac{\mathbf{r}(t+\delta t) - \mathbf{r}(t+\delta t)}{2\delta t} \tag{2.41}$$

But as one can quickly tell, this can only be calculated when new position of $r(t+\delta t)$ is calculated. Often time, we are interested in simulation which can give us velocity associated with the position at the same timestep, e.g. flux. To address this issue, a modified Verlet

velocity algorithm is adopted. By taking velocity into account explicitly, position and velocity are integrated at the same timestep using:

$$\mathbf{r}(t+\delta t) = \mathbf{r}(t) + \mathbf{v}(t)\delta t + \frac{1}{2}\mathbf{a}(t)\delta t^2 \tag{2.42}$$

$$\mathbf{v}(t+\delta t) = \mathbf{v})(t) + \frac{1}{2}[\mathbf{a}(t+\delta t) + \mathbf{a}(t)]\delta t \tag{2.43}$$

The explicit algorithm is implemented following:

1. $r(t)$ and $v(t)$ are used to compute $\mathbf{a}(t)$, at time t.
2. Calculate $r(t+\delta t)$ using equation 2.43.
3. Calculate $V(t+\frac{\delta t}{2})$ using equation 2.44
4. Calculate new forces using $r(t+\delta t)$ to get $a(t+\delta t)$.
5. Calculate final velocities $v(t+\delta t)$ using equation 2.43.

With Verlet velocity algorithm, velocity can be obtained directly from the integration while retaining the same level of accuracy as Verlet algorithm. Finaly, before fully advance to the next timestep, all interested physical observation like energy or temperature would be recorded for that sampled phase space points. The whole simulation, once initialized, is kept iterated from step 2 through step 4 until the desired convergence is reached.

CHAPTER 3

Model Building of VCE

3.1 Formalism of VCE

Thanks to Kanzaki's theory which layout an intuitive and useful scheme, a clear physical pictures can be further exapnded based on it. Unlike CE sample energy at relaxed or ensemble averaged position, Kanzaki shows we could turn an LD problem into configuration dependent function by using ideal, high symmetry structure. The configurational effect then can be shown in force terms as Kanzaki force. But obviously, the configurational effect does not occur on force term only, the change of occupation is expected to change across all orders of FCTs in LD. VCE model inherited the spirit from the Kanzaki force and further generalizes the higher order force constant to be configuration dependent. The full Hamiltonian of VCE can be formulated as:

$$\begin{aligned} H_{tot} &= H_{LD} + H_{CE} + H_{coup} = U_0 + \Phi_i u_i + J_{\text{ß}}\sigma_i \\ &+ \frac{1}{2!}\Phi_{ij}u_i u_j + K_i^j u_i\sigma_j + J_{ij}\sigma_i\sigma j \\ &+ \frac{1}{3!}\Phi_{ijk}u_i u_j u_k + \frac{1}{2!}K_{ij}^k u_i u_j\sigma_k + K_i^{jk}u_i\sigma_j\sigma_k + J_{ijk}\sigma_i\sigma_j\sigma_k + \cdots \end{aligned} \tag{3.1}$$

Where the coupling terms takes both vibrational and configurational degree of freedom as:

$$H_{coup} = K_i^j u_i\sigma_j + \frac{1}{2!}K_{ij}^k u_i u_j\sigma_k + K_i^{jk}u_i\sigma_j\sigma_k + ... \tag{3.2}$$

Before further derivation and discussion, we start from the definition of clusters notation

used in our VCE.

To concrete the idea of clusters, let us start from the natural way to define our cluster $\alpha = (\alpha_1, \alpha_2, \cdots, \alpha_N)$ as an N-tuple flatten cluster, where N is the number of total lattice sites. Each α_i here represents the ith lattice on the parent lattice site. For example, a cluster α=(0,1,1,0,0,...0), represents a cluster composed of a pair-cluster with one vertex at lattice site 2, and another on lattice site 3. Since the index can be predefined without loss of generality, one can define their indexing once they decide the way to arrange their parent lattice site. With site-index predefined, we can also represent this in terms of their site-index as $\{i, i', \cdots\}$. Taking the previous example, we can have one cluster $\alpha \equiv (0, 1, 1, 0.., 0) = \{2, 3\}$. After have clear definition of cluster, one significant distinct between configurational cluster in CE and vibrational cluster in LD is the fact that there is no duplicated site for configurational cluster. This is understandable since unlike LD's self-clusters which originate from the polynomial Taylor expansion, CE's basis is composed by the inter-product of site basis $(\theta_0, \theta_1(\sigma))^{\mathrm{T}}$. Based on whether there are duplicated sites, we can define proper cluster and improper cluster. A proper cluster does not contain any duplicated lattice site, which is $a_i \leq 1$, otherwise it is an improper cluster. For example $\alpha = (1, 1, 0, ..) = \{1, 2\}$ is a proper cluster while $\alpha = (3, 0, \cdots) = \{1, 1, 1\}$ is an improper cluster. From now on, we use A to represent a configurational cluster(proper clusters only) and α to represent a vibrational cluster(improper clusters included) for CE and LD, respectively. To make the notation compact through our discussion, following multi-index notation is defined:

$$|\alpha| = \sum_i \alpha_i \tag{3.3}$$

$$\alpha! = \prod_i \alpha_i! \tag{3.4}$$

$$u^\alpha = \prod_i u_i^{\alpha_i} \tag{3.5}$$

$$\partial^\alpha = \prod_i \partial^{\alpha_i} / \partial u_i^{\alpha_i} \tag{3.6}$$

These notations can help us better track the numerous pre-factors in expansion as well. Take previous proper cluster α=(1,1,0,....0) as an example, the number of atoms is 2 can easily be obtained from $|\alpha|$ and the factorial $\alpha!$ is $(1! \times 1! \times 0! \times 0!)$=1. For improper cluster α=(3,0), its factorial is just $(3! \times 0! \times 0!)$=6. One can thus use these compact notations to rewrite LD and CE as

LD:

$$\begin{aligned} E_{LD} &= \sum_{\alpha} \frac{1}{\alpha!} \sum_{I} \Phi_I(\alpha) u_I^{\alpha} \\ &\equiv \frac{1}{\alpha!} \Phi_I(\alpha) u_I^{\alpha} \end{aligned} \tag{3.7}$$

CE:

$$\begin{aligned} E_{CE} &= \sum_{A} J(A) \sigma^A \\ &\equiv J(A) \sigma^A \end{aligned} \tag{3.8}$$

To derive the expression of VCE in equation 3.1 explicitly, we start from the LD model. The key insight of VCE is realizing FCT actually is a configurational dependent funtional with given reference point lattice $\mathbf{u} \in \mathbf{R}_a^N$. With above lattice constraint, the FCT $\Phi_I(\alpha)$here is no longer constant but configuration dependent $\Phi_I(\alpha, \sigma)$. With the same spirit as Kanzaki force, we can thus apply CE in FCT $\Phi_I(\alpha, \{\sigma\})$:

$$\Phi_I(\alpha, \{\sigma\}) = \sum_{A} K_I(\alpha, A) \sigma^A \tag{3.9}$$

Finally, we have the compact expression for VCE by inserting equation 3.7 into equation 3.9:

$$\begin{aligned} E &= E_{LD} \otimes E_{CE} \\ &= \frac{1}{\alpha!} K_I(\alpha, A) u_I^{\alpha} \sigma^A \end{aligned} \tag{3.10}$$

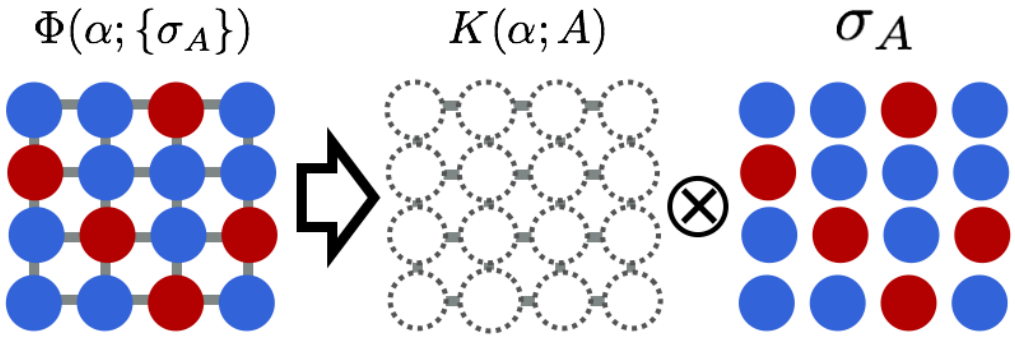

Figure 3.1: Schematic illustration of symmetry constraints in VCE. The original configuration dependent FCTs Φ(left) with low symmetry can be derived from the configuration independent CFCs K, which thus preserves symmetry of parent lattice, and known configurations(right).

equation 3.10 is identical to euqation 3.1. And mathematically we can soon realize it is actually nothing more than a tensor product between CE and LD. Here we define K as configurational force constant (CFC) and $\alpha(\alpha, A)$ as compound cluster(CC). Similar as Kanzaki force, One can interpret $K_I(\alpha, A)$ as the difference of strain on cluster α along I direction when configuration of cluster A changes. This makes it falls back to many-body Kanzaki expression if cluster α is singlet. Few strong advantages are worth mentioning for VCE here, First and arguably the greatest advantage of VCE is, since configurational and vibrational variables can be explicitly treated, rapid sampling of configurational dependent PES can be achieved once $\{K\}$ is found. This makes accurate PES modeling for arbitrary disorder alloys possible. Secondly, since both LD and CE are derived from exact method, VCE is also an exact method. This makes arbitrary accuracy can be done in VCE with controlled approximation. Unlike empirical potentials highly tailor to specific materials, VCE lays out a systematic improvable path which is adaptive to different targeting materials. Finally, with given reference lattice, CFCs are configurational independent. This merit serves great computational simplification to model large alloy supercell. In contrast, in LD FCTs have virtually no symmetry for alloys due to the random atomic configurations. It makes model building for alloy supercell computationally prohibitive. However in VCE, CFCs share the

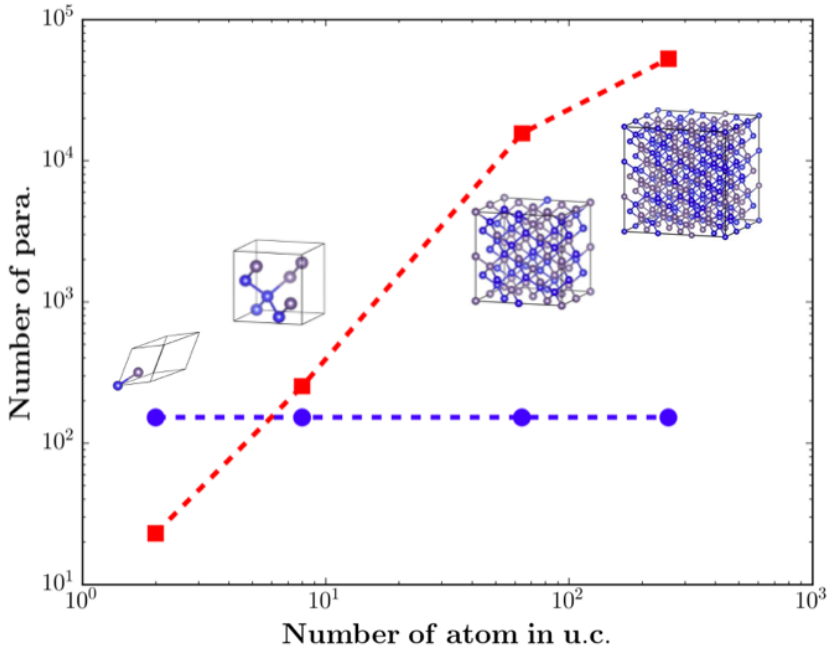

Figure 3.2: Comparison of required parameters in the model between VCE and LD with respect to different size of alloy modeling cell for Si-Ge. The number of parameters from VCE with converged CE cut-off represented by blue circle dots remain constant regardless the size of modeling cell. The red square dots is the required parameters for LD which scale with the size of modeling cell. Both VCE and LD use the same cut-off for vibrational clusters. Inset is the modeling cell.

same symmetry property as the underlying lattice structure. In general, the higher symmetry the underlying lattice preserves, the fewer actual independent CFC required in model building process. More details will be discussed in following sections. The reason of this great advantage of preserved symmetry is schematically shown in Figure 3.1. Because of translational symmetry which can not be used in LD but VCE, we can use primitive cell to efficiently model the alloy supercell with well converged configuration cluster cut-off. Simply by applying translational symmetry, number of parameters remain constant in VCE while grow in the fashion of N in LD as shown in Figure 3.2, where N is the number of modeled alloy cell.

This great simplification practically makes VCE the only option to model accurate PES for large alloy supercell. In the following section, we will discuss how we take advantage of symmetry properties to reduce our number of independent CFCs.

However the multiplicity of CE and LD inevitably causes the combinatorial increase of CFC terms. Since The selection of cut-off is not a prior here, yet unlike LD or CE, which has various well-studied examples, a proper choice of cut-off is not straightforward in VCE. In the best case, we should try to include as large cut-off as possible. It inevitably cause the large number of parameters in VCE. Though it is way fewer than direct LD modeling, to robustly and accurately infer these parameters is still a challenging task. To address this issue we need to leverage our understanding of VCE system. We can easily observe that for most of the systems only those short range clusters have significant contributions to VCE system. Given either FCTs or ECI decrease rapidly for clusters with sites which are far apart from each other, we should also expect CFC also decrease rapidly for long distance clusters. Intuitively, we can expect $\lim_{d(\alpha,A)\to\infty} K_I(\alpha, A) = 0$. With this property in mind, it is safe to assume our system is a sparse system, which is the system in which only a very few basis have non-zero values. Later on, we would discuss how this sparsity can help us reduce the required fitting input thanks to compressive sensing. In contrast to tedious integer programming, compressive sensing allows parameter selection and fitting be done in one shot. With compresseive sensing, a robust, efficient and accurate VCE model building can be easily achieved.

3.2 Linear Force relation

Theoretically one can fit CFC from energies of each different configurational and vibrational structures. However, considering the cost from first-principles calculations, fitting force is a more efficient option. Thanks to the LD property in VCE, the explicitly captured vibrational degree of freedom enables us to construct a force-to-CFC relation directly through the well-know force-displacement relationship:

$$\mathbf{F}_a = \partial_a E = \frac{1}{\alpha!} K_I(\alpha, A)\sigma^A \partial_a u_I^\alpha \tag{3.11}$$

On the left-hand side, we can generalize F_a as a vector consisting sampled forces for each individual atom along certain directions. Also, thanks to the advantage of using one-dimensional array representation of CFC, we can concatenate all CFC tensors from representative clusters to form a vector as well. We then can construct a "sensing" matrix $\mathbb{A}$ based on the configuration and displacement from the sampled system. To be more explicit, from above equation, we can calculate each entry in $\mathbb{A}$ by:

$$\mathbb{A} = \begin{bmatrix} -1 & -\sigma_b^1 & -u_{\mathbf{b}}^1 & -u_{\mathbf{b}}^1\sigma_b^1 & \dots \\ & \dots & \dots & & \\ -1 & -\sigma_b^L & -u_{\mathbf{b}}^L & -u_{\mathbf{b}}^L\sigma_b^L & \dots \end{bmatrix} \tag{3.12}$$

for an N-atom modeling cell with L different training configurations. These linear relations, though easy to construct, has great redundancy in the model due to the lack of physical set constraints on our CFCs. Moreover, without applying these constraints, numerical non-exact calculations would cause the artificial discrepancy between CFCs which are meant to be identical, e.g. the translational identical CFCs. It can cause artifact effect like the violation of acoustic sum rule(ASR), which makes acoustic phonon has artificial imaginary frequency at Γ point. Therefore, it is both computational and physically important to apply physical constraints to find the independent CFCs.

3.3 Independent Configurational Force Constant

We can reduce the number of CFCs in fitting by finding out symmetry-invariant CFC. In our current study, by applying physical constraints, three kind of invariances are used. They are

1. commutativity

2. space group symmetry

3. translational symmetry

For high symmetry crystals, these constraint can greatly reduce the number of CFCs by finding the independent CFCs.

3.3.1 Commutativity

Commutativity comes from the fact that for a smooth enough energy surface, the derivatives do not depend on the order of partial differentiation. In solids, since we are still within the framework of LD, where ions only moderately move away from their ideal position, It is safe to apply this commutativity. In our VCE context, since we already pre-defined the order of our lattice site in cluster, we should not worry about commutativity in our proper cluster. To examine this, we can make up a permutation operator π. π can take in any index series and output the index series after the permutation. We can clearly see our $K_{x,y}^{\{1,2\}}$ for cluster $\alpha = \{1,2\}$ will not be identical to $K_{\pi(x,y)}^{\{1,2\}} = K_{y,x}^{\{1,2\}}$. One can understand this as the force from site 2's y-direction to site 1'x-direction, is different from site 1's x-direction to site 2's y-direction, and thus no commutative CFC needs to be concerned when $\pi(\alpha) \neq \alpha$. However, the commutativity still plays an important role for "improper" clusters. For example, if $\alpha = \{1,1,1\}$ then obviously $\pi(\alpha)$ is still equal to $\alpha = \{1,1,1\}$. In other words, this is impossible to tell the order in which lattice site 1 acts on the other lattice sites 1. Base on this invariance, we then can set up the commutative relation for CFC:

$$K_{\pi(I)}(\alpha, A) = K_I(\alpha, A) \quad \forall \quad \pi(\alpha) = \alpha \tag{3.13}$$

3.3.2 Space group symmetry

Energy is invariant under an operation if the operator commute with the Hamiltonian. We can thus utilize space group symmetry for the parent lattice site to find out the CFC which

are subject to this invariance. By knowing space group operator $S = \{\hat{s}\}$ one can map α to $\hat{s}\alpha = \alpha'$ and A to $\hat{s}A = A'$. We can construct the following general linear relation:

$$\begin{aligned} K_I(\hat{s}\alpha, \hat{s}A) &= \Gamma_{IJ}(\hat{s}) K_J(\alpha, A) \\ K_I(\alpha, A) &= \Gamma_{IJ}(\hat{s}^{-1}) K_J(\hat{s}\alpha, \hat{s}A) \end{aligned} \tag{3.14}$$

where Γ_{IJ} is a $3^{|\alpha|} \times 3^{|\alpha|}$ matrix.
The relation can be derived from linear transformation of displacement for each vertex.

$$\mathbf{u'}_j = \boldsymbol{\gamma} \mathbf{u}_{\pi(j)} \tag{3.15}$$

The original potential energy formed by the original cluster is given by

$$E = K_{i_1 i_2 .. i_n}(\alpha, A) u_{1,i_1} u_{2,i_2} ... u_{n,i_n} \tag{3.16}$$

and the energy formed by the symmetry transformed cluster is

$$\begin{aligned} E &= \mathbf{K}(\alpha', A) \cdot (u'_1 \otimes u'_2 \otimes ... u'_n) \\ &= \mathbf{K}(\alpha', A) \cdot ((\gamma \cdot u_1) \otimes (\gamma \cdot u_2) \otimes ... (\gamma \cdot u_n)) \\ &= K(\alpha', A')_{i'_1 i'_2 .. i'_n} \gamma^{i'_1}_{i_{\pi(1)}} ... \gamma^{i'_n}_{i_{\pi(n)}} u_{\pi(1),i_1} ... u_{\pi(n),i_n} \end{aligned} \tag{3.17}$$

We apply operator π to permute the index is because in general the symmetry transformation can change the order of pre-defined index. Permutation of index can be examined if the translational symmetry is preserved. After index permutation, the summation can be

written as:

$$
\begin{aligned}
E &= K(\alpha', A')_{i'_1 i'_2 .. i'_n} \gamma^{i'_1}_{i_{\pi(1)}} ... \gamma^{i'_n}_{i_{\pi(n)}} u_{\pi(1),i_1} ... u_{\pi(n),i_n} \\
&= K(\alpha', A')_{i'_1 i'_2 .. i'_n} \gamma^{i'_1}_{i_{\pi(1)}} ... \gamma^{i'_n}_{i_{\pi(n)}} u_{1,i_1} ... u_{n,i_n}
\end{aligned} \tag{3.18}
$$

With this expression, we can easily formulate the relation between $K(\alpha, A)$ and $K(\hat{\alpha}, \hat{A})$:

$$
K(\alpha, A)_{i_1 i_2 .. i_n} = K(\hat{s}\alpha, \hat{s}A)_{i'_1 i'_2 .. i'_n} \gamma^{i'_1}_{i_{\pi(1)}} ... \gamma^{i'_n}_{i_{\pi(n)}} \tag{3.19}
$$

and the γ part can be written as:

$$
\Gamma_{IJ}(\hat{s}^{-1}) = \gamma^{j_1}_{i_{\pi(1)}} ... \gamma^{j_n}_{i_{\pi(n)}} \tag{3.20}
$$

Since the matrix γ, and Γ have the same orthogonality,

$$
\begin{aligned}
\Gamma_{IJ}(\hat{s}) &= \gamma^{j_1}_{i_{\pi^{-1}(1)}} ... \gamma^{j_n}_{i_{\pi^{-1}(n)}} = \gamma^{i^{-1}_{\pi(1)}}_{j_1} ... \gamma^{i^{-1}_{\pi(n)}}_{j_n} \\
&= \gamma^{i_1}_{j_{\pi(1)}} ... \gamma^{i_n}_{j_{\pi(n)}} = \Gamma(\hat{s}^{-1})
\end{aligned} \tag{3.21}
$$

Equation is then derived.

Obviously, if we change the origin to another points in our lattice system, the index will shift but energy still remains the same. We can therefore assure that if we translate our cluster to another lattice position, which is, if each vertex change the same N lattice points, then CFC for these two clusters should be the same although the index is changed. This relation is the so called translational relation. In our VCE system translational relation is preserved if two clusters's parent lattice structure are all changed with same N, $N \in \mathbb{N}$ lattice, and if at the same time, each vibrational cluster and configuration cluster also move with the

same N-lattice,i.e. $T(C_1, C_2) = T(\alpha_1, \alpha_2) = T(A_1, A_2) = \mathbf{v}$. Where T is a function takes in two different clusters's underlying lattice index and give the translational vector $\mathbf{v}$. Once translational symmetry is defined, we can build the space group symmetry relation for each cluster.

Two clusters are considered symmetrically identical only when there is a space group operator $\hat{s} \in S$ that transforms one clusters to the other clusterss while preserving translational relation. With this symmetry relation, we can construct our model by finding the representative clusters, which is the minimal set of clusterss that can be mapped to all possible clusterss in parent lattice through $\hat{s} \in S$. Obviously, this minimal set are mutually symmetry distinctive, and we call this set of clusters as our representative clusters. Once the representative clusters is selected, all clusterss then can be grouped into "orbitals". Each orbital is a set of clusterss which can be transformed into the same representative clusters. Once the orbitals are found, instead of finding all CFC for all clusters, we only need to find the CFC for representatives clusters and construct the corresponding Γ from their transformation group $\hat{s}$. And then we can construct all CFCs for all clusters by applying equation 3.20.

Within each orbital, we can even further reduce the number of our independent CFCs by grouping each translationally identical clusters as isotropy group S_α. Knowing that CFC is the same for translational identical clusters, we can have the linear relation:

$$K_I(\hat{s}\alpha, \hat{s}A) = \Gamma_{IJ}(\hat{s}) K_J(\alpha, A) = K_I(\alpha, A) \quad \forall \quad \{\alpha', A'\} = T(\{\alpha, A\}) \tag{3.22}$$

$$(\Gamma_{IJ}(\hat{s}) - \mathbb{I}) K_J(\alpha, A) = \mathbb{B} K_J(\alpha, A) = 0 \tag{3.23}$$

This relation lets us set up the constraint on CFC for each representative clusters to further reduce the number of required parameters.

3.3.3 Translational symmetry

In translational symmetry, we presume that uniform translation of the crystal makes no change in terms of both energy and force for any atom. This assumption leads to the famous

acoustic sum rule(ASR) for pair interaction, which can be written as:

$$\Phi(\{a,a\}) = -\sum_{b\neq a}\Phi(\{a,b\}) \tag{3.24}$$

This equation tells us that improper FCT of improper pair cluster on atom a should be the summation of all FCT from other proper clusters include atom a regardless of the the configuration. This rule can be generalized to higher order FCTs and CFCs as well. Higher order ASR for FCTs can simply be derived by replacing the singlet cluster to arbitrary high order clusters. We then have

$$\sum_{a}\Phi_I(\{a,b,c,...\}) = 0 \tag{3.25}$$

For CFC, we can expand Φ_I into configurational basis. Since ASR can be applied to any arbitrary configuration as well, a CFC version of high order ASR can be written as:

$$\sum_{a,A}K_I^A(\{a,b,c,...\}) = 0 \tag{3.26}$$

Since we have already grouped clusters in terms of orbits, we can easily rewrite equation 3.26 into orbits as:

$$\sum_{a,A}K_I^A(\{a,b,c,...\}) = \sum_{\alpha}\Gamma_{IJ}(\hat{s})K_J^A(\alpha) = 0 \tag{3.27}$$

This is the same as what we did in space group symmetry. Equation 3.27 lets us setup another linear constraint to further reduce the number of required independent parameters in CFC.

Other more complicated invariances like rotational invariance can be implemented in the future, but is not discussed in this study.

As discussed in previous section, to easily implement all of these constraint for high order CFC, we transform any n-dimensional CFC tensors into 1 dimensional arrays with 3^N elements. By using this expression, we can easily include all invariant constraint effects into one linear equation. This includes improper commutativity, isotropy group, and translational invariance as the physical constraints for independent CFCs:

$$\mathbb{B}K_J(\alpha, A) = 0 \tag{3.28}$$

We then only consider the basis that spans the null space of $\mathbb{B}$ as our independent parameter k for our model fitting. By applying different null-space reduction methods, the basis may vary, but the dimensionality shall be invariant with respect to the choice of null-space reduction method. These null space basis can thus construct a linear transformation matrix that transforms these independent parameters back to the original clusters as

$$K = \mathbb{C}k \tag{3.29}$$

where $\mathbb{C}$ is a $N_K \times N_k$ matrix. These constraints can siginificantly help us reduce the computational cost. Since these constraints are based on real physical models, it also future-proof our CFC away from some unphysical effect caused by numerical inaccuracy.

By applying the invariance of equation 3.29, the whole linear equation is reduced to

$$\mathbb{A}K = \mathbb{A}\mathbb{C}k \equiv \mathbb{A}'k = \mathbf{F} \tag{3.30}$$

3.4 Compressive sensing of VCE

Due to the vast amount of CFC, a robust, accurate and computationally efficient signal recovery technique is highly desired. In general, the number of CFC parameter is far greater than the number of calculated forces, and hence we have an under-determined linear equation. This system is also known to have very few dominant terms like NN-pair, while most are zero or close to zero. In this kind of situation, compressive sensing offers a very robust, accurate, and computationally efficient approach for us to recover CFC from known force samples. Known for the capability to efficiently and robustly extract the exact(near exact) solution for sparse system even under underdetermined conditions, CS has been widely used in the computer science community like computer vision, data analysis, etc. Unlike conventional regression process, the performance of compressive strongly depends on the choice of basis and the training data acquisition process. To best recover the signal at minimum cost, the sensing basisΦ should be as incoherent with the representation basis Ψ as possible.

$$\min \quad \sqrt{N} \cdot \max_{1 \leq k,j \leq N} | \langle \psi_k, \phi_j \rangle | \tag{3.31}$$

where ϕ_k and ψ_k is the element in each basis. However, sometimes the representation basis can not be selected freely especially in physical-based problems. In the setup of vibrational cluster expansion, the measurement basis is the atomic configuration with a particular displacement and the representation basis is our coupled clusters. Though with fixed measurement and representation basis, identically independently distributed(i.i.d.) entries has high possibility[64] to construct low coherent basis with almost any representation basis. Theoretically, a Monte-Carlo simulation can help us to find the training structures which construct the maximum incoherent sensing matrix $\mathbb{A}$. However, it is computationally expensive even for small structures. A more heuristic yet practical approach is discussed later.

Compressive sensing has been successfully applied to CE[68] and LD[52]. As a generalization of both, VCE is expected to exhibit the same success with the application of CS. In VCE, we construct the objective function following the one in [52].

$$k^{CS} = \arg\min_{k} \|k\|_1 + \frac{\mu}{2} \|\mathbf{F} - \mathbb{A}k\|_2^2 \tag{3.32}$$

Equation 3.32 is the classical CS problem with noise. μ in equation 3.32 can be seen as the weight factor that controls solution between sparsity and accuracy. With a higher/lower value of μ, the optimization tends be regularized more by l_1/l_2 norm and the solution hence become less/more sparse. As shown in previous CS-CE paper[68], the value of μ is reciprocal to the noise level, but a precise choice of μ is not needed to precisely recover the signal. In practice, the optimal value of μ can be found by minimizing prediction errors with chose cross validation scheme.

3.4.1 Split Bregman iteration

Various optimization techniques have been proposed for l_1 normalization. Given the fitting size in VCE, split-Bregman iteration[75] is opted for its capability to deal with a large system. The advantage of split-Bregman iteration is that it separates $\|\mathbb{A}k - \mathbf{F}\|$ from the original l_1 and l_2 mixing case as seen in equation 3.32 by rewriting it as

$$k = \arg\min_{u,d} \|d\|_1 + \frac{1}{2} \|\mathbf{F} - \mathbb{A}k\|_2^2 + \frac{\lambda}{2} \left\| d - \frac{1}{\mu} k \right\|_2^2 \tag{3.33}$$

Where d is an introduced variable that enables us to separate the l_1 and the l_2 norms. The last term in equation 3.33 makes sure $d = \mu k$ in minimization limit. This allow us to efficient recover signal without any complicated pre-conditioner for the sensing matrix $\mathbb{A}$. The basic iteration algorithm in split Bregmann iteration method is:

$$k^{n+1} = \arg\min_{u} \frac{1}{2} \|\mathbb{A}k - \mathbf{F}\|_2^2 + \frac{\lambda}{2} \|d^n - \mu u - b^n\|_2^2 \tag{3.34}$$

$$d^{n+1} = \arg\min_{d} |d|_1 + \frac{\lambda}{2} \left\|d - \mu k^{n+1} - b^n\right\|_2^2 \tag{3.35}$$

$$b^{n+1} = b^n + \mu k^{n+1} - d^{n+1} \tag{3.36}$$

We can efficiently solve equation 3.36 by techniques such as conjugate gradient(CG) or other standard convex optimization techniques. Once k is acquired,equation 3.35 can be easily solved entry by entry using the shrinking operator without the need to deal with the matrix:

$$d_i^{n+1} = \text{shrink}(\mu k_i^{n+1} + b_i^n, 1/\lambda) \tag{3.37}$$

Where the shrinking operator is defined as:

$$\text{shrink(x,u)} = \arg\min_{y} \mu|y| + \frac{1}{2} \|x - y\|^2 = \begin{cases} x - \mu, & x \geq \mu, \\ 0, & |x| \leq \mu, \\ x + \mu, & x \leq -\mu \end{cases} \tag{3.38}$$

The final step in equation 3.36 is imposed to reduce the noise and convergence cycles by adding back the residue after $n - th$ iteration[68]. λ in general does not affect the results significantly as long as it is not terribly off. Usually the optimal λ can be easily found within few trial by fixing μ. Overall, split Bregmann iteration yields very stable and efficient converging results

3.5 Relation between CFC and FCT

Although one can directly calculate alloy related thermodynamic and phonon properties from CFC, constructing an explicit transformation from CFC to FCT can help the compatibility

of VCE to existing methods, and also enhance the interpretablity of strain effects in alloy. Obviously, the relation between CFC and FCT depend on the configuration of the system. Therefore, to define the CFC/FCT relation, a given configuration $\{\sigma\}$ is required. Map CFC to FCT is a three step process. The First step is to collect all the effects of configuration from the configurational cluster to a given vibrational cluster by equation 3.9:

$$\Phi_I^{Id}(\alpha, \{\sigma\}) = \sum_A K_I(\alpha, A)\sigma^A \tag{3.39}$$

Here, we use Φ^{Id} to represent FCT expanded from ideal position. The Second step is a coordinate transformation due to different reference position between VCE and LD. In most LD calculations, the FCT expansion is done from the equilibrium position. However, in VCE, the expansion is from the ideal position. To address this difference, a relaxation process is required. In the Kanzaki force context, this relaxation is a linear equation since no order higher than the harmonic orders are considered. However, in VCE, we include higher orders to account for anharmonic effects. The relaxation process then need to be done by various structure optimization algorithms that minimize force. To keep simplicity, volume expansion is not taken into account in this study. Finally, the coordinate transformation based on displacement between the optimized structure and the ideal structure can be accomplished by a renormalization process. We can construct an explicit relation between FCT expanded from the ideal position(Φ^{Id}) and FCT from the equilibrium position(Φ^{Eq}):

$$\Phi_I^{Eq}(\alpha) = \partial_{u_\alpha} E = \sum_\gamma \frac{1}{\beta!}\Phi_J^{Id}(\gamma) \cdot \delta_J(\beta) \quad \gamma \in \{\alpha, \beta\} \tag{3.40}$$

β here represents all possible clusters in system, and $\delta(\beta)$ represents the relaxation configuration in β. Mapping CFC back to FCT does not introduce any new physics, but it helps us to validate phonon properties like dispersion, density of states, and phonon life time, etc by comparing our VCE results directly with other first-principle calculations. Also, the mapped FCT makes it easier for others to infer more complicated properties from our VCE model.

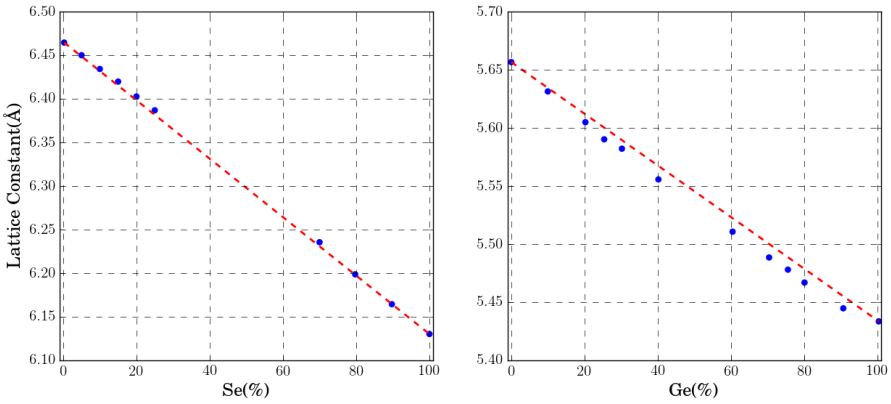

Figure 3.3: Lattice constant dependency of concentration for (a)PbTe-Se[30] and (b)SiGe[76]. Strong linear relation following Vegard's law in both materials is a strong evidence of solid solution.

3.6 Alloy PES of Si-Ge and PbTe-Se

We choose Si-Ge and PbTe-Se as two alloy systems to demonstrate the validity of our VCE model. Few incentives make these two materials interesting to be studied for our VCE model. First is both materials are widely studied and plays important role in microelectronics[77] and thermoelectrics[78]. Secondly, they posses very different anharmonicity characteristics. Si-Ge, a widely adopted electronic materials which is well known for its weak anharmonicity and high thermal conductivity[79]. On the other end, PbTe-Se shows strong anharmonicity[78] and thus low thermal conductivity. Because of its low thermal conductivity, PbTe-Se has been demonstrated in various high performance thermoeletric materials[30].

Third, as depicted in Figure 3.3, experimental studies also show both materials lattice constant follow Vegard's law, which is an important indication showing both of them are substitutional alloys from end to end. Finally, both materials have been extensively studied by state-of-art computational techniques[80, 40, 41] and experimental characterizations[81, 30, 82]. This assures us to benchmark with others state-of-art methods and to be validated by experimental data.

3.6.1 Training structure selections

To accurately reconstruct the PES, representative training structures are essential. Few criteria need to be met for an optimal training structure. First question need to be asked is how can we use small supercell to model bulk materials. A common technique to model bulk materials with small supercell is applying periodic boundary condition with $\mathbf{u}(r) = \mathbf{u}(r+R)$, where R is the size of supercell. Periodic boundary condition can remove the surface effect and ensures the indefinitely long interaction(Γ point in reciprocal space), however, it also reduces the interaction range between independent atoms. The idea can easily be understood as the image atom. That is the case when you reach out the atom at R_i which the distance if larger than you supercell size $R_i > L$. Because of periodic boundary condition, one is actually getting the interaction between the atom R_0 and $R_i - L$. Though depending on the shape of the supercell, most common practice is your supercell size should be two time larger than the longest interaction you are interested in. To make the alloys more close to the real random cell it is desired to have large supercell to mimic the realistic alloys. However, since DFT calculations typically scale with $O(n^2 logn)$[83], large supercell calculations can become prohibitive expensive. In practice, we find a good trade-off between cut-off and computational feasiblity is using size with 4x4x4 FCC supercell. In Si-Ge and PbTe-Se, it means 512 atoms in each supercell structure. With a chosen supercell size, it effectively determines the longest cut-off in our VCE models and allows us to set the upper bound of radius cut-off in our model. With determined supercell size, the next question is how to efficiently sample the configurational space and vibrational space. For the vibrational part, although it is intuitive to adopt MD trajectory as sample points given those are the phase space sample, has high possibility to be visited by the system, the strong correlation between MD trajectory would inhibit the recovery power of CS. On the other hand, directly construct a highly uncorrelated sensing matrix is challenging due to the symmetry constraint matrix. A rigorous way out is using Monte-Carlo to explore the possible phase space and disregard the samples which are highly correlated. But this step is computationally expensive even for small supercells. Here, we adopted a more heuristic approach by randomly displaced

atom with ≈ 0.1Å on top of random alloys. Though depending on the number of clusters is included, the number of supercell training set usually requires less than 10. Finally, for different concentrations, we adopted Vegard's law to decide the macroscopic lattice constant for the supercells. Our results show our VCE model performs exceptionally with this training structure selections process.

3.6.2 DFT calculations

After the selection of supercell structures, we use the Vienna Ab initio simulation package(VASP)[83] to accomplish DFT force calculations. For Si-Ge, we use Perdew-Becke-Ernzerhof exchange correlation functional form based[84] on projector-augmented wave formalism[85]. While for PbTe-Se we use local density approximation functional fit to Ceperley-Alder elctron gas method[86]. The reason of these choices are based on our previous studies on which potential forms give rise to best phonon properties. Given the purpose of this work is trying to demonstrate VCE model can well recover ab initio PES, we would not discuss the validations of these functinoal forms. The energy cut-off for Si-Ge and PbTe-Se are 600 eV and 400 eV, respectively. All of the training cell use Gamma only K-mesh calculation.

3.6.3 Models and Results

In both cases, we use up to 4th order vibrational clusters with good convergence. For Si-Ge the cut-off for 2nd, 3rd, and 4th order are 8 6 3. While for PbTe-Se the cut-off are 11 7 6. The inclusion of longer pair cut-off for PbTe-Se is due to stronger long-range force which cause non-negligible long range force constant.

The trained model then are used to predict with materials with random configurations which had not been involved in the training. The selected supercell structures are then put into AIMD simulation at 300K. The randomly selected snapshots of MD configuration are calculated in VASP to serve as the cross validation data set. By comparing the force prediction between VCE and DFT calculations in Figure 3.4, we can see our VCE predicted forces match DFT calculations exceptionally well. In Si-Ge, the prediction error is less than

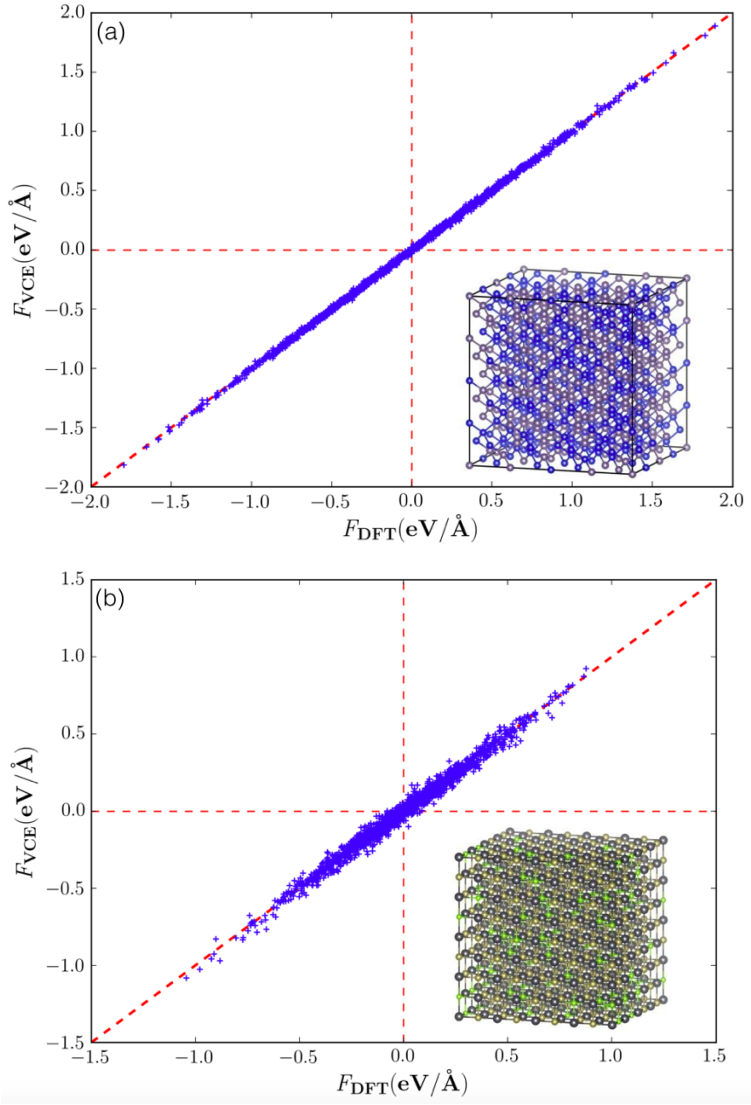

Figure 3.4: Predictive forces from VCE compared against DFT calculated forces using the MD trajectory corresponding to 300K for (a) a 512 atom $Si_{0.8}Ge_{0.2}$ random alloy supercell and (b) a 512 atom $PbTe_{0.75}Se_{0.25}$ random alloy supercell. The diagonal red line represents perfect match.

3%. This results demonstrated the capability of VCE to accurately reconstruct PES of arbitrary random configurations. In PbTe-Se, however, due to the strong Columnb interaction, as manifested by the large Born effective charge, FCT decays much slower than Si-Ge. To handle this situation, we include long pair interaction up to half of the supercell size. Despite the strong long-range force, we still find our VCE gives satisfying results with less than 8% prediction error. One thing worth pointing out here is that the error is not due to the lack of high order anharmonicity. From our calculations and the phonon plot, we know the main reason for its higher prediction error is mainly due to the pair cluster cut-off, which is mainly limited by supercell size, can not fully capture long-range force. Unlike anharmonicity which plays important role in thermal conductivity calculations, long-range force is known to have minimal effect in thermal conductivity. The reason of it is because long-range force would only affect optical mode near Gamma point which has close to zero group velocity and thus virtually contribute nothing to the heat transportation.

To further assure the accuracy of the PES, we use our trained VCE model to generate sampling atomic configuration for CSLD. Ordered FCC Si-Ge unitcell and PbTe-Se unitcell corresponding to $Si_{0.5}Ge_0.5$ and $PbTe_{0.75}Se_{0.25}$ with small displacement is predicted both in DFT and VCE. Due to non-negligible long-range interaction in PbTe-Se, dielectric constant and Born effective charge is calculated in VASP and used to account for non analytic correction following the method introduced in [89]. Strong LO-TO splitting is a clear evidence on the strength of long-range interaction and again explain why pair FCT decay slowly in PbTe-Se. The exciting results from our VCE is that not only the force prediction is accurate across different type of alloys with arbitrary configurations, it also accurately describes the vibrational properties, which is crucial for accurate thermal conductivity calculations. To the best of our knowledge, this is the first ever model which can accurately predict the PES of arguably any type of crystalline alloys. The consistent model building process of VCE for alloys free us from the burden to design various functional form for complicated materials. Inherited from its parent LD and CE, VCE also preserves the controlled approximation property, which allows us to adjust the necessary cut-off to meet the desired accuracy. By

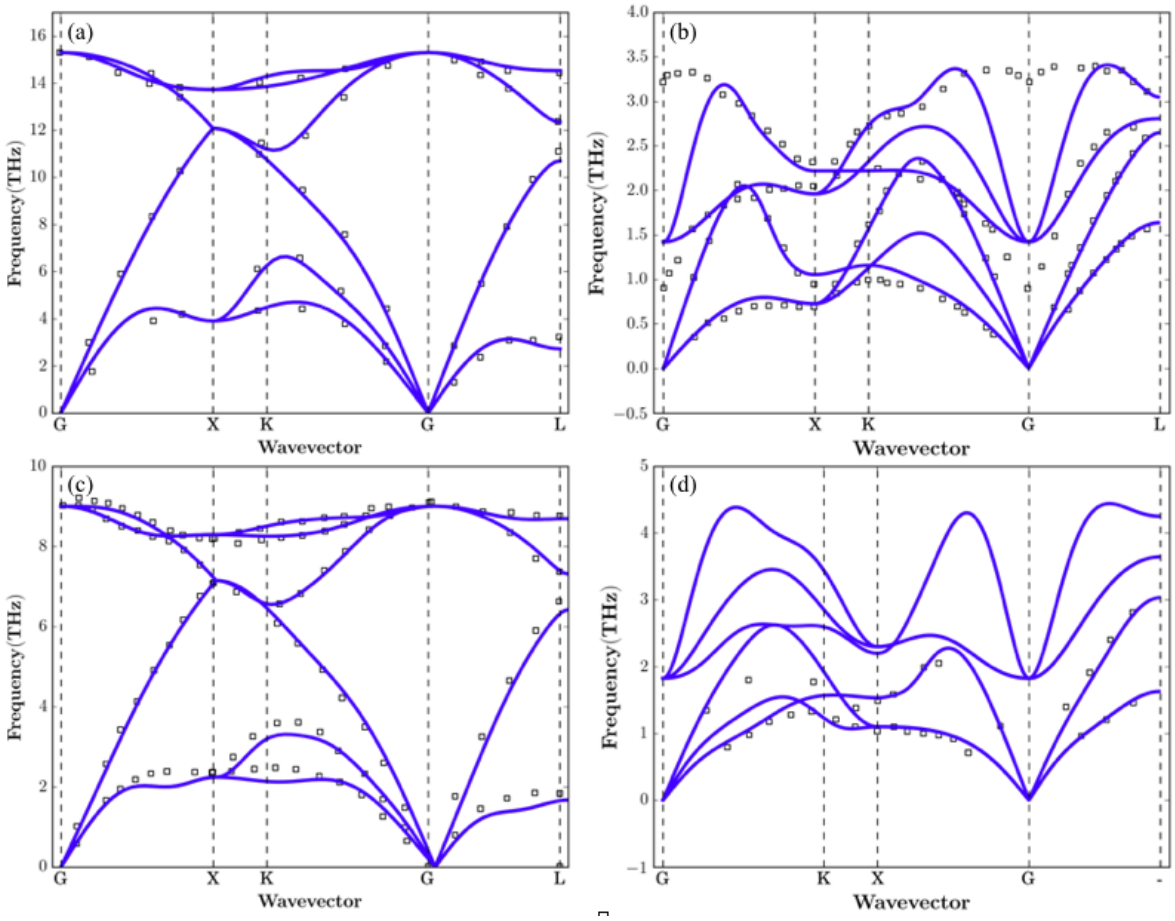

Figure 3.5: Phonon dispersion comparison between first-principle VCE calculations(curve) and experiments(dots) for (a) Si[87], (b) Ge[87], (c) PbTe[88] and (d) PbSe[88]. The results demonstrate the accuracy of DFT calculations of force and force constant inferred by VCE

expanding force constant into configurational space, we can greatly reduce the dimension into one which preserves important environmental information.

These advantages becomes significant for PbTe-Se especially. Due to the poor transferability between empirical potentials and poor description of anharmonicity, no sophisticated empirical potential form has been successfully proposed for PbTe-Se. The long-range interaction in PbTe-Se also requires large cut-off for converged pair FC. All of the above issues make accurate FCTs can hardly be obtained numerically. But with compressive sensing, our model building processes are extremely facile, efficient and the predicting results are accurate

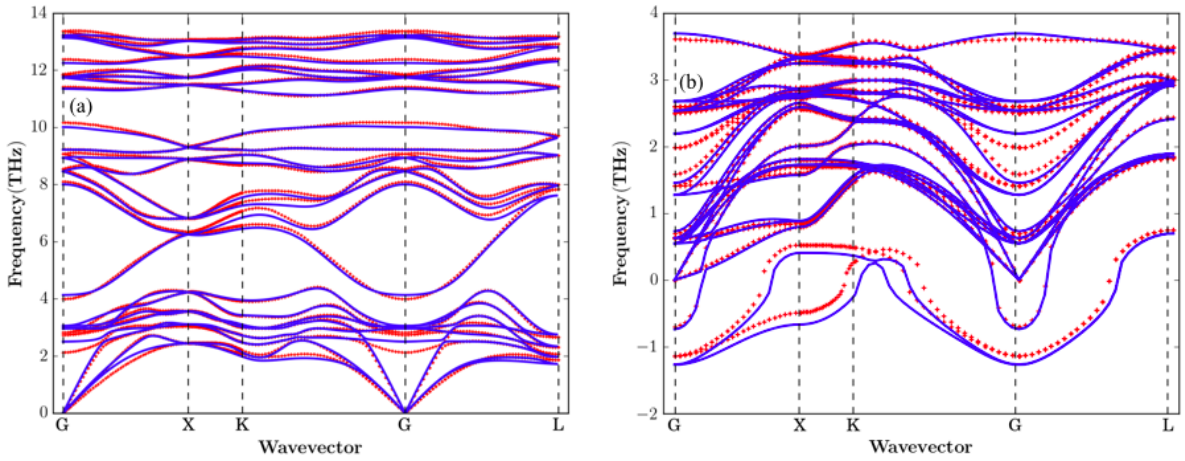

Figure 3.6: With finite displacement forces calculated from VCE and DFT, phonon dispersion calculated in CSLD for (c) FCC $Si_{0.5}Ge_{0.5}$ and (h) FCC $PbTe_{0.75}Se_{0.25}$ are shown in solid and dashed line, respectively.

and robust. Our VCE model is the first ever PES representation which can reach such high accuracy not only in force but even phonon properties for PbTe-Se alloys as demonstrated in Figure 3.6.

Given the fact that alloys play important role in thermoelectric materials development, our VCE method successfully paves a general and efficient process to obtain accurate PES across wide materials classes. Though the constructed PES can be used to calculate wide-range of thermodynamics properties, In the following chapter, we focus our discussion on the application of thermal conductivity calculations, which no existing methods can accurately predict the thermal conductivity of PbTe-Se yet.

CHAPTER 4

Lattice thermal Conductivity Calculations

Thermal conductivity is a fundamental material feature which directly relate to numerous applications. And due to the thermodynamic law, all materials at finite temperature would incorporate certain level of impurities which makes disorder a necessary component in the discussion of heat transportations. As discussed in the Introduction, finding a proper way to accurately predict thermal conductivity of alloys is still a very challenging task, even with all the advancements of first-principles calculations. Though direct thermal conductivity calculation via DFT is theoretically possible, it is computationally prohibitive due to the scale required in time and length. Another common approach is through the multi-scale modeling. Instead of directly using DFT to simulate arbitrary time and length scale, we can first extract few important parameters which is smooth and insensitive within our interested scope. These parameters then can be used as pre-calculated parameters for computationally tractable model for larger system. Two invaluable methods have been widely applied for multi-scale modeling thermal conductivity calculations are Boltzmann transport and molecular dynamics. Boltzmann transport is based on phonon theory while molecular dynamics utilize classical Newtonian dynamics in real space. By utilizing these two methods with VCE inferred PES, we can further validate if our VCE-PES is indeed an accurate model to push the boundary of modern first-principles thermal conductivity calculations for alloys.

4.1 Boltzmann Transport Calculations

Also known as phonon Boltzmann transport(PBT), Botzmann transport equation(BTE) was first formulated by Perial to describe the intrinsic lattice thermal conductivity from

microscopic point of view apart from scattering from boundary or defects[34]. Though the formulation has been proposed, the accurate solution has long been considered very hard to solve. Few techniques like relaxation time with Debye approximation[90] has thus been proposed to alleviate the computational complexity. Thanks to the development of iterative method[91] we are finally be able to get the exact solution for BTE. To explain how BTE be derived to calculate lattice thermal conductivity, it starts with the description of non-equilibrium process of phonons. In lattice thermal conductivity, phonon is the sole carrier to transport heat. To model intrinsic lattice thermal conductivity, Perial applies perturbation theory. Given a small temperature perturbation, phonon distribution would be kicked off from their equilibrium distribution. The intrinsic heat flow then is generate when phonon return back to equilibrium states. The caused heat flow can be expressed as the collection of phonons as:

$$q = \frac{1}{N_0 \Omega} \sum_{\lambda} \hbar\omega(\lambda) v_{\alpha\lambda} f_{\lambda} = -k_{\alpha,\beta} |\Delta T|_{\beta} \tag{4.1}$$

where λ is a tuple comprise both branch index ν and wave vector$q$. v,f represents phonon group velocity and distribution, respectively, and α, β refers to the Cartesian coordinate. The toughest part to handle in this equation is phonon population f_{λ}. To handle how n_{λ} would respond to the fluctuation ΔT, the resulting heat flow can be decomposed into the diffusion part and scattering part. The conservation of energy and momentum ensures the balance:

$$- v_{\lambda} \Delta T (\frac{\partial f_{\lambda}}{\partial T}) + \frac{\partial f_{\lambda}}{\partial t}|_{scatter} = 0 \tag{4.2}$$

Equation 4.2 is the basic formulation of BTE. In perfect harmonic crystal, all the harmonic phonon modes are independent and thus no interaction occurs. It caused the vanished scattering part and thus no finite thermal conductivity can be obtained. To allow finite thermal

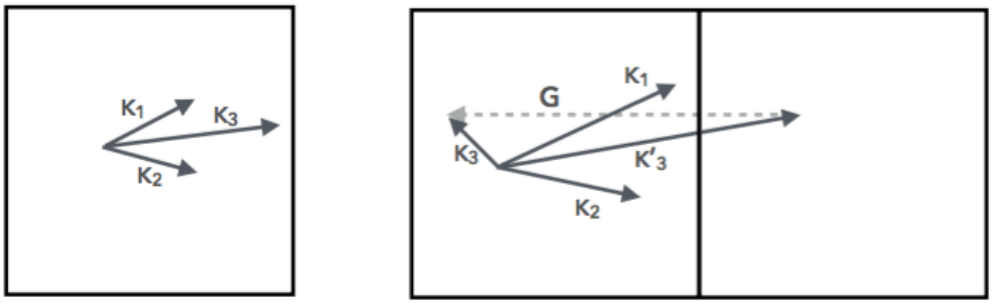

Figure 4.1: Two type of phonon generation process involves three phonons describe by Callaway. (a) is the normal process which the generated phonon is still within its own Brillouin zone(BZ). (b) is the umklapp process of which the generated phonon is outside of its own BZ. The equivalence of K_3 and $K_3{}'$ can be interpreted by the scattering of crystal momentum G

conductivity in perfect crystal, introducing of anharmonicity is the only way to allow phonon scattering. To understand how phonon interaction can induce finite thermal conductivity, Callaway propose the quasi-momentum model[92]. From Callaway's scattering model, two type of phonon scattering can occur in crystals. Figure 4.1 shows the simplest three phonon coalescence interaction. With this three phonon interaction, the first type is the normal scattering, which is after the generation of new phonon, the phonon momentum is still within its own Broullion Zone(BZ). The second type of phonon interaction is when the new generated phonon's momentum is beyond its own BZ. However, due to the periodicity, it's new momentum K_3' is actually equivalent to $K_3{}' - G$ where G is the width of BZ. Callaway refers the first type of phonon scattering as normal scattering while the second type as Umklapp, abnormal in Germany, scattering. Since no momentum change in first type, it contribute nothing to thermal resistance. But the second one brings back the phonon, and directly cause the finite thermal thermal conductivity. In most practical case, the small value of norm $|dT|$ allows one to apply linear expansion of population f_λ into $f_0(\omega_\lambda) - \mathbf{F}_\lambda \nabla T \frac{df_0}{dT}$, where f_0 is the equilibrium phonon distribution. When only less than three phonon interactions are involved, the resulting linearized BTE can be written as:

$$\mathbf{F}_\lambda = \tau_\lambda^0(\mathbf{v}_\lambda + \delta_\lambda) \tag{4.3}$$

Where τ_λ is relaxation time of mode λ, and the term δ_λ is showing how the system is deviated away from constant relaxation time. The omit of $\delta_{\{}\lambda\}$ is commonly referred to single mode relaxation time approximation. In single mode relaxation time approximation, only one mode involved in the interaction is being pushed out of the equilibrium while all others mode are remained equilibrium. This often not the realistic case but all modes involved in the interaction are relaxed simultaneously. The reason to introduce the δ_λ terms is to address what is missing in single mode relaxation process. δ_λ can thus be regarded as the correction term which is depending on how much the relaxation process is deviated away from normal relaxation time process. Obviously, δ_λ would be depending on the population of other modes, and can be explicitly expressed as:

$$\begin{aligned}\delta_\lambda =& \frac{1}{N}\sum_{\lambda_i\lambda_j}\Gamma^+_{\lambda_i\lambda_j\lambda_k}(\zeta_{\lambda_i\lambda_k}\mathbf{F}_{\lambda_j} - \zeta_{\lambda_i\lambda_j}\mathbf{F}_{\lambda_j}) + \\ & \frac{1}{N}\sum_{\lambda_i\lambda_j}\frac{1}{2}\Gamma^-_{\lambda_i\lambda_j\lambda_k}(\zeta_{\lambda_i\lambda_k}\mathbf{F}_{\lambda_k} + \zeta_{\lambda_i\lambda_j}\mathbf{F}_{\lambda_j}) + \\ & \frac{1}{N}\sum_{\lambda_i}\Gamma_{\lambda_i\lambda_j}\zeta_{\lambda_i\lambda_k}\mathbf{F}_{\lambda_j}\end{aligned} \tag{4.4}$$

where $\zeta_{\lambda_{i,j}}$ is the ratio of $\omega_{\lambda_i}/\omega_{\lambda_j}$ and relaxation time constant τ_λ^0 is:

$$\tau_\lambda^0 = \frac{1}{N}(\sum_{\lambda_i\lambda_j}\Gamma^+_{\lambda_i\lambda_j\lambda_k} + \frac{1}{2}\sum_{\lambda_i\lambda_j}\Gamma^-_{\lambda_i\lambda_j\lambda_k} + \sum_{\lambda_j}\Gamma_{\lambda_i\lambda_j}) \tag{4.5}$$

Γ here represents the scattering rate between modes. The scattering rate of phonon can then be calculated through Fermi's golden rule to describe the generation and annihilation of phonons. With three phonon interactions:

$$\Gamma^{+}_{\lambda_i\lambda_j\lambda_k} = \frac{\hbar\pi}{4}\frac{f_0^i - f_0^j}{\omega_{\lambda_i}\omega_{\lambda_j}\omega_{\lambda_k}}|V^{+}_{\lambda_i\lambda_j\lambda_k}|^2\delta(\omega_{\lambda_i} + \omega_{\lambda_j} - \omega_{\lambda_k}) \tag{4.6}$$

$$\Gamma^{=}_{\lambda_i\lambda_j\lambda_k} = \frac{\hbar\pi}{4}\frac{f_0^i + f_0^j + 1}{\omega_{\lambda_i}\omega_{\lambda_j}\omega_{\lambda_k}}|V^{-}_{\lambda_i\lambda_j\lambda_k}|^2\delta(\omega_{\lambda_i} - \omega_{\lambda_j} - \omega_{\lambda_k}) \tag{4.7}$$

δ function assures the energy conservation during generation and annihilation process. Through the scattering equation, whole scattering events strongly depend on 1) phonon distribution f_ω, which represent how many phonons are available to be interacted, and 2) the overall area of phase space which can be calculated from scattering matrix V:

$$V^{\pm}_{\lambda_i\lambda_j\lambda_k} = \sum_{\mathrm{i}\in\mathrm{u.c.}}\sum_{\mathrm{jk}}\Phi_{\mathrm{ijk}}\frac{\hat{e_i}\hat{e_j}\hat{e_k}}{\sqrt{M_{\mathrm{i}}M_{\mathrm{j}}M_{\mathrm{k}}}} \tag{4.8}$$

Since F_λ exists in life time τ^0_λ, the explicit F_λ is solved iteratively for exact answer with three phonon interactions. With given second and third order FCT, group velocity and scattering rate and finally thermal conductivity can be calculated. We use shengBTE[37] to be our phonon BTE solver for full iterative solution of thermal conductivity. The key for accurate thermal conductivity calculations then is the accurate FCTs. The importance of Φ_{ijk} shows how anharmonicity plays crucial role for accurate scattering rate. To accurate recover anharmonicity, however, remains a computational challenging task. Various technique has been proposed to extract accurate third order FCT. DFPT with 2n+1 approach has been first demonstrated by [36] for Si and Ge. Frozen phonon based methods like finite difference methods also show good performance in [37]. With compressive sensing, Fei et. al[52]. shows how accurate and robust high order force constant can be accurately recovered, and accurate thermal conductivity for compounds can thus be acquired.

4.1.1 VCA and Mass disorder

To allow the disorder in phonon calculation scheme, VCA is the only possible approach to work hand in hand with BTE. The center piece of VCA is assuming the disorder should

be treated as the perturbation on top of the ordered virtual atoms with weight averaged physical and chemical properties. The only disorder left in VCA is the mass disorder, which is treated using Klemens' method[93] for point defects. In Klemens' discussion, point defect only would interact with harmonic phonon, and thus only harmonic PES is considered here. The unperturbed Hamiltonina of virtual crystal and mass disorder perturbation can be written as:

$$H = H_0 + H_I \tag{4.9}$$

Where H_0 and H_1 are:

$$H_0 = \frac{1}{2}\sum_{\alpha} \bar{m}(\alpha)\mathbf{u}_(^2\alpha) + V_{\mathrm{Har}} \tag{4.10}$$

$$H_I = \frac{1}{2}\sum_{\alpha} \delta m(\alpha)\mathbf{u}_(^2\alpha) \tag{4.11}$$

Where α is the atomic position and $\delta m = m(\alpha) - \bar{m}(\alpha)$. By converting equation 4.11 into eigen mode along with Fermi's golden rule and knowing random distribution of masses yields:

$$\langle \delta M_i \delta M_j \rangle = \left\langle [\delta M_i]^2 \right\rangle \delta_{ij} \tag{4.12}$$

we can have the scattering rate:

$$\Gamma_{\lambda_i\lambda_j} = \frac{\pi\omega^2}{2}\sum_{\alpha} g(\alpha) < \hat{e(\alpha)}_{\lambda_i} \hat{e(\alpha)}_{\lambda_j} > \tag{4.13}$$

Where $g(\alpha) = \sum_s f_s(\alpha)[1 - M_s(\alpha)/\bar{M}(\alpha)]^2$ and $\bar{M}$,f_s are the average mass and relative concentration of species s,respectively. Though starting as the perturbation method which

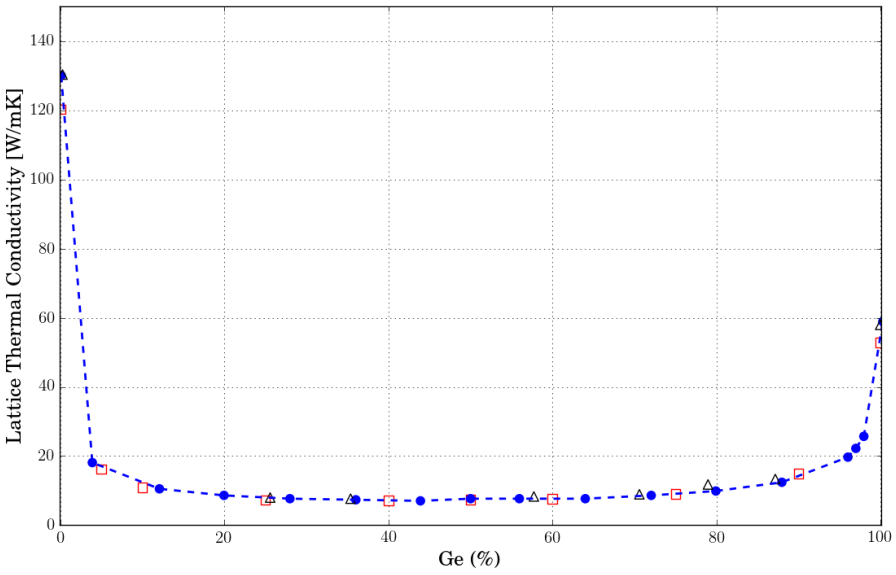

Figure 4.2: κ_L calculation by VCA for Si-Ge in VCE(square) and experimental(triangle)[94] and DFPT from Garg et. al.[39](circle)

aims for small mass fluctuation, VCA works surprisingly good for large mass contrast alloys, e.g. NiPd, SiGe. Garg et al. perfectly predict SiGe thermal conductivity using VCA from DFT calculations.

4.1.2 Thermal conductivity of Si-Ge and PbTe-Se in VCA

Given DFPT shows accurate results compared to experimental data, it is expected our VCE generated potential should also give very accurate results. We first use the trained VCE model for Si-Ge to predict the pure Si and Ge configurations. To approximate VCA effect in VCE, all of the occupancy variables are replaced with $\sigma = 2c - 1$ for Si_cGe_{1-c}. With this replacement, the idea of averaged virtual atom can be explicitly implemented instead of just weight averaging FCT, like the one proposed in [95]. Our VCA results of Si-Ge is compared to experimental values and Garg's DFPT[40] calculations in Figure 4.2. As expected, our VCA model with VCE generated potentials shows great match between Garg's and experimental results.

Though with great success in Si-Ge, common overestimations are found in VCA when there is 1) mass contrast and 2) strong anharmonicity. Poor agreement between experiments and VCA in PbTe-Se is a famous example, in which both large lattice mismatch and strong anharmonicity are found. As depicted in figure 4.7 later, the significant overestimation is observed in our VCA calculations. A very similar trend also appears in InGaAs and most pseudobinary alloys[96]. From our further finding, we realize strong anharmonicity would strongly interplay with configurations. Even in Garg's report, they found when temperature in Si-Ge is getting higher, noticeable disagreement between experiments and VCA can only be reduced by deriving anharmonic relaxation time with explicit supercell configuration. Indeed, this phenomenological approach seems arbitrary and the need of relaxation time from explicit supercell further assures the importance of including local configuration is crucial for general thermal conductivity calculations.

4.2 Molecular Dynamics

The impotence of phonon in handling local configuration for strong anharmonic alloys is from the fact that phonon becomes ill-defined idea when zero or very low periodicity are preserved in the system. Beside it, the computational complexity for phonon interaction higher than 3rd order makes it inaccessible to strong anharmonicity. Unlike phonon based calculations, molecular dynamics offers another microscopic intrinsic thermal conductivity view by tracking atomic trajectory in real space. Because of its real space property, it makes no ambiguity when one apply large long-range disorder supercells to explicit model random configurations. Moreover, since all phonon interaction are represented in the form of trajectory, it can directly includes phonon interaction to full order. All these properties makes MD a convincing alternative when it comes to thermal conductivity calculations of alloys. The real issue of MD is the lack of high quality potentials which can accurately model PES. To address this issue, we propose our VCE potential as the alternative solution. By using VCE as potential, a strong constraint need to be applied is atoms are not allowed to diffuse. In other words, atom in VCE enabled MD system can only move, or say vibrate,

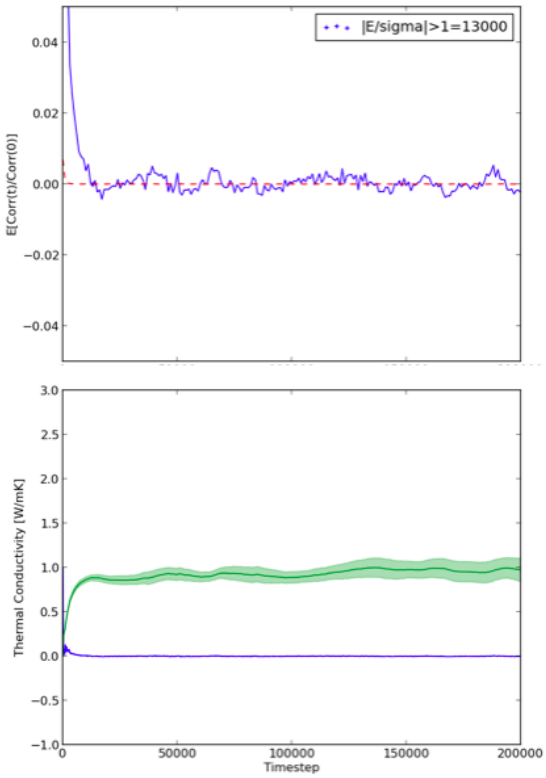

Figure 4.3: Upper figure shows the value of $\sigma(ACF)$ and $E(ACF)$ in red dashed line and blue line, respectively. By Choosing where the $\sigma(ACF) > E(ACF)$, which is 13000 fs here, can be used to infer the thermal conductivity from integrated ACF in lower figure.

around the equilibrium position. The reason this is a required constraint is because VCE is derived from LD, which describe only solids which atom is considered to vibrate only within its potential well. In solids, this constraints pose no serious concern since we are interested in materials which is well below its melting points. We thus call this lattice MD(LMD)[97] to differentiate our VCE enable MD from the rest of general MD systems. Depends on the scheme of ensemble, MD can be categorized into equilibrium MD and non-equilibrium MD. In equilibrium MD, thermal conductivity is calculated from the perturbation point of view[98, 99]. In contrast, non-equilibrium MD[100] applies external heat source and sink to simulate the Fourier's law with constant temperature gradient. To make our calculations between BTE and MD comparable, we would focus on the equilibrium MD given both of them are deriving from the intrinsic heat diffusivity from perturbation.

4.2.1 Equilibrium MD

Origin from the discovery of Brownian motion, that even a macroscopically equilibrium system would still has thermal fluctuation in atomic level. With the closed system, a micro canonical ensemble condition, the characteristic variables are number of atom N, volume V, and total energy E. To extract thermal conductivity from MD, the first thing need to be defined is the form of heat flux. In crystalline materials without convection, heat flux $\mathbf{q}$ is commonly defined as:

$$\mathbf{q}(t) = \frac{d}{dt}\frac{1}{V}\sum_{i}^{N}\mathbf{r}_i(t)e_i(t) \tag{4.14}$$

Where $\mathbf{r}_i$ and e_i are the position and energy of particle i, respectively, at time t with volume V of material. Though in the equilibrium, these three variables may seems constant in average, and $< \mathbf{q} >$ should be zero. The discovery of Brownian motion demonstrate spontaneous local fluctuations and dissipations would result in non-zero energy transfer within the system. To model fluctuation-dissipation, Einstein offers a terse yet straightforward derivation, which is also known as Einstein relation. Einstein link the diffusivity D to the fluctuation profile by:

$$D = \lim_{t\to\infty}\frac{1}{2t}\left\langle[\mathbf{r}(t) - \mathbf{r}(0)]^2\right\rangle \tag{4.15}$$

This could be understood easily by realizing if materials have strong dissipation, then the width would be narrow due to strong decay, and vice versa. And since we know the profile differences at different time t is

$$\mathbf{r}(t) - \mathbf{r}(0) = \int_0^t \mathbf{q}(t')d(t') \tag{4.16}$$

we can rewrite equation 4.15 into

$$\begin{aligned} D &= \lim_{t\to\infty}\frac{1}{2t}\int_0^t dt_1\int dt_2\left\langle q(t_1)q(t_2)\right\rangle \\ &= \int_0^\infty \left\langle q(t_0)q(t_0+t)\right\rangle dt \end{aligned} \tag{4.17}$$

by assuming $\lim_{t\to\infty} \langle q(t_0)q(t_0+t)\rangle\, dt = 0$. With the help of Einstein relation, the thermal conductivity through Green-Kubo formalism then can be formulated as:

$$\kappa_{\alpha\beta} = \frac{1}{Vk_BT^2}\int_0^\infty \langle J_\alpha(0)J_\beta(t)\rangle\, dt \tag{4.18}$$

Where α and β represent the direction and J is the heat current related to the flux via $J = V\mathbf{q}$. $\langle J_\alpha(0)J_\beta(t)\rangle$ is the autocorrelation function representing the degree of dissipation while the instantaneous fluctuation is induced. Since thermal conductivity calculated from Green-Kubo[98, 99] are directly derived from the fluctuation, it shows the intrinsic property of the materials without the worries from dependence of temperature gradient. Though theoretically one can obtain perfect answer from equation 4.18, in reality MD is notorious for their ambiguity and uncertainty issue. Two major issue in MD is called finite time effect and finite size effect. With different approach to address these two issues, the calculated results often would vary too. In following discussion, we try to select the extrapolation scheme which shows good consistency and sensible in practice.

4.2.2 Finite Time Effect

With all the great merits in EMD, the fact that it is intractable to approach the limit that $t \to \infty$ brings all the problems. In MD's context, it means it is impossible to realize ergodicity[60]. The lack of real ergodicity cause the noticeable fluctuation around zero while theoretically it should drops to zero quickly due to the finite thermal conductivity. The ever-existing fluctuation often cause the diverged integrated autocorrelation function, and so as the thermal conductivity. The time serial property in MD makes large time-scale calculations prohibitively expensive. To resolve this issue, it is common to use multiple random initial states to simulate same systems. Though it is not equivalent to one long simulation time, by choosing correlation between these initial states and parallelizing MD simulation makes the ergodicity more accessible. The ensemble averaged EMD simulation then can be used to calculate thermal conductivity with finite time τ:

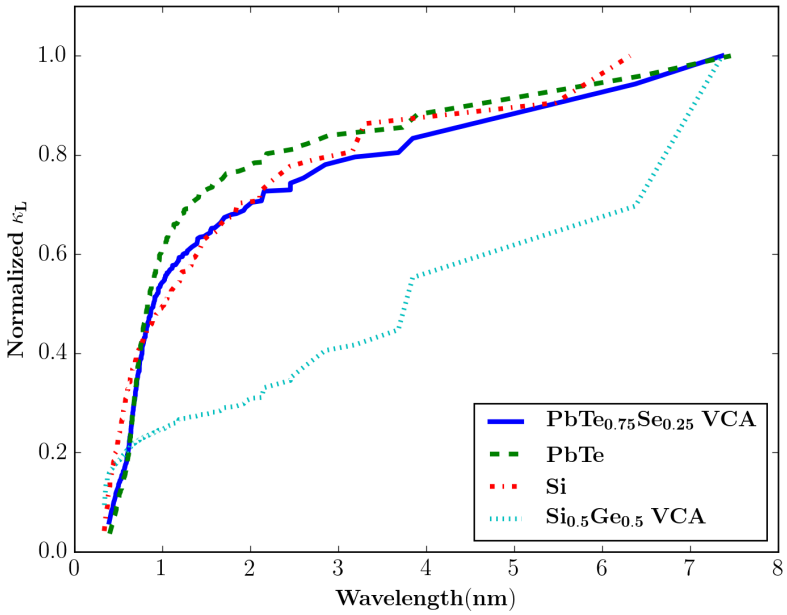

Figure 4.4: Normalized accumulation thermal conductivity with respect to wavelength. The alloy calculations is based on VCA. It is clearly mass-disorder is a strong scattering center for Si-Ge but not as significant for PbTe-Se

$$\kappa_{\alpha\beta} = \frac{1}{Vk_BT^2}\frac{1}{N}\sum_{n}^{N}\int_0^{\tau}\langle J_\alpha(0)J_\beta(t)\rangle\, dt \tag{4.19}$$

Where N is the number of parallel MD simulations.

Though the ensemble simulation can inhibit the divergence, a well stabilized thermal conductivity still rarely is the case. The question now is how do we pinpoint the thermal conductivity. Since the accumulated noise in the simulation would be more dominant toward the long simulation time and the fact that finite thermal conductivity is expected, the selected time to determine the thermal conductivity should be close to the origin point. In other words, the thermal conductivity in MD is only reliable up to a small finite time. But how close to the origin point is arguable. One of the commonly adopted and simple method is pick the time where autocorrelation first touch zero. Though it is a fairly empirical approach,

it originates from the idea that theoretically the thermal conductivity is characterized when no more autocorrelation is observed[101]. This method works fine for some of more trivial materials like Si, Ge, and NaCl. Commonly, these materials can also be well characterized by two exponential decaying functions, one corresponding to long wavelength oscillation and the other one accounts for short wave length oscillation. However, in more complex materials, one would find out the fluctuation does not really follows asymptotically exponentially decaying curve but strongly oscillate around zero autocorrelation value. To handle materials with these autocorrelation characteristics, McGaughey et. al.[102] propose to smooth the fluctuation, and use the location where the first plateau occurs. In practice, we find it is hard to quantitatively identify where is the turn on point of the plateau. In this report, we adopt the more recent approach proposed by Chen et al.[103]. It is trying to identify how noise accumulating in our MD simulation and find the cut-off when the noise overtake the signals by defining the relative fluctuation in ACF, $\left|\frac{\sigma(ACF)}{E(ACF)}\right|$ where σ and E represent the variance and the mean value of ACF. By choosing a proper averageing timespan δ and the desired threshold for $\left|\frac{\sigma(ACF)}{E(ACF)}\right|$, and compared with independent calculations we can have consistent thermal conductivity calculations with well defined selection criteria as depicted in figure 4.3.

4.2.3 Finite Size Effect

Unlike finite time effect which is universal among all the MD calculations, finite size effect depends heavily on materials. With supercell size L, the use of boundary condition allows only the commensurate wavelength and thus exclude wavelength longer than $2\pi/L$. Unlike finite-time effect, whether there is a strong finite size effect in EMD calculations is still arguable in the community. Often times one can find MD converges in cell size which is far smaller than the commensurate long-wave length size. One common belief of why this magical converging thermal conductivity occurs even with a moderated supercell size is due to the omitted phonons. The omitted phonon can either play as the contribution to the thermal conductivity and the channel for the scattering [60].

By borrowing the BTE frame, thermal conductivity contribution from different cut-off can be formulated as:

$$k_{cut}(\lambda^*) = \sum_{q,\nu} C_v(q\nu) v_g^2(q,\nu)\tau(q,\nu) \tag{4.20}$$

$$\tag{4.21}$$

The cut-off frequency λ^* related to the size of supercell with $2\pi C/L$, where C is the long-wavelength limit group velocity. The lack of long phonon wavelength as the heat transportation carriers would cause the underestimation of thermal conductivity. However, on the other hand, due to the three phonon energy $\omega - \omega_1 - \omega_2$ needs to be less than the phonon line-width. In the finite cell size, this constraint can be harder to reach due to the lack of phonon contribution from long-wavelength and thus would limit these scattering process. It would then overestimate the life-time of phonon, and consequently, thermal conductivity. Due to these two counter effects, one can hardly predict whether the thermal conductivity is converging or simply in a lucky range. To quantify these effects, Wang et. al.[104] found though it could be either over-estimation or under-estimation, by using the wavelenth accumulated thermal conductivity, it is possible to know how big the size of supercell would guarantee the convergence.

As depicted in figure 4.4, the plot of thermal conductivity with respect to phonon wavelength indicate in Si-Ge, it shows strong dependency on long wavelength limit while its weaker in PbTe-Se. And that is the case in our LMD simulations as well. Unlike some compound systems whose thermal conductivity can be largely carried by moderate to short wavelength, in alloy materials, most short wavelength are scattered and makes long wavelength vibration be the dominant heat carrier. To tell the trend of size effect, we apply no magic method but running multiple cell size to study its size effect. Limited by the computational power, an extrapolation scheme is required to account for those long wavelength vibrations. To apply the extrapolation scheme, an assumption need to be made first. Presumably, in long wave-

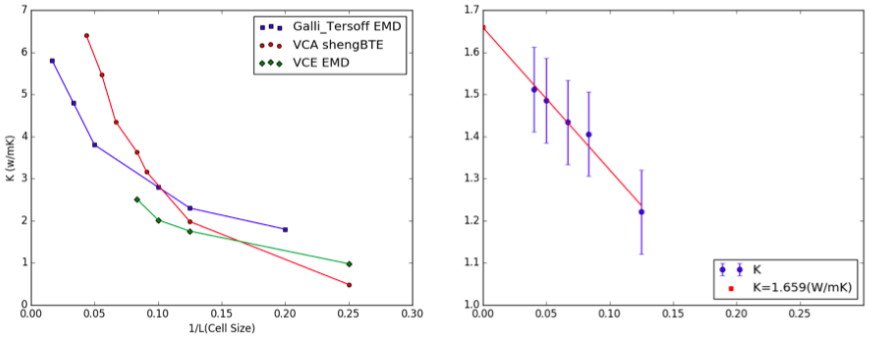

Figure 4.5: Size effect in (a) Si-Ge and (b) PbTe-Se. In Si-Ge, due to the strong size effect, Si-Ge can hardly be approximated by extrapolation scheme proposed by Gang et. al. However, in PbTe-Se, a strong linear dependency shows validity of the extrapolation. The G. Galli et al. work is from [105]

length limit, phonons would hardly be scattered by the local environments. This is believed to be true since in long-range limit, each adjacent atom can hardly feel the displacement and thus the local configurational dependent strain becomes irrelevant. In other words, we can safely use VCA to treat the long-wavelength limit. The long wavelength limit then can be approximated by the Klemens' formula to estimate long wavelength life time:

$$\frac{1}{\tau_\lambda^{\text{Klemens}}} = \gamma_\lambda^2 \frac{2k_bT}{Mv_g^2(\lambda)} \frac{\omega_\lambda^2}{\omega_\nu^{\max}} \tag{4.22}$$

Where γ_λ^2 is Gruneisen parameter. By plugging Klemens' formula into the spectrum accumulated thermal conductivity one can derive a linear extrapolation scheme:

$$\begin{aligned} \kappa(L) &= \kappa(\infty) - A\int_0^{\omega_{\text{cut}}} \frac{1}{\omega^2} f(\omega)d\omega = \kappa(\infty) - D\omega_{\text{cut}} \\ &= \kappa(\infty) - E\frac{1}{L} \end{aligned} \tag{4.23}$$

By assuming the low frequency, $C_v \approx k_B$ and $v_g(\omega)$ is the same as the acoustic velocity.

In practice, to numerically estimate what is the proper length scale the local environment has negligible effect to the phonon carriers. we use the κ_L calculated from harmonic mass-disorder scattering and anharmonic scattering within VCA framework to see the strength of size effect. As shown in figure 4.4, Simply by comparing these two distributions, a qualitative estimation of the applicability of linear extrapolation scheme can be derived. In principle, one with stronger anharmonicity would exhibit smaller onset size to apply the linear extrapolation since soon anharmoncity become the most dominant scattering mechanism. By comparing PbTe-Se to SiGe in figure 4.5, we can clearly see in SiGe, due to its weak anharmonicity, the onset point to apply linear extrapolation is far larger than PbTe-Se. And in our MD simulation we also find it is extremely hard to converge Si-Ge and underestimated thermal conductivity is observed due to the significant contribution from long wave-length vibration while PbTe-Se is dominated by anharmonicity. We then use the extrapolated thermal conductivity to derive the κ_L with respect to alloy concentration of PbTe-Se.

4.3 The Effect of Configuration on Anharmonicity

By applying the extrapolation scheme, our EMD simulation shows great match to the experimental results as depicted in figure 4.6. The first thing we are interested here is to understand what cause this overestimation using VCA in PbTe-Se but Si-Ge. To study this effect, we use MD to simulate VCA by using averaged FCT but explicit mass distribution. In other words, all of the bond has the same strain while each atom preserves its own atomic mass to introduce mass disorder effect. We compare the following 3 scenarios: 1) SiGe/PbTe-Se with explicit mass and explicit FCT depending on the configuration 2) SiGe/PbTe-Se with explicit mass and same averaged FCT. 3) SiGe/PbTe-Se with same averaged mass and explicit FCT. All of the cells are computed in a 4x4x4 FCC supercell with random configuration.

By directly comparing these scenarios in MD, we are able to distinguish the effect from mass disorder and strain disorder, which is configuration dependent FCT. The result is shown in table 4.1. The result clearly explains the reason of overesitmation in VCA is due to the lack of description for strain disorder. Due to small mass contrast in PbTe-Se,

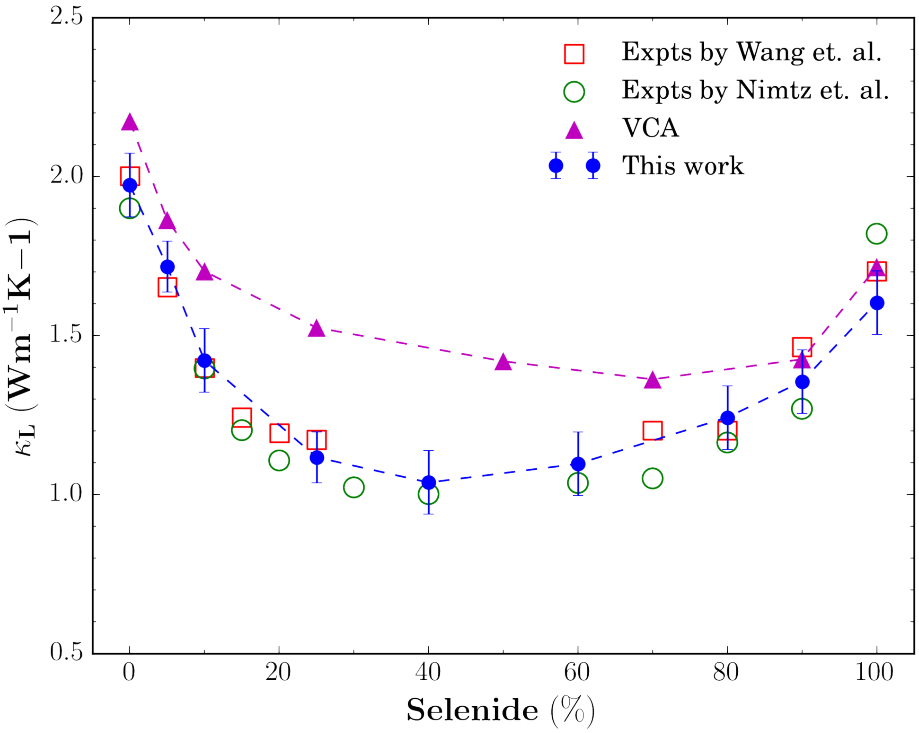

Figure 4.6: κ_L calculation by VCA for Si-Ge in VCE(square) and experimental(triangle)[94] and DFPT from Garg et. al.[39](circle)

mass disorder is fairly small in terms of reducing thermal conductivity. In contrast, Si-Ge shows strong mass disorder effect which further corroborate the observations that why VCA excellent match to experimental data. To dig deeper on how strain disorder affect the thermal conductivity and how it interplays with the environmental configurations , we calculate phonon dispersion of FCC PbTe-Se and Si-Ge supercell with concentration corresponding to $PbTe_{0.75}Se_{0.25}/Si_{0.75}Ge_{0.25}$ and $PbTe_{0.25}Se_{0.75}/Si_{0.25}Ge_{0.75}$ using averaged FCTs and explicit FCTs from VCE.

As can be seen in figure 4.7, for Si-Ge, the differences between VCA and explicit phonon is fairly small near the long wavelength area and the change of concentration barely affect the acoustic mode in Si-Ge. However, there are significant differences between VCA and explicit supercell calculations for $PbTe_{0.75}Se_{0.25}$ and $PbTe_{0.25}Se_{0.75}$. The significant imaginary mode in $PbTe_{0.75}Se_{0.25}$ shows strong phonon softening after the doping of Se atoms. From

Table 4.1: κ_L(W/mK) for Si-Ge and PbTe-Se with different methods

Case	Si-Ge	PbTe-Se
Exp. Mass/Exp. FCT	0.97	0.81
Exp. Mass/Avg. FCT	1.23	1.52
Avg. Mass/Exp. FCT	113	0.86

partial phonon density of state and phonon mode in figure 4.7(d), it clearly shows the coupling between Pb which is closest to Se and Se atom induce strong ferroelectric-like instability and hence significant phonon scattering is expected to be observed. On the other hand, in $PbTe_{0.75}Se_{0.25}$ FCC cell, no imaginary mode is observed. The evidence above clearly demonstrate how local environment would significantly affect vibrational properties in random alloys, while VCA can hardly capture these effects. To intuitively describe why Te rich alloys posses stronger phonon softening effect than Se rich one, we first use VCE to generate a defect in 512 parent compound for Si-Ge and PbTe-Se. Figure 4.8 gives on-site FCT minus pure compound on-site force constant. Unlike Si-Ge which barely change their on-site FCT after substitution, Se substitute has a significant softening of their on-site FCT and thus a flatter on-site potential well than Te substitute. This is a direct result of much weaker interaction between Pb and Se compared to Pb and Te and leads to unstable vibrational modes in Te rich alloys as depicted in Figure 4.7. Meanwhile, to understand the source of strong flattening, we calculate phonon dispersion of FCC $PbTe_{0.75}Se_{0.25}$ cell with lattice constant identical to $PbTe_{0.25}Se_{0.75}$ and no imaginary modes are found. The absence of imaginary modes clearly shows size effect reinforce the configuration disorder effect in phonon softening by trapping a small Se atom in a large PbTe cell. This result also explains why VCA shows relatively better prediction of κ_L near PbSe end but deviated significantly near PbTe end. At near PbSe end, the thermal conductivity drop is mainly due to the mass disorder perturbation as evidenced by small dispersion change. However, at near PbTe end, on top of mass disorder, configuration disorder brings in strong anharmonicity manifested by imaginary mode, and thus stronger scattering. Our calculations gives clear and

direct evidences on why incorporating configuration dependent force constant is necessary to reproduce scattering mechanism for accurate thermal conductivity calculations. To achieve phonon gas electron crystal for high performance thermoelectric materials, common belief of alloying effect is to bring down k_l mainly through mass disorder scattering. However, our study of PbTe-Se shows force constant disorder plays important role to further lower thermal conductivity and its effect can be observed simply by calculating phonon dispersion of few supercells. This study process can thus serve as a guideline for better design of thermoelectrics by introducing stronger force constant disorder.

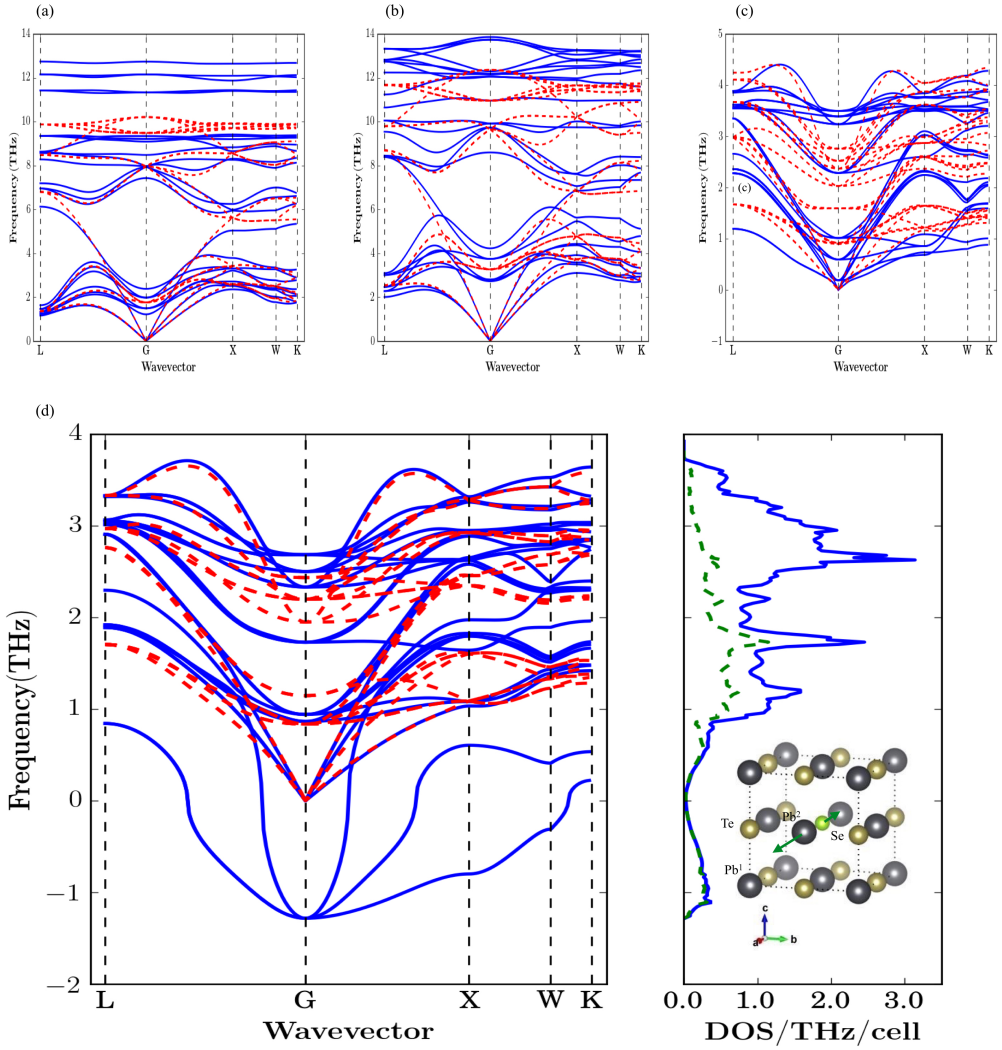

Figure 4.7: (a) and (b) shows phonon dispersion of $Si_{0.75}Ge_{0.25}$ and $Si_{0.25}Ge_{0.75}$, respectively. Solid line is the direct calculation of explicit FCC random cell from VCE, while dashed line is calculated by VCA. Same phonon dispersion comparison is calculated for (c)$PbTe_{0.25}Se_{0.75}$ and (d)$PbTe_{0.75}Se_{0.25}$. Total density of state and partial density of state of Pb^2 is plotted in solid and dashed line, respectively. FCC cell and one of three degenerated imaginary modes at gamma point is depicted in inset.

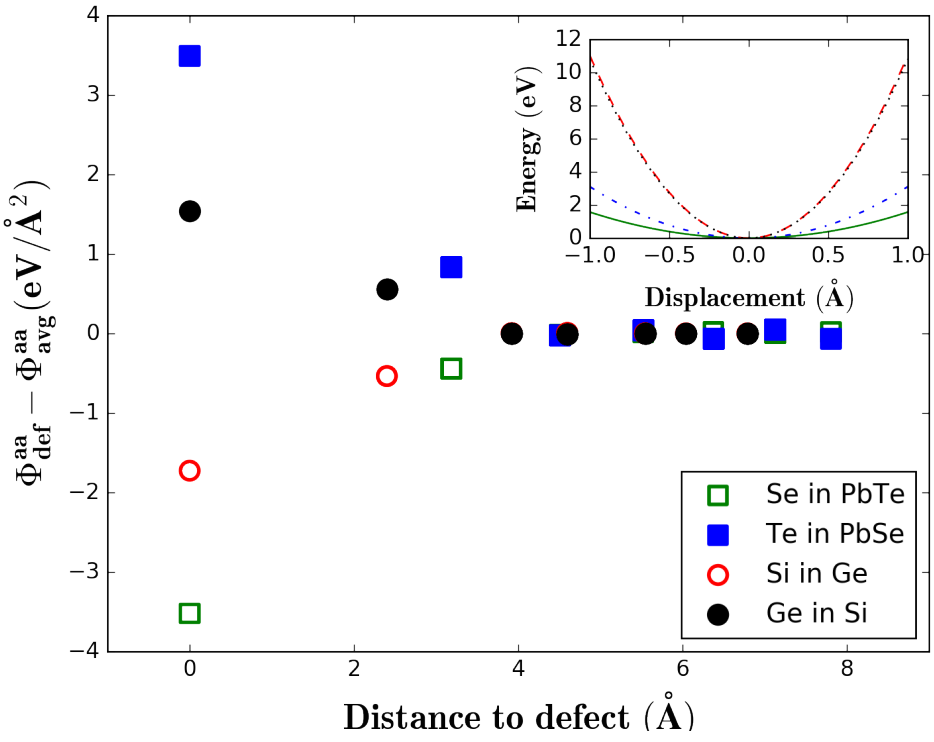

Figure 4.8: Calculated on-site FCT of defect and its surrounded atom minus parent compounds' on-site FCT. Inset shows the on-site potential curve $\frac{1}{2}\Phi^{aa}_{def}u^2$ to visualize the differneces. The deviation of defect's on-site energy from parent compound clearly shows the substitute effect is more drastic in PbTe-Se than Si-Ge

CHAPTER 5

Potential Applications of VCE

We have successfully demonstrated VCE as the unique tool to handle thermal conductivity in alloys by constructing accurate PES model incorporating explicit configurational degrees of freedom. With an accurate PES which can describe materials in realistic situations, great amount of applications can be reached beyond thermal conductivity. One of the valuable applications is calculations of free energy for alloys at finite temperature.

5.1 Introduction

Free energy is one of the most important thermodynamic properties. With accurate free energy in hand, one can quickly derive thermal expansion, heat capacity, compressibility and most importantly, the phase transition condition. A common picture to understand phase transition can be understood as the process that materials transit from higher Gibbs free energy to minimum one as depicted in figure 5.1. From grand canonical, Gibbs free energy can be expressed as the function in the phase characterized by temperature and pressure:

$$G(T, P) = U - TS + PV \tag{5.1}$$

where U, T, S, P and V are the internal energy, temperature, entropy, pressure and volume, respectively. Although often time Gibbs free energy is a much better phase transition indicator given the fact that both temperature and pressure are experimentally measurable and controllable quantity. However, controlling pressure turn out is a computationally demanding process in atomic simulations compared to fixed volumes. An alternative free energy

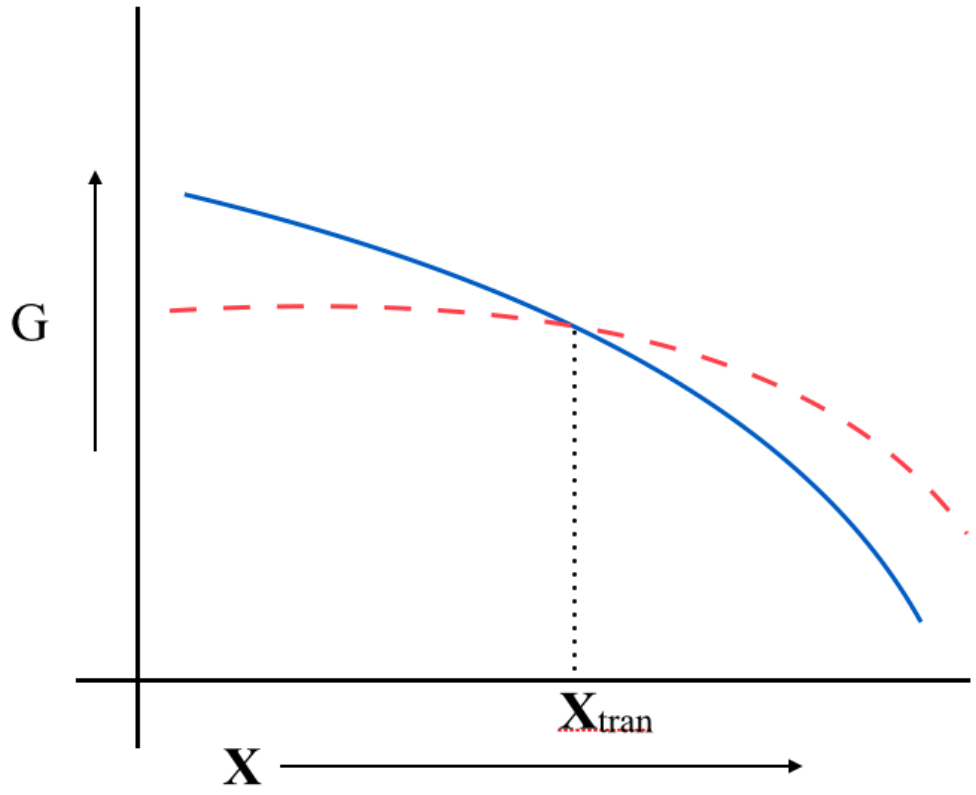

Figure 5.1: Schematic illustration of phase transition. The phase transition occurs at condition X where $G_n$ew(solid line) is lower than $G_o$ld (dahsed line)

commonly used is Helmholtz free energy F, which instead is characterized by temperature and volume,

$$F(T, V) = U - TS \tag{5.2}$$

Using F is particularly a good approximation to model realistic phase transitions for solids given the volume expansion in solid usually are small. The Helmholtz free energy of alloys can be written as,

$$F(x, T) = \Delta U_{\text{mix}}(x, T) - T[\Delta S^{\text{ideal}}_{\text{mix}}(x) + \Delta S^{\text{xs}}(x, T)] \tag{5.3}$$

where $\Delta S^{\text{ideal}}_{\text{mix}}$ for binary alloys can easily be derived as:

$$\Delta S_{\text{mix}}^{\text{ideal}} = -k_B[x \log x + (1-x)\log(1-x)] \tag{5.4}$$

ΔE_{mix} and $\Delta S_{\text{mix}}^{xs}$ is a mixing energy and excess entropy which is composed by 1) Mixing energy and mixing entropy at zero temperature, 2) electron excitation energy and mixing entropy, 3) the mixing energy and entropy from spin which is directly related to magnetism and 4) mixing energy and entropy from atomic vibrations. In semiconductor and non-magnetic materials, both 2) and 3) can be ignored in alloy states. For a long time, it is believed in alloys $\Delta S_{\text{mix}}^{\text{ideal}}$ is the dominant terms. However, the contribution of vibrational free energy is found to be significant in recent discoveries. As depicted in figure 5.2 , free energy without taking vibrational effect into account significantly overestimate the phase transition temperature in Al-.

5.2 Existing methods

To handle the vibrational effect in alloys with explicit configuration disorder, special quasi-random structure(SQS)[107] is a popular method. Based on CE, SQS cleverly find the structure which resembles the true random alloys by exploiting the cut-off range of configuration clusters. Phonon property is then calculated based on the derived structure. The vibrational part of free energy then are computed through harmonic approximation:

$$F^{\text{vib}} = k_b T \int g(\omega) \ln(2 \sinh \frac{h\omega}{2k_b T}) d\omega \tag{5.5}$$

The above equation, however, can not handle the anharmonicity which is particularly crucial for thermal expansion. A simple modification is quasi-harmonic approximation[108], which incorporates thermal expansion with moderate increase of computational cost. The idea of QHA is fairly simple yet effective: let phonon frequency be volume dependent by allowing FCT a function depends on volumes. The effect of volume dependent phonon often are captured by the Gruneisen parameter[109],

$$\gamma_{jq} = -\frac{\partial \log \omega_{jq}}{\partial \log V} \tag{5.6}$$

which can be calculated from first principle calculations. Though SQS work well along with QHA in wide range of materials, there are still some issues limiting their applicabilities. First issue is related to the adoption of SQS. It is known some materials can hardly be modeled by small SQS, especially for those which has relatively strong long-range force. This can be easily examined if there is slow convergence of effective cluster interactions in CE. These large cells would make calculations of FCT impractical as we discussed previously in Chapter 3. Second issue is about QHA. Though being reliable for most of the case, the Achilles' heel of QHA is lack of the ability to handle dynamically unstable materials. As many metals with BCC structure at high temperature, they have elastic constant violating the Born stability condition that materials which would simply fall flat at zero temperature. These materials can easily be identified with their characteristic imaginary modes. These imaginary modes can be intuitively understood by setting up a double well potentials. As depicted in figure 2.3, the equilibrium position at finite temperature(which is the hill-top between two valley) is not the energy minimum at zero Kelvin. This negative potential energy curvature caused imaginary mode and is ill-defined in QHA. The renormalization phonon[110, 111] has been developed to address this issue by sampling harmonic phonon at high temperature to construct the temperature or average displacement sensitive effective harmonic potentials to remove the imaginary modes. However, these methods tend to specialize on specific materials and specific temperature range rather than a general applicable solution. And again, the uncontrolled approximation approach also makes it hard to be optimized when discrepancy is observed.

5.3 Free energy calculation with VCE

To solve above issues in one-shot and construct a general formalism to accurately acquire anharmonic lattice vibrations in alloys, we can use VCE to model PES of alloys. With compact representation of vibrational property thanks to the configurational dependent force constant, VCE can easily infer accurate FCTs for large supercell with arbitrary random atomic configurations. This elegantly release us from the computational constraints on SQS. To handle anharmoniciy in free energy calculations, we apply thermodynamic integration, a well established and robust method which can take in arbitrary high order vibrational effects. Due to the path independent property of free energy, one can get the full free energy by integrating along arbitrary path from any referential points A common approach is first separating potential energy U_λ into U_{har} and U_{anh} as:

$$U_\lambda = \lambda U_{\text{har}} + (1-\lambda) U_{\text{vce}} \tag{5.7}$$

Unlike QHA calculate the harmonic potential by extracting FCT from ground state, thermodynamic integration allows one to choose referential point on one's own will. One can thus choose a well-defined harmonic potential well U_{har} as the referential starting point. Finding the renormalized phonon modes is the underlying idea among all methods developed to find the well-defined harmonic potentials. Methods including self-consistent phonon abinitio lattice dynamics(SCAILD)[110], temperature dependent effect potential(TDEP)[111] are well-known methods to find harmonic phonons incorporating temperature effect to get rid of imaginary modes in dynamically unstable materials. Unlike above mentioned method that renormalized harmonic part is the sole contribution for free energy, and thus sophisticate sampling schemes are required. In thermodynamic integration, a rough approximation is enough. In our prototypical test, we can quickly generate large random displacement configuration with its root mean square roughly equal to the corresponding displacement from equation 2.38. As demonstrated in Figure 5.3, these configurations can thus be served as the

training data which incorporate temperature effects to remove imaginary mode. Artificial free energy F_λ then are calculated along the path from $F(U_{\text{har}})$ to $F(U_{\text{vce}})$:

$$F_{\text{vce}} = F_{\text{har}} + \int_0^1 \frac{\partial F_\lambda}{\partial \lambda} \tag{5.8}$$

By definition, Helmholtz free energy can be calculated from corresponding potential by:

$$F_\lambda = kT \ln Z_\lambda \tag{5.9}$$

Where Z is the partition function can be obtained from potential energy with:

$$Z_\lambda = \int dr^N e^{(-\beta(U_\lambda)} \tag{5.10}$$

, and $\partial F_\lambda / \partial \lambda$ can be derived from:

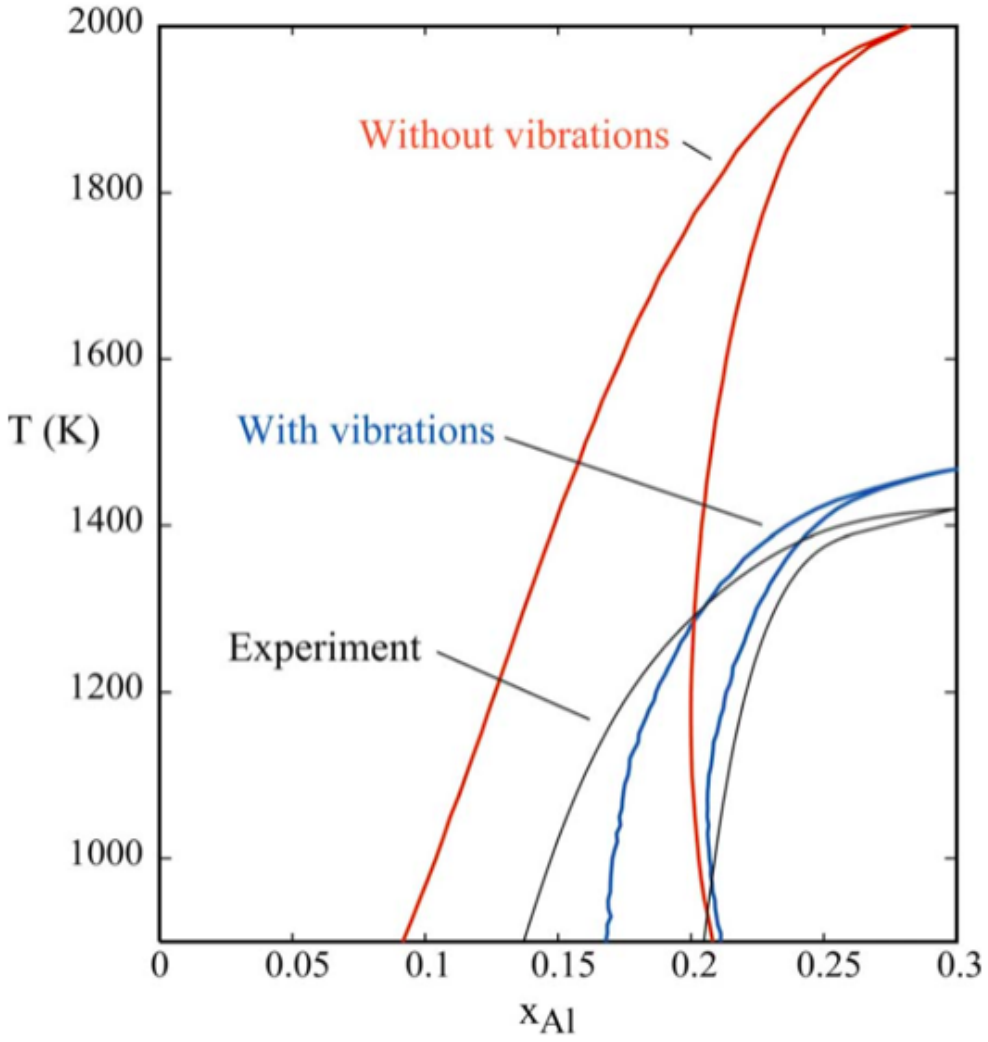

Figure 5.2: Phase transition calculation from [106] for Al-Sc intermetallic compounds. The inclusion of vibrational disorder effect significantly match much better to the experimental results compared to configuration disorder only calculations

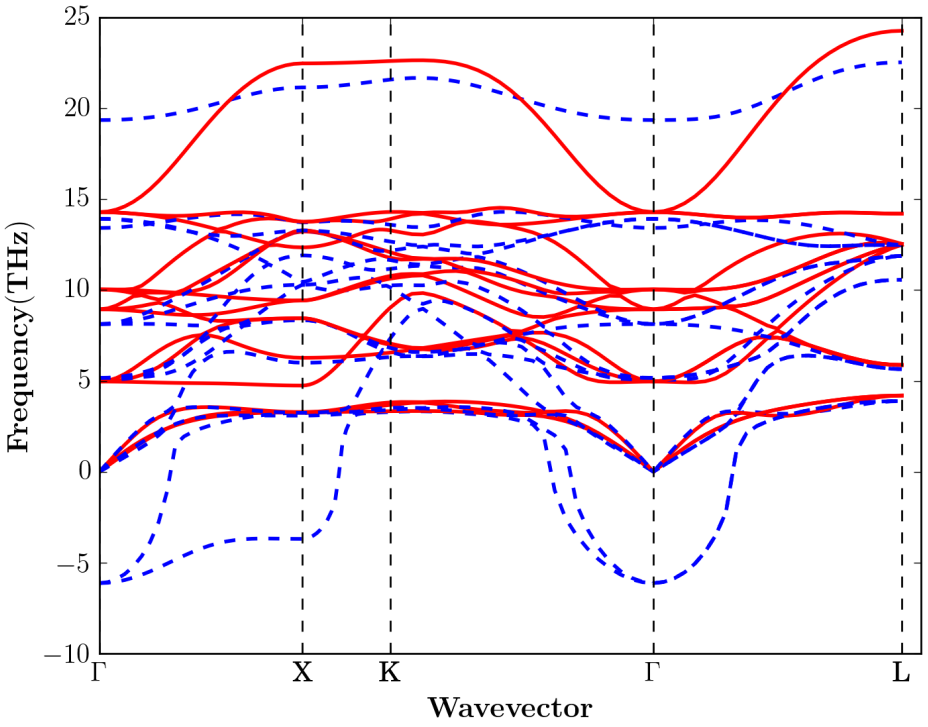

Figure 5.3: The phonon dispersion calculated by fitting FCTs with different displacement training structure. The dashed line is calculated from small displacement which would recover the true PES while solid line is calculated from large displacement which resembles displacement at high temperature to remove the imaginary part of phonon dispersion

CHAPTER 6

Conclusions

Due to the strong need of functional materials with exceedingly high performance and astronomically large number of materials, discovering solely from intuition and experiences can hardly catch up the iteration speed. Thanks to the recent advancement of computational powers and techniques, the idea of virtual lab has been demonstrated as an important approach to narrow down the required exploratory process and offer meaningful insight and guidance. The recent advancement of both computational techniques and powers makes the idea of virtual lab no longer an distant goal. Well limited by calculating 0 Kelvin and perfect crystalline materials set a hard cap to extend first principle calculations to directly quantify materials properties under realistic conditions. To extend the modern first calculation methods, in this report, we demonstrated an efficient and accurate multi-scale scheme to model realistic materials from first-principles calculations. Our VCE model shows by combining lattice dynamics and cluster expansion, one can actually construct a PES model to explicitly incorporate both vibrational and configurational degree of freedoms. The fact that both LD and CE are exact methods, as a combination of both, the exact property of VCE allows controlled approximation for straightforward tuning between desired accuracy and computational cost. This PES model can then be used as the surrogate model of DFT calculations to rapidly sample materials with both thermal and configuration disorder. Our VCE model is built and parameterized from DFT calculations to incorporate the power of parameter free calculations. Given the fact that DFT calculations is expensive while the dimension of our parameter space is large, group symmetry is applied for dimension reduction and compressive sensing is adopted to efficiently, robustly and accurately infer the sparse representation of our model. By comparing Si-Ge and PbTe-Se with random configurations, we showed our

VCE can accurately predict the force calculated from DFT. The phonon comparisons of FCC Si-Ge and PbTe-Se between DFT and VCE again demonstrated that the vibrational property is also well preserved. Unlike empirical potentials which requires well tailored functional form, thanks to the exact form of VCE and compressive sensing to retain large number of degree of freedoms, VCE is a materials-agnostic model building process for crystalline alloys and minimum prior knowledge is needed to design the model of PES. Indeed, from Si-Ge to PbTe-Se, barely any change is needed between these two systems. Unlike other first principle machine learning models, no sophisticate function design feature selections or concurrent sampling is needed in VCE. Guided by the underlying assumptions of compressive sensing and our empirical study, randomly displaced atomic displacement on top of low-fidelity AIMD trajectory of a moderate size supercell with random atomic configurations commonly yield accurate PES. By using our VCE generated PES incorporating explicit configuration disorder in lattice MD calculations, We demonstrated explicit configuration disorder is crucial to accurately predict thermal conductivity of PbTe-Se, which is overestimated by VCA in phonon calculations. Our phonon spectrum study on FCC PbTe-Se further shows this discrepancy is due to the strong interactions between high order anharmonicity and local environments. In PbTe-Se, it is manifested by the strong ferroelectric-like damping which cause significantly enhanced anharmonic scattering. A quick glance of how our VCE has potential to be a powerful tool to calculate free energy for complicated alloy systems is also shown. We propose that by sampling large displacement, it is possible to generate a harmonic potential without imaginary modes in dynamically unstable materials. The free energy can then be calculated through thermodynamic integration along this unphysical path from this harmonic potentials all the way to full VCE potentials. It is a robust, facile, and most importantly, general process to quantify free energy in alloy systems. We belive the accurate, materials-agnostic, and effecient evaluation properties in VCE can unlock a wide range of thermal properties calculations for alloys which can hardly be matched by exisiting methods.

BIBLIOGRAPHY

[1] National Research Council et al. *Materials in the New Millennium: Responding to Society's Needs*. National Academies Press, 2001.

[2] Walter Kohn, Axel D Becke, and Robert G Parr. "Density functional theory of electronic structure". In: *The Journal of Physical Chemistry* 100.31 (1996), pp. 12974–12980.

[3] Pierre Hohenberg and Walter Kohn. "Inhomogeneous electron gas". In: *Physical review* 136.3B (1964), B864.

[4] Walter Kohn and Lu Jeu Sham. "Self-consistent equations including exchange and correlation effects". In: *Physical review* 140.4A (1965), A1133.

[5] Ricky A Kendall et al. "High performance computational chemistry: An overview of NWChem a distributed parallel application". In: *Computer Physics Communications* 128.1-2 (2000), pp. 260–283.

[6] Mohamed Hacene et al. "Accelerating VASP electronic structure calculations using graphic processing units". In: *Journal of computational chemistry* 33.32 (2012), pp. 2581–2589.

[7] Alberto Franceschetti and Alex Zunger. "The inverse band-structure problem of finding an atomic configuration with given electronic properties". In: *Nature* 402.6757 (1999), p. 60.

[8] G Ceder, MK Aydinol, and AF Kohan. "Application of first-principles calculations to the design of rechargeable Li-batteries". In: *Computational materials science* 8.1 (1997), pp. 161–169.

[9] Kisuk Kang et al. "Electrodes with high power and high capacity for rechargeable lithium batteries". In: *Science* 311.5763 (2006), pp. 977–980.

[10] Byoungwoo Kang and Gerbrand Ceder. "Battery materials for ultrafast charging and discharging". In: *Nature* 458.7235 (2009), p. 190.

[11] Xu Lu et al. "High performance thermoelectricity in earth-abundant compounds based on natural mineral tetrahedrites". In: *Advanced Energy Materials* 3.3 (2013), pp. 342–348.

[12] Surbhi Lal, Stephan Link, and Naomi J Halas. "Nano-optics from sensing to waveguiding". In: *Nature photonics* 1.11 (2007), p. 641.

[13] Gérard Férey et al. "Crystallized frameworks with giant pores: are there limits to the possible?" In: *Accounts of chemical research* 38.4 (2005), pp. 217–225.

[14] M Claudia Troparevsky et al. "Criteria for predicting the formation of single-phase high-entropy alloys". In: *Physical Review X* 5.1 (2015), p. 011041.

[15] Christopher C Fischer et al. "Predicting crystal structure by merging data mining with quantum mechanics". In: *Nature materials* 5.8 (2006), p. 641.

[16] Anubhav Jain et al. "A high-throughput infrastructure for density functional theory calculations". In: *Computational Materials Science* 50.8 (2011), pp. 2295–2310.

[17] Anubhav Jain et al. "Commentary: The Materials Project: A materials genome approach to accelerating materials innovation". In: *Apl Materials* 1.1 (2013), p. 011002.

[18] James E Saal et al. "Materials design and discovery with high-throughput density functional theory: the open quantum materials database (OQMD)". In: *Jom* 65.11 (2013), pp. 1501–1509.

[19] Hans J Queisser and Eugene E Haller. "Defects in semiconductors: some fatal, some vital". In: *Science* 281.5379 (1998), pp. 945–950.

[20] Tevye Kuykendall et al. "Complete composition tunability of InGaN nanowires using a combinatorial approach". In: *Nature materials* 6.12 (2007), p. 951.

[21] Jürgen Rödel et al. "Perspective on the development of lead-free piezoceramics". In: *Journal of the American Ceramic Society* 92.6 (2009), pp. 1153–1177.

[22] J-W Yeh et al. "Nanostructured high-entropy alloys with multiple principal elements: novel alloy design concepts and outcomes". In: *Advanced Engineering Materials* 6.5 (2004), pp. 299–303.

[23] GL Yuan, Siu Wing Or, and Helen Lai Wa Chan. "Structural transformation and ferroelectric–paraelectric phase transition in Bi1- x Lax FeO3 (x= 0–0.25) multiferroic ceramics". In: *Journal of Physics D: Applied Physics* 40.4 (2007), p. 1196.

[24] CY Wang and Venkat Srinivasan. "Computational battery dynamics (CBD)—electrochemical/therm coupled modeling and multi-scale modeling". In: *Journal of power sources* 110.2 (2002), pp. 364–376.

[25] Marc GD Geers, Varvara G Kouznetsova, and WAM Brekelmans. "Multi-scale computational homogenization: Trends and challenges". In: *Journal of computational and applied mathematics* 234.7 (2010), pp. 2175–2182.

[26] Furio Ercolessi and James B Adams. "Interatomic potentials from first-principles calculations: the force-matching method". In: *EPL (Europhysics Letters)* 26.8 (1994), p. 583.

[27] Max Born and Robert Oppenheimer. "Zur quantentheorie der molekeln". In: *Annalen der Physik* 389.20 (1927), pp. 457–484.

[28] Allon I Hochbaum et al. "Enhanced thermoelectric performance of rough silicon nanowires". In: *Nature* 451.7175 (2008), p. 163.

[29] BC Sales et al. "Filled skutterudite antimonides: Electron crystals and phonon glasses". In: *Physical Review B* 56.23 (1997), p. 15081.

[30] Yanzhong Pei et al. "Convergence of electronic bands for high performance bulk thermoelectrics". In: *Nature* 473.7345 (2011), p. 66.

[31] Abraham Pais. "Einstein and the quantum theory". In: *Reviews of Modern Physics* 51.4 (1979), p. 863.

[32] M Born and Th Von Karman. "Vibrations in space gratings (molecular frequencies)". In: *Z. Phys* 13 (1912), pp. 297–309.

[33] Rudolf Ernst Peierls and Rudolf Sir Peierls. *Quantum theory of solids*. Oxford University Press, 1955.

[34] John M Ziman. *Electrons and phonons: the theory of transport phenomena in solids*. Oxford university press, 2001.

[35] Paolo Giannozzi et al. "Ab initio calculation of phonon dispersions in semiconductors". In: *Physical Review B* 43.9 (1991), p. 7231.

[36] DA Broido, A Ward, and N Mingo. "Lattice thermal conductivity of silicon from empirical interatomic potentials". In: *Physical Review B* 72.1 (2005), p. 014308.

[37] Wu Li et al. "ShengBTE: A solver of the Boltzmann transport equation for phonons". In: *Computer Physics Communications* 185.6 (2014), pp. 1747–1758.

[38] Philip B Allen and Joseph L Feldman. "Thermal conductivity of disordered harmonic solids". In: *Physical Review B* 48.17 (1993), p. 12581.

[39] Jivtesh Garg. "Thermal conductivity from first-principles in bulk, disordered, and nanostructured materials". PhD thesis. Massachusetts Institute of Technology, 2011.

[40] Jivtesh Garg et al. "Role of disorder and anharmonicity in the thermal conductivity of silicon-germanium alloys: A first-principles study". In: *Physical review letters* 106.4 (2011), p. 045901.

[41] Zhiting Tian et al. "Phonon conduction in PbSe, PbTe, and PbTe 1- x Se x from first-principles calculations". In: *Physical Review B* 85.18 (2012), p. 184303.

[42] William Graham Hoover. *Computational statistical mechanics*. Elsevier, 2012.

[43] Jerry Tersoff. "Empirical interatomic potential for silicon with improved elastic properties". In: *Physical Review B* 38.14 (1988), p. 9902.

[44] Frank H. Stillinger and Thomas A. Weber. "Computer simulation of local order in condensed phases of silicon". In: *Phys. Rev. B* 31 (8 1985), pp. 5262–5271. DOI: 10.1103/PhysRevB.31.5262. URL: https://link.aps.org/doi/10.1103/PhysRevB.31.5262.

[45] Ashton Skye and Patrick K Schelling. "Thermal resistivity of Si–Ge alloys by molecular-dynamics simulation". In: *Journal of Applied Physics* 103.11 (2008), p. 113524.

[46] D. A. Broido, A. Ward, and N. Mingo. "Lattice thermal conductivity of silicon from empirical interatomic potentials". In: *Phys. Rev. B* 72 (1 2005), p. 014308. DOI: 10.1103/PhysRevB.72.014308. URL: https://link.aps.org/doi/10.1103/PhysRevB.72.014308.

[47] Christian Carbogno, Rampi Ramprasad, and Matthias Scheffler. "Ab initio Green-Kubo approach for the thermal conductivity of solids". In: *Physical review letters* 118.17 (2017), p. 175901.

[48] John P. Perdew and Wang Yue. "Accurate and simple density functional for the electronic exchange energy: Generalized gradient approximation". In: *Phys. Rev. B* 33 (12 1986), pp. 8800–8802. DOI: 10.1103/PhysRevB.33.8800. URL: https://link.aps.org/doi/10.1103/PhysRevB.33.8800.

[49] Albert Einstein. *Investigations on the Theory of the Brownian Movement*. Courier Corporation, 1956.

[50] Max Born and Kun Huang. *Dynamical theory of crystal lattices*. Clarendon press, 1954.

[51] Nina Shulumba et al. "Temperature-dependent elastic properties of Ti1- x Al x N alloys". In: *Applied Physics Letters* 107.23 (2015), p. 231901.

[52] Fei Zhou et al. "Lattice anharmonicity and thermal conductivity from compressive sensing of first-principles calculations". In: *Physical review letters* 113.18 (2014), p. 185501.

[53] David B Laks et al. "Efficient cluster expansion for substitutional systems". In: *Physical Review B* 46.19 (1992), p. 12587.

[54] Jiří Čížek. "On the use of the cluster expansion and the technique of diagrams in calculations of correlation effects in atoms and molecules". In: *Advances in chemical physics* (1969), pp. 35–89.

[55] Walter RL Lambrecht and Benjamin Segall. "Anomalous band-gap behavior and phase stability of c-BN–diamond alloys". In: *Physical Review B* 47.15 (1993), p. 9289.

[56] Ernst Ising. "Beitrag zur theorie des ferromagnetismus". In: *Zeitschrift für Physik* 31.1 (1925), pp. 253–258.

[57] M Asta et al. "Effective cluster interactions from cluster-variation formalism. I". In: *Physical Review B* 44.10 (1991), p. 4907.

[58] GD Garbulsky and G Ceder. "Linear-programming method for obtaining effective cluster interactions in alloys from total-energy calculations: Application to the fcc Pd-V system". In: *Physical Review B* 51.1 (1995), p. 67.

[59] D De Fontaine. *Solid State Physics, H. Ehrenreich, F. Seitz and D. Turnbull, eds., vol. 34*. 1979.

[60] Keivan Esfarjani, Gang Chen, and Harold T Stokes. "Heat transport in silicon from first-principles calculations". In: *Physical Review B* 84.8 (2011), p. 085204.

[61] H Kanzaki. "Point defects in face-centred cubic lattice-II X-ray scattering effects". In: *Journal of Physics and Chemistry of Solids* 2.2 (1957), pp. 107–114.

[62] O Shchyglo et al. "Theory of size mismatched alloy systems: many-body Kanzaki forces". In: *Journal of Physics: Condensed Matter* 20.4 (2008), p. 045207.

[63] Ivan Zhuravlev, Joonhee An, and Kirill Belashchenko. "Generalized Kanzaki-Krivoglaz model of lattice relaxations in concentrated size-mismatched substitutional alloys applied to Cu-Au and Fe-Pt systems". In: *APS Meeting Abstracts*. 2014.

[64] Emmanuel J Candès and Michael B Wakin. "An introduction to compressive sampling". In: *IEEE signal processing magazine* 25.2 (2008), pp. 21–30.

[65] Emmanuel J Candès, Justin Romberg, and Terence Tao. "Robust uncertainty principles: Exact signal reconstruction from highly incomplete frequency information". In: *IEEE Transactions on information theory* 52.2 (2006), pp. 489–509.

[66] Michael Lustig et al. "Compressed sensing MRI". In: *IEEE signal processing magazine* 25.2 (2008), pp. 72–82.

[67] Jian Sun, Huibin Li, Zongben Xu, et al. "Deep ADMM-Net for compressive sensing MRI". In: *Advances in Neural Information Processing Systems*. 2016, pp. 10–18.

[68] Lance J Nelson et al. “Compressive sensing as a paradigm for building physics models”. In: *Physical Review B* 87.3 (2013), p. 035125.

[69] Savas Berber, Young-Kyun Kwon, and David Tománek. “Unusually high thermal conductivity of carbon nanotubes”. In: *Physical review letters* 84.20 (2000), p. 4613.

[70] Sebastian G Volz and Gang Chen. “Molecular dynamics simulation of thermal conductivity of silicon nanowires”. In: *Applied Physics Letters* 75.14 (1999), pp. 2056–2058.

[71] Masao Doi. “Molecular dynamics and rheological properties of concentrated solutions of rodlike polymers in isotropic and liquid crystalline phases”. In: *Journal of Polymer Science: Polymer Physics Edition* 19.2 (1981), pp. 229–243.

[72] David A Pearlman et al. “AMBER, a package of computer programs for applying molecular mechanics, normal mode analysis, molecular dynamics and free energy calculations to simulate the structural and energetic properties of molecules”. In: *Computer Physics Communications* 91.1-3 (1995), pp. 1–41.

[73] Loup Verlet. “Computer" experiments" on classical fluids. I. Thermodynamical properties of Lennard-Jones molecules”. In: *Physical review* 159.1 (1967), p. 98.

[74] William C Swope et al. “A computer simulation method for the calculation of equilibrium constants for the formation of physical clusters of molecules: Application to small water clusters”. In: *The Journal of Chemical Physics* 76.1 (1982), pp. 637–649.

[75] Tom Goldstein and Stanley Osher. “The split Bregman method for L1-regularized problems”. In: *SIAM journal on imaging sciences* 2.2 (2009), pp. 323–343.

[76] JP Dismukes, L Ekstrom, and RJ Paff. “Lattice parameter and density in germanium-silicon alloys1”. In: *The Journal of Physical Chemistry* 68.10 (1964), pp. 3021–3027.

[77] Karl Brunner. “Si/Ge nanostructures”. In: *Reports on Progress in Physics* 65.1 (2001), p. 27.

[78] Elad Joseph and Yaron Amouyal. "Enhancing thermoelectric performance of PbTe-based compounds by substituting elements: A first principles study". In: *Journal of Electronic Materials* 44.6 (2015), pp. 1460–1468.

[79] CJ Glassbrenner and Glen A Slack. "Thermal conductivity of silicon and germanium from 3 K to the melting point". In: *Physical Review* 134.4A (1964), A1058.

[80] B Abeles. "Lattice thermal conductivity of disordered semiconductor alloys at high temperatures". In: *Physical Review* 131.5 (1963), p. 1906.

[81] B Abeles et al. "Thermal conductivity of Ge-Si alloys at high temperatures". In: *Physical review* 125.1 (1962), p. 44.

[82] Heng Wang et al. "The criteria for beneficial disorder in thermoelectric solid solutions". In: *Advanced Functional Materials* 23.12 (2013), pp. 1586–1596.

[83] Jürgen Hafner. "Ab-initio simulations of materials using VASP: Density-functional theory and beyond". In: *Journal of computational chemistry* 29.13 (2008), pp. 2044–2078.

[84] John P Perdew, Kieron Burke, and Matthias Ernzerhof. "Generalized gradient approximation made simple". In: *Physical review letters* 77.18 (1996), p. 3865.

[85] Peter E Blöchl. "Projector augmented-wave method". In: *Physical review B* 50.24 (1994), p. 17953.

[86] David M Ceperley and BJ Alder. "Ground state of the electron gas by a stochastic method". In: *Physical Review Letters* 45.7 (1980), p. 566.

[87] G Nilsson and G Nelin. "Study of the homology between silicon and germanium by thermal-neutron spectrometry". In: *Physical Review B* 6.10 (1972), p. 3777.

[88] ER Cowley, JK Darby, and GS Pawley. "The lattice dynamics of tin telluride". In: *Journal of Physics C: Solid State Physics* 2.11 (1969), p. 1916.

[89] Fei Zhou et al. "Compressive sensing lattice dynamics. II. Efficient phonon calculations and long-range interactions". In: *arXiv preprint arXiv:1805.08903* (2018).

[90] P Debye, HR Anderson Jr, and H Brumberger. "Scattering by an inhomogeneous solid. II. The correlation function and its application". In: *Journal of applied Physics* 28.6 (1957), pp. 679–683.

[91] M Omini and A Sparavigna. "An iterative approach to the phonon Boltzmann equation in the theory of thermal conductivity". In: *Physica B: Condensed Matter* 212.2 (1995), pp. 101–112.

[92] Joseph Callaway. "Model for lattice thermal conductivity at low temperatures". In: *Physical Review* 113.4 (1959), p. 1046.

[93] PG Klemens. "The scattering of low-frequency lattice waves by static imperfections". In: *Proceedings of the Physical Society. Section A* 68.12 (1955), p. 1113.

[94] H Stöhr. "H. Stöhr and W. Klemm, Z. Anorg. Allg. Chem. 241, 305 (1939)." In: *Z. Anorg. Allg. Chem.* 241 (1939), p. 305.

[95] Samuel Huberman et al. "Unifying first-principles theoretical predictions and experimental measurements of size effects in thermal transport in SiGe alloys". In: *Physical Review Materials* 1.5 (2017), p. 054601.

[96] Marco Arrigoni et al. "First-principles quantitative prediction of the lattice thermal conductivity in random semiconductor alloys: The role of force-constant disorder". In: *Phys. Rev. B* 98 (11 2018), p. 115205.

[97] Weston Graham Nielson. "A Robust Approach to Lattice Thermal Conductivity". PhD thesis. UCLA, 2015.

[98] Melville S Green. "Markoff random processes and the statistical mechanics of time-dependent phenomena. II. Irreversible processes in fluids". In: *The Journal of Chemical Physics* 22.3 (1954), pp. 398–413.

[99] Ryogo Kubo. "Statistical-mechanical theory of irreversible processes. I. General theory and simple applications to magnetic and conduction problems". In: *Journal of the Physical Society of Japan* 12.6 (1957), pp. 570–586.

[100] Giovanni Ciccotti, Raymond Kapral, and Alessandro Sergi. "Non-equilibrium molecular dynamics". In: *Handbook of materials modeling*. Springer, 2005, pp. 745–761.

[101] Ju Li, Lisa Porter, and Sidney Yip. "Atomistic modeling of finite-temperature properties of crystalline β-SiC: II. Thermal conductivity and effects of point defects". In: *Journal of Nuclear Materials* 255.2-3 (1998), pp. 139–152.

[102] AJH McGaughey and M Kaviany. "Thermal conductivity decomposition and analysis using molecular dynamics simulations: Part II. Complex silica structures". In: *International Journal of Heat and Mass Transfer* 47.8-9 (2004), pp. 1799–1816.

[103] Jie Chen, Gang Zhang, and Baowen Li. "How to improve the accuracy of equilibrium molecular dynamics for computation of thermal conductivity?" In: *Physics Letters A* 374.23 (2010), pp. 2392–2396.

[104] Zuyuan Wang and Xiulin Ruan. "On the domain size effect of thermal conductivities from equilibrium and nonequilibrium molecular dynamics simulations". In: *Journal of Applied Physics* 121.4 (2017), p. 044301.

[105] Marcello Puligheddu, Francois Gygi, and Giulia Galli. "First-principles simulations of heat transport". In: *Phys. Rev. Materials* 1 (6 2017), p. 060802. DOI: 10.1103/PhysRevMaterials.1.060802. URL: https://link.aps.org/doi/10.1103/PhysRevMaterials.1.060802.

[106] Axel van de Walle, Gautam Ghosh, and Mark Asta. "Ab initio modeling of alloy phase equilibria". In: *Applied computational materials modeling*. Springer, 2007, pp. 1–34.

[107] Alex Zunger et al. "Special quasirandom structures". In: *Physical Review Letters* 65.3 (1990), p. 353.

[108] Göran Grimvall. *Thermophysical properties of materials*. Elsevier, 1999.

[109] K Brugger. "Generalized Grüneisen parameters in the anisotropic Debye model". In: *Physical Review* 137.6A (1965), A1826.

[110] Petros Souvatzis et al. "The self-consistent ab initio lattice dynamical method". In: *Computational materials science* 44.3 (2009), pp. 888–894.

[111] Olle Hellman et al. “Temperature dependent effective potential method for accurate free energy calculations of solids”. In: *Physical Review B* 87.10 (2013), p. 104111.